

DIGITAL PROTECTION OF POWER CONVERTERS
EMPLOYED IN DOUBLY-FED INDUCTION GENERATOR
AND INDUCTION MOTOR USING WAVELET
TRANSFORM

UKASHATU ABUBAKAR

FACULTY OF ENGINEERING
UNIVERSITY OF MALAYA
KUALA LUMPUR

2021

**DIGITAL PROTECTION OF POWER CONVERTERS
EMPLOYED IN DOUBLY-FED INDUCTION
GENERATOR AND INDUCTION MOTOR USING
WAVELET TRANSFORM**

UKASHATU ABUBAKAR

**THESIS SUBMITTED IN FULFILMENT OF THE
REQUIREMENTS FOR THE DEGREE OF DOCTOR OF
PHILOSOPHY**

**FACULTY OF ENGINEERING
UNIVERSITY OF MALAYA
KUALA LUMPUR**

2021

UNIVERSITY OF MALAYA
ORIGINAL LITERARY WORK DECLARATION

Name of Candidate: UKASHATU ABUBAKAR

Matric No: 17028395/1

Name of Degree: Doctor of Philosophy

Title of Project Paper/Research Report/Dissertation/Thesis ("this Work"):

**DIGITAL PROTECTION OF POWER CONVERTERS EMPLOYED IN DOUBLY-FED
INDUCTION MOTOR AND INDUCTION MOTOR USING WAVELET TRANSFORM**

Field of Study: Fault Analysis in Renewable Energy and Power Electronics

I do solemnly and sincerely declare that:

- (1) I am the sole author/writer of this Work;
- (2) This Work is original;
- (3) Any use of any work in which copyright exists was done by way of fair dealing and for permitted purposes and any excerpt or extract from, or reference to or reproduction of any copyright work has been disclosed expressly and sufficiently and the title of the Work and its authorship have been acknowledged in this Work;
- (4) I do not have any actual knowledge, nor do I ought reasonably to know that the making of this work constitutes an infringement of any copyright work;
- (5) I hereby assign all and every right in the copyright to this Work to the University of Malaya ("UM"), who henceforth shall be owner of the copyright in this Work and that any reproduction or use in any form or by any means whatsoever is prohibited without the written consent of UM having been first had and obtained;
- (6) I am fully aware that if in the course of making this Work I have infringed any copyright whether intentionally or otherwise, I may be subject to legal action or any other action as may be determined by UM.

Candidate's Signature

Date:

Subscribed and solemnly declared before,

Witness's Signature

Date:

Name:

Designation:

**DIGITAL PROTECTION OF POWER CONVERTERS EMPLOYED IN
DOUBLY-FED INDUCTION GENERATOR AND INDUCTION MOTOR
USING WAVELET TRANSFORM**

ABSTRACT

This work comprises two sections, firstly, the execution of an alternative to crowbar for the DFIG-based wind energy conversion system (WECS) is proposed. The deployed crowbar protection scheme is based on a digital algorithm oriented to utilize the d-q axis of the 3- Φ rotor currents. The application of wavelet transforms enables the effective capture, of essential information contained in the high frequency current signals. The crowbar functions to protect the rotor side converter (RSC) from damage, against the high inrush current during short or open circuit fault in the rotor or at the grid. The working of the traditional crowbar is usually characterized with the absorption of reactive power from the grid, which is considered undesirable for the topology presented herein. Furthermore, the presented digital crowbar can discriminate between the actual fault occurrence and momentarily transient. Additionally, the flexibility of wavelet packet transform (WPT) predisposes it to be incorporated within the rotor controller structure and adapted to work as crowbar. The developed d-q WPT-based digital crowbar is capable of generating a faster trip signal with shorter restoration time of $\leq 7.1ms$, than the discrete Fourier transform (DFT) based algorithm or the conventional crowbar. The protection for the grid side power converter (GSC) is implemented in somewhat similar fashion but is reinforced with H_{∞} controller, which is incorporated in the main controller to minimize the absorption of reactive power, and to limit the grid disturbances yet further. This proposed topology will minimize the grid disturbance issues, which is desirable for the high-powered applications. Secondly, the protection that entails the protection of power converters in the induction motors, involves the robustification of the motors by the

implementation of strategy for the individual controllers that collectively work in an induction motor (IM) drive by interswitching from one form of a control strategy to another. The interswitching occurs between voltage by frequency (V/f) open-loop control, closed-loop (V/f) control, sensorless vector control and sensor vector control. Optimal performance capabilities are attained with vector control, whereas V/f is a setup that is commonly affordable but with increased speed. The underlying principle is to realize a fault-tolerant control (FTC) scheme towards the robustification of the motor and hence the inverter, to attain enduring reliability in safety-critical applications. The faults tackled in this study are open and short circuits winding faults, speed sensor failures and stator winding faults. When the severity of the fault is high, an embedded protection entity interrupts the motor. Wavelet transform is applied for detecting the fault. A novel Enhanced Model Reference Adaptive System (EMRAS) is employed for sensorless vector control to assess the motor speed with minimal tuning time. Both the software and hardware simulation of the IM drive indicates that the framework is effective in detecting the fault, while the smooth interoperability of the quadric-control ensures the robustness of the FTC scheme. Thus, by default this robust protection scheme that renders the motor almost indestructible, guarantees the safety of the fragile power converters in the motor.

Keywords: Doubly-Fed Induction Generator, Induction Motor, Wavelet analysis, Fault Tolerant Control, Faults, Digital protection

**PERLINDUNGAN DIGITAL PENUKAR KUASA DIGUNAKAN DALAM
PENJANA ARUHAN BERGANDA TERSUAP DAN MOTOR ARUHAN
MENGUNAKAN PENGUBAH WAVELET**

ABSTRAK

Penyelidikan ini mengandungi dua bahagian, pertama pelaksanaan alternatif tuil-besi untuk DFIG berdasarkan sistem penukaran kuasa (WECS) dicadangkan. Skim perlindungan tuil-besi adalah berdasarkan algoritma digital untuk menggunakan paksi d-q untuk arus-arus pemutar 3- Φ . Penggunaan pengubah wavelet membolehkan mendapatkan informasi secara cekap untuk isyarat arus berfrekuensi tinggi. Fungsi tuil-besi adalah untuk melindungi pemutar sisi penukar (RSC) daripada kerosakan disebabkan oleh arus pusuan tinggi semasa litar pintas atau litar buka pada pemutar atau pada grid. Jalan kerja tuil-besi tradisional kebiasaannya dicirikan dengan menyerap kuasa regangan daripada grid, yang mana dianggap tidak dikehendaki untuk topologi yang dipersembahkan di sini. Tuil-besi digital yang dicadangkan boleh membezakan di antara arus gagal sebenar dengan fana sementara. Tambahan pula, kebolehlenturan WPT terdedah untuk digandingkan dengan struktur pemutar pengawal dan diambil untuk sebagai tuil-besi. Tuil-besi digital berdasarkan d-q WPT yang dibina berupaya menghasikan isyarat pembuka pantas dengan masa pemulihan yang singkat $\leq 7.1ms$ berbanding algoritma berdasarkan DFT atau tuil-besi biasa. Perlindungan untuk kuasa pengubah grid (GSC) dilaksanakan sama tetapi dikuatkan dengan pengawal H_{∞} , yang mana digandingkan dengan pengawal utama untuk mengurangkan penyerapan kuasa regangan, dan mengurangkan gangguan pada grid. Topologi yang dicadangkan akan mengurangkan isu gangguan grid, yang sangat penting untuk aplikasi kuasa tinggi. Kedua, perlindungan yang melibatkan perlindungan penukar kuasa dalam motor aruhan, melibatkan keteguhan motor dengan pelaksanaan strategi untuk pengawal individu yang secara kolektif bekerja dalam pemacu motor aruhan (IM) dengan bersilang dari satu

bentuk strategi kawalan kepada yang lain. Persimpangan berlaku antara voltan oleh kawalan gelung terbuka frekuensi (V/f), kawalan gelung tertutup (V/f), kawalan vektor tanpa sensor dan kawalan vektor sensor. Keupayaan prestasi optimum dicapai dengan kawalan vektor, manakala V/f adalah persediaan yang biasanya berpatutan tetapi dengan kelajuan yang meningkat. Prinsip asas adalah untuk merealisasikan skim kawalan yang tidak bertoleransi (FTC) terhadap keteguhan motor dan dengan itu penyongsang, untuk mencapai kebolehpercayaan dalam aplikasi kritikal keselamatan. Kegagalan yang ditangani dalam kajian ini adalah kegagalan pada belitan untuk litar terbuka dan pintas, kegagalan sensor kelajuan dan kegagalan belitan pemegun. Apabila keterukan kegagalan adalah tinggi, entiti perlindungan tertanam mengganggu motor. Transformasi wavelet digunakan untuk mengesan kegagalan. Sistem Penyesuaian Rujukan Model Dipertingkatkan novel (EMRAS) digunakan untuk kawalan vektor tanpa sensor untuk menilai kelajuan motor dengan masa penalaan yang minimum. Kedua-dua simulasi perisian dan perkakasan pemacu IM menunjukkan bahawa rangka kerja itu berkesan dalam mengesan kegagalan, manakala kelancaran keboleharapan kawalan kuadrik memastikan keteguhan skim FTC. Oleh itu, secara lalai skim perlindungan yang kuat ini yang menjadikan motor hampir tidak dapat diganggu, menjamin keselamatan penukar kuasa rapuh dalam motor

Katakunci: Penjana Aruhan Dua Suapan, Motor Aruhan, Analisa Wavelet, Kawalan Boleh Terima Kegagalan, Kegagalan, Perlindungan Digital

ACKNOWLEDGEMENTS

ALHAMDULILLAH, I am particularly delighted to reach this milestone in my PhD program. For this reason, I want to extend my appreciation and deepest gratitude to my supervisors Professor Saad Mekhilef and Professor Hazlie bin Mokhlis for their immense support and contributions until this stage of thesis submission. My special thanks go to Mouaz Al Kouzbary and Khalaf Gaeid for their help during the software experiment and the manuscript preparation for both the thesis and the published journal papers.

Furthermore, I am indebted to my friends Mukhtar Fatihu Hamza, Toufiq Al Yemeni, Leong Wen Chek, Shameem Ahmad and Alireza Pourdaryaei for their tireless counselling towards the successful presentations and administrative guidance. Not forgetting the kindness of the amazon philosopher in person of Suzanna Ramli for her angelic gestures and who always offers to help even before soliciting, in times of difficulty and challenges. My appreciation to my friend in person of Dr Awwal for assisting me with the responsibilities of printing and binding work.

Special thanks go to my parents and family especially to my children, Jeddah and Muhammad for their utmost patience during my long sojourn here in Malaysia, for PhD studies at the University of Malaya.

TABLE OF CONTENTS

ABSTRACT.....	III
ABSTRAK.....	V
ACKNOWLEDGEMENTS.....	VII
TABLE OF CONTENTS.....	VIII
LIST OF FIGURES	XII
LIST OF TABLES	XVI
LIST OF SYMBOLS AND ABBREVIATIONS	XVII
CHAPTER 1: INTRODUCTION.....	1
1.1. Introduction.....	1
1.2. Problem Statement.....	3
1.3. Research Objectives.....	7
1.4. Scope of the Research.....	7
1.5. Thesis Outline.....	9
CHAPTER 2: LITERATURE REVIEW.....	12
2.1 Introduction.....	12
2.1.1 Transient Models of Associate Components in WECS.....	14
2.1.1.1 Wind Turbine Generator Transient Model.....	14
2.1.1.2 Wind Turbine Transient Model.....	16
2.1.1.3 Circuit Breaker Transient Models	17
2.1.2 Transient Analysis in WECS.....	18
2.1.2.1 Transient Stability Analysis in WECS.....	22
2.1.3 Methods for Mitigation and Control of Transients in Wind Turbine Generators.....	28
2.1.3.1 Transient Control Techniques in WECS.....	29
2.1.3.2 Transient Fault Protection Techniques on WECS.....	37

2.2	Methods for Control and Detection of Faults in the Induction Motor Drives	43
2.2.1	Induction Motor Faults	44
2.2.1.1	Stator Opening, Shorting Phase Winding.....	45
2.2.1.2	Shorted Rotor Winding	45
2.2.1.3	Broken Rotor Bar and Crack End Ring.....	46
2.2.2	Wavelet-Based Faults Diagnosis.....	47
2.2.2.1	Gear Box and Bearing Faults	48
2.2.2.2	Stator Open and Short Winding Faults.....	50
2.2.2.3	Shorted Rotor Field Winding	51
2.2.2.4	Broken Rotor Bar and Crack Ring	51
2.3	Fault Tolerant Control (FTC) Survey	53
2.3.1	Stator Winding Fault Tolerant.....	57
2.3.2	Design Methodologies.....	58
2.4	Inverter Faults	64
2.5	Summary.....	68
CHAPTER 3: RESEARCH METHODOLOGY.....		70
3.1	Introduction.....	70
3.1.1	Proposed Protection Scheme for RSC and GSC	70
3.1.1.1	Implementation of the Wavelet-Based Digital Crowbar	71
3.1.1.2	Implementation of the Wavelet-Based Digital Protection for GSC	73
3.1.2	d-q Axis wavelet transform applications.....	74
3.1.3	H_{∞} Controller Design for the DFIG.....	77
3.2	Proposed Control and Protection Techniques for the Induction Motor.....	80
3.2.1	Wavelet Index Algorithm for the Induction Motor	84
3.2.2	The Platform of the Fault-Tolerant Control.....	87

3.3	Summary.....	95
CHAPTER 4: : RESULTS AND DISCUSSION		96
4.1	Introduction	96
4.2	Platform of Simulation Studies and Results for the DFIG	96
4.2.1	Simulation Results During an Open Circuit Fault in the Rotor Windings	97
4.2.2	Simulation Results During a Short Circuit Fault in the Rotor Windings .	99
4.3	Non-Fault Transient Events in the Rotor Circuits.....	101
4.3.1	Transients due to the rotor speed changes.....	101
4.3.2	Flickers in the Rotor Owing to the Wind Speed Changes.....	102
4.4	Transient Fault Events in the Stator Circuit	103
4.4.1	Simulation Results During an Open Circuit in the Stator Winding/Grid.....	103
4.4.2	Simulation Results During a Short Circuit in the Stator Windings or in the Grid.....	106
4.5	Non-Fault Transient Events in the Stator Circuits.....	110
4.5.1	White Gaussian noise in the grid.....	110
4.5.2	Voltage Spikes and Dips	112
4.6	Mitigation of Grid Reactive Power with H_{∞} Optimization.....	114
4.7	Results and Discussion for the Induction Motor	117
4.8	Summary.....	130
CHAPTER 5: CONCLUSION AND FUTURE WORK.....		131
5.1	Conclusion.....	131
5.2	Future Works	132

REFERENCES	134
LIST OF PUBLICATIONS.....	157
APPENDIX A: SIMULINK DIAGRAM OF THE DOUBLY-FED INDUCTION GENERATOR TOPOLOGY	158

Universiti Malaya

LIST OF FIGURES

Figure 2.1 DFIG-equipped wind turbine (Lei et al., 2006)	15
Figure 2.2: Transient model performance during disruption of a short-line fault using the SF6 test circuit breaker (BRK) (CIGRE, 1990).	18
Figure 2.3: Equivalent circuit of DFIG viewed from the rotor side (D. Zhu et al., 2016)	19
Figure 2.4: Single-line diagram representation of ASEA Brown Boveri (ABB) wind cable laboratory (CIGRE, 1990).	21
Figure 2.5: Fixed-speed wind turbine (FSWT) attached to the infinite bus (Rahimi & Parniani, 2009).	25
Figure 2.6: Feed-forward transient compensation (FFTC) structural scheme for DFIG with additional computation (in red) for FFTC implementation. RSC, rotor-side converter (J. Liang et al., 2013).	29
Figure 2.7: Control scheme for direct-drive PMSG-based wind turbine with adaptive-speed (J. Chen et al., 2014).	30
Figure 2.8: Variable-band vector-based hysteresis current regulator (VBHCR) employed in RSC control structure representation (Mohseni et al., 2011).	34
Figure 2.9: System configuration (Todeschini & Emanuel, 2011)	39
Figure 2.10 Fault-tolerant inverter-fed motor drives and the fault modes.	44
Figure 2.11 IM faults percentages according to IEEE	48
Figure 2.12 Basic block diagram of the FTC scheme	59
Figure 2.13 Proposed FTC technique with 3-phase four-leg inverter (X. Jiang et al., 2016)	60
Figure 2.14 Percentage of component failures in ASD.	65
Figure 2.15 Percentage of component failures in switch mode power supply	66
Figure 3.1: Digital Crowbar Implementation Topology	71
Figure 3.2: Conventional Crowbar Implementation Topology	73
Figure 3.3: Digital Protection Topology for GSC	74

Figure 3.4: Control Structure for H_{∞} Controller Design	78
Figure 3.5: The reference frame for vector control	81
Figure 3.6: The EMRAS implementation in Simulink	83
Figure 3.7: Entropy proportion in percentage	85
Figure 3.8: The scaling factor (red) and the Daubechies Wavelet function (db10).....	85
Figure 3.9: Wavelet decomposition and reconstruction.....	86
Figure 3.10: Simulink wavelet index implementation	87
Figure 3.11: Fault-tolerant control algorithm.....	88
Figure 3.12: Fault detection and isolation unit implementation in Simulink.....	88
Figure 3.13: Trip data for the individual controllers executed in Simulink.....	89
Figure 3.14: Simulink model of FTC scheme	89
Figure 3.15: Multisensory control scheme block diagram.....	90
Figure 3.16: Switching fashion for the space vector PWM	92
Figure 3.17: Low pass filter (0-10) kHz magnitude and phase response.....	93
Figure 3.18: High pass filter (9.76-19.5313) Hz magnitude and phase response	93
Figure 3.19: FTC Strategy flowchart using the multisensory control technique	94
Figure 4.1: Simulation Response of 3-phase rotor current during the open circuit fault in phase A.....	98
Figure 4.2: Simulation Response of the direct and quadrature axis rotor current during the rotor open circuit fault.....	99
Figure 4.3: Simulation Response of the Three-phase Rotor Current during Short-Circuit Fault.....	100
Figure 4.4: Simulation Response of the direct-quadrature Rotor Current during Short-Circuit Fault.....	101
Figure 4.5: Simulation of the Wind Speed Changes	102
Figure 4.6: Simulation Response of wind Variation in DFIG with Flickers	103

Figure 4.7: Simulation Response of the Three-Phase Stator Currents During an Open Circuit Test.....	104
Figure 4.8: Simulation Response of the direct-quadrature Stator current during an Open Circuit Fault.....	105
Figure 4.9: Simulation Response of the Three-phase stator current during an open circuit fault.....	106
Figure 4.10: Simulated Response to the short circuit fault in the Stator of the generator with Spikes and Dips.....	107
Figure 4.11: Simulation Response of the Direct-axis Stator Current during the Short Circuit Fault.....	107
Figure 4.12: Simulation Response of the direct-quadrature Axis Stator Current during the Short Circuit Fault.....	108
Figure 4.13: Simulation Response of the d-q WPT Digital Protection and its Localization Ability.....	109
Figure 4.14: Simulation Response of the d-q WPT and its Localization Effects on the Fault.....	109
Figure 4.15: Simulation Response to the Injected Noise to a Grid connected to the Stator of a generator.....	111
Figure 4.16: Simulation Response of the Non-fault events, such as the Spikes and Dips at the grid during the DFIG Operation.....	113
Figure 4.17: Simulation Response of Reactive Power under H_{∞} Control Optimization.....	116
Figure 4.18: Simulation Response of Reactive Power under Classical PI-Vector Control.....	116
Figure 4.19: wavelet analysis in faultless motor.....	117
Figure 4.20 Experimental DC level in the healthy inverter.....	118
Figure 4.21 Experimental DC level in the faulty inverter.....	118
Figure 4.22: Laboratory scheme to analyze the short-circuit fault in the stator with wavelet index.....	119
Figure 4.23: Laboratory procedure for assessing the open-circuit fault in the stator, with wavelet index.....	119

Figure 4.24: Induction motor setup	119
Figure 4.25: Speed difference with the binary indication	121
Figure 4.26: SVM control signal with 0 binary indication in healthy induction motor	121
Figure 4.27: Stator current with fault injection	122
Figure 4.28: Wavelet decomposition	122
Figure 4.29: Speed reaction and recovery time	123
Figure 4.30: Monitoring outputs for faults at 2 sec	123
Figure 4.31: Stator current with fault injection	124
Figure 4.32: Wavelet decomposition	124
Figure 4.33: Multiple faults at different times	125
Figure 4.34: stator current	126
Figure 4.35: Signal from the SVM to control the inverter under various control technique	127
Figure 4.36: Different values of wavelet index correspond to stator resistance	130

LIST OF TABLES

Table 2.1: Results of the transient stability of two-mass, three-mass and six-mass models (ignoring all types of damping) (Muyeen et al., 2007). S, steady; U, unsteady.....	24
Table 2.2: Results of the transient stability of two-mass, three-mass and six-mass models (considering all types of damping) (Muyeen et al., 2007).	24
Table 2.3: Transient stability evaluations techniques in various WECS applications. IISG, inverter interface synchronous generator.	27
Table 2.4: Summary of various Control/Protection Techniques for Mitigating Transient Faults	42
Table 2.5: Induction Motor frequency characteristics formulas	53
Table 2.6: Common Procedures for Diagnostic Techniques of IM	62
Table 4.1: Comparison of the proposed techniques and existing ones	114
Table 4.2: The IEEE standard for observing the parameters of induction motor	120
Table 4.3: The induction motor parameters	120
Table 4.4: Comparison of recent fault diagnostic techniques of the Induction motor, using advance signal processing techniques	129

LIST OF SYMBOLS AND ABBREVIATIONS

Ψ	Mother Wavelet
Φ	Father Wavelet
db10	Daubechies 10 wavelet
W_{index}	wavelet Index
a	scaling parameter
b	Localization factor
x_h	high-frequency band limit
x_l	Low-frequency band limit
$E_{(S)}$	Shannon Entropy
f	fundamental frequency
\bar{D}_{SV}	Diagnostic Space Vector
w	width or window
$S_{(n)}$	partial sum sequence entropy
Ψ	mother/original wavelet
$(Hs)_k$	low pass operator
$(Gs)_k$	High pass operator
x	time in wavelet analysis
$L_2(R)$	multiresolution frame
T_e	electrical torque
p	number of poles
v/f	voltage/frequency
$d - q$	direct-quadrature axis orientation
v_d, v_q	direct-quadrature voltages
L_m	magnetizing inductance
$T_s f_s$	sampling time and frequency
$T_0 T_1 T_2$	switching time duration
I_S	main stator current

v_{ds}, v_{qs}	stator voltages
i_{sd}, i_{sq}	stator currents
R_s, L_s	resistance and Inductance of stator
R_r, L_r	resistance and Inductance of rotor
$\lambda_{dr}, \lambda_{qr}$	rotor direct-quadrature flux linkages
$\lambda'_{dr}, \lambda'_{gr}$	referenced rotor flux linkages
$\frac{di_{ds}}{dt}, \frac{di_{qs}}{dt}$	derivatives of stator currents
σ	leakage coefficient
Φ_{airgap}	air gap flux
E_{airgap}	air gap EMF
N	rate limiter input
T	time
δ	rising slew rate
ω_0	initial angular speed
$\omega_{Enhancer}$	enhanced angular speed
$\omega,$ $\omega_{reference}$	original and reference angular speed
ε	speed error
$O_{\frac{O}{P}}(i)$	rate limiter output
α	angle
γ	falling slew rate
N	nth order
Y_{dq}	Convolution function
SF_6	Sulphur Hexafluoride
X_{dq}	unbiased function
h_4	Convolution matrix
W_p	Weighing function of H_{∞} controller input
W_u	Weighing function of H_{∞} controller Output
APF	Active Power Filtering

AZPWM	Active Zero Pulse Width Modulation
BFCL	Bridge-type Fault Current Limiter
CHB	Cascaded H-Bridge
CMV	Common Mode Voltage
CWT	Continuous Wavelet Transform
DFIG	Doubly-Fed Induction Generator
DFT	Discrete Fourier Transform
DLSTM	Deep Long Short-Term Memory
DSP	Digital Signal Processing
DVR	Dynamic Voltage Regulator
DWT	Discrete Wavelet Transform
EAC	Equal Area Criterion
EEAC	Extended Equal Area Criterion
EMRAC	Enhanced Model Reference Adaptive Control
EWT	Empirical Wavelet Transform
FDI	Fault Diagnostic and Isolation
FD-DWT	Frequency Domain Discrete Wavelet Transform
FFT	Fast Fourier Transform
FFTC	Feed Forward Transient Compensation
FNGBM	Fourier Nonlinear Grey Bernoulli Model
FPGA	Field-Programmable Gate Array
FSIG	Fixed Speed Induction Generator
FTC	Fault Tolerance Control
GSC	Grid Side Converter
IISG	Inverter Interface Synchronous Generator
IPMSM	Interior Permanent Magnet Synchronous Motor
IM	Induction Motor

IMD	Induction Motor Drive
KS	Controller Stability
LVRT	Low Voltage Ride Through
MCSA	Machine Current Signature Analysis
MIMO	Multi Input Multi Output
MMC	Multi-Modular Converter
MMPC	Modulated Model Predictive Control
MPPT	Maximum Power Point Tracking
MPTC	Model Predictive Torque Control
OEWIM	Open-Ended Wound Induction Motor
OWFMP	Optimal Wavelet Function Matching Pursuit
PBLFC	Passivity Based Linear Feedback Control
PCC	Point of Common Coupling
PIR	Proportional Integral Resonance
PMG	Permanent Magnet Generator
PMSG	Permanent Magnet Synchronous Generator
PR-VC	Proportional Resonant-Vector Control
PSCAD	Power System Computer Aided Design
PTC	Predictive Torque Control
PWM	Pulse Width Modulation
RP	Robust Performance
RS	Robust Stability
RSC	Rotor Side Converter
RSSD	Resonance-Based Sparse Signal Decomposition
RTDS	Real Time Digital Simulator
RTTF	Rotor Turn-to-Turn Fault
SFTC	Sensorless Fault Tolerant Control

SISO	Single Input Single Output
SMGLC	Sliding Mode Guidance Law Controller
SMO	Sliding Mode Observer
SMIB	Single Machine Infinite Bus
STFT	Short Term Fourier Transform
SVM	Support Vector Machine
SWPT	Stationary Wavelet Packet Transform
TSI	Transient Stability Index
VBHCR	Variable-band Vector-Based Hysteresis Current Regulator
VSI	Voltage Source Inverter
WECS	Wind Energy Conversion System
WPP	Wind Power Plant
ZOH	Zero-Order Hold
ZSV	Zero Sequence Voltage
1D-LBP	One Dimensional Local Binary Pattern

CHAPTER 1: INTRODUCTION

1.1. Introduction

The operation of doubly fed induction generator (DFIG) is found to be transient in nature, and thus the dominant faults in DFIG-based wind energy conversion system (WECS) is transients. A state-of-the-art technique is needed to specifically determine whether such a transient is related to fault or non-fault events (S. Saleh, Radwan, & Rahman, 2007), (S. A. Saleh, Scaplen, & Rahman, 2011). In case of fault occurrence in doubly fed induction generator (DFIG) based wind farm, the rotor current increases sharply to an unsafe value. Therefore, should be decoupled from the grid within few milliseconds, to protect the power electronic converter at the rotor side of the generator from being damaged. The protection that is commonly devised for this application, is referred to as crowbar circuit. A crowbar is used for the protection of circuits or equipment, under fault conditions and in high powered applications where the conventional circuit cannot be used (John, 2019).

A crowbar is made up of thyristor with a voltage-or-current sensitive firing circuit. In wind energy conversion system employing DFIG the crowbar circuit is retrofitted between the rotor of the generator and the rotor side converter RSC (Z. Chen, Guerrero, & Blaabjerg, 2009) (J. Liang, Qiao, & Harley, 2011) and (Stojčić, Pašanbegović, & Wolbank, 2014). The wavelets/phaselet has a localization property that can be applied, to capture the salient features of the rotor current during actual fault occurrence and just the momentarily transients due to change of speed or load changes (S. Saleh et al., 2015).

The induction motor (IM) has been the most prominent drive employed in industrial applications and energy conversion systems for the past decades. This prominence is due to its rugged design, ease of maintenance and cost-effectiveness. During the operation of an IM, various types of faults are encountered as a result of electrical, mechanical,

magnetic, thermal and environmental forces (Hassan, Amer, Abdelsalam, & Williams, 2018). Identifying and diagnosing these faults require a combination of control and fault classification techniques for the reliable operation of the motor. The control techniques include fault-tolerant control (FTC), which is implemented concurrently with fault diagnostic methods. These methods include thermal imaging, conventional relays (current, voltage and thermal) and monitoring of mechanical vibrations. They all facilitate the FTC and help to obtain an excellent post-fault performance (J. Zhang, Zhan, & Ehsani, 2019). However, the growing number of power electronic converter applications in motor drives have rendered most of these techniques ineffectual (Amini & Moallem, 2016). Therefore, to improve the robustness of the motor drives, digital protection techniques are needed in motor drives.

The procurement order for induction motor drives (IMDs) has spiked in the industry, due to its reliability and optimal-performance. This has sparked a major research interest regarding the design of state-of-the-art controllers required for a wide range of applications. The intelligent (fuzzy logic, neural networks, and genetic algorithm, etc.), vector, proportional-derivative-integral, sliding mode and direct torque controllers are among the numerous controllers proposed to achieve the optimal-performance from motor drives (Farah et al., 2019) (J.-H. Lee, Pack, & Lee, 2019) (D. Jiang et al., 2019) (Barrero & Duran, 2015). Model predictive control (MPC) for power converters and drives can be considered as a standardized scheme for research and development. However, efforts are required to take this technology to the commercial and industrial stages. The categories of MPC techniques are based on optimization standards (Vázquez Pérez, Rodríguez, Rivera, García Franquelo, & Norambuena, 2017). Model reference adaptive control (MRAC) is usually employed in machine drives, including the (IM) (Fei, Deng, Li, Liu, & Shao, 2019), to manage the speed of the motor. This is achieved by manipulating parameters such as the back EMF, flux and reactive power is naturally

unaffected by the stator resistance (Teja, Verma, & Chakraborty, 2015). Nonetheless, such architecture is incapable of handling the stability properly while in the regenerative mode (Seshadrinath, Singh, & Panigrahi, 2013).

1.2. Problem Statement

Various protection schemes in distributed generation systems exist especially in the wind energy conversion system. Owing to the stochastic nature of the wind, the operation of the generators can adversely be affected, because of the erratic nature of the supply frequency. The location of the faults in a power system even at distance position, from the turbine installations, would result in the sudden fall of the grid voltage. This will result in an over voltage in the dc bus and consequently over current in the rotor circuit of the generator (Climente-Alarcon, Riera-Guasp, Antonino-Daviu, Roger-Folch, & Vedreno-Santos, 2012) (Toma, Capocchi, & Capolino, 2012) (S. Saleh, R. Meng, R. McSheffery, S. Buck, & E. J. I. T. o. I. A. Ozkop, 2017b). Without the provision of any protection scheme would lead to the destruction of the power converter. Although, most of the techniques make use of extra sensors that complicates the condition observer and fault detection scheme to become cost-prohibitive (Daneshi-Far, Capolino, & Henao, 2010). Another setback is that these sensors are also susceptible to small defects, that would lead to unintended failure. Thus, techniques need to be devised on the basis of generator's electrical parameters, such as the stator/rotor current or voltage to simplify the complication of the control scheme (Stojčić et al., 2014).

The crowbar control system employs crowbar circuit, which is also incorporated with the RSC and for FRT. The utilization of crowbar protection techniques disconnects the RSC in the event of fault occurrence (Haidar, Muttaqi, & Hagh, 2017), which predisposes the DFIG to operate like squirrel-cage induction generator. This resulted in drawing enormous amount of reactive power from the utility grid and resulted in the stability

problem in the grid (Firouzi & Gharehpetian, 2017). Distributed Static Compensator (DSTATCOM) has been utilized to monitor and control the voltage during grid fault (Sitharthan, Sundarabalan, Devabalaji, Nataraj, & Karthikeyan, 2018).

According to (W. Jin, Lu, & Huang, 2019) the steady positive impedance of the DFIG was found to differ from the transient positive impedance; thus, there is a speed-frequency component in positive sequence fault current. Under this condition the LVRT approach of DFIG-based wind turbine is the insertion of crowbar resistance. Moreover, when inserting the crowbar resistance, a substantial attenuation course in the positive sequence current was observed. In order to counter these shortcomings (Semwal, Selvaraj, Desingu, Chelliah, & Joseph, 2019) developed a two-stage protection circuit (dc link chopper + crowbar), design in the manner to protect multi-channeled power electronic converter from excess voltage in the event of grid disturbances. Analogy of crowbar using traditional ignition scheme, involving a three-phase controlled rectifier, during which the automatic voltage regulator (AVR) was improvised by (Hasani, Haghjoo, Bak, & da Silva, 2019) in protection scheme employing real time digital simulator (RTDS).

The proposed detection and classification methods of transient's faults is designed to extracts the magnitudes and phases of the high-frequency sub-band contents available in d-q-axis components of the crowbar currents for the RSC protection and the PCC current for the grid side converter (GSC) protection especially during islanding (S. Saleh, R. Meng, R. McSheffery, S. Buck, & E. Ozkop, 2017a) and (S. Saleh, Aljankawey, Ozkop, & Meng, 2016), respectively. The extraction of the magnitudes of the high-frequency from the sub-band content is achieved by modulated filter bank that is made up six digital high-pass filters (HPFs) (S. A. Saleh, Ozkop, & Aljankawey, 2016).

For the case of Induction motor (IM), the original works on digital protection in motor drives were established based on the electric machine models. The adoption of

negative/zero sequence currents, voltages, and impedance values have been used for fault detection and classification owing to their affinity towards asymmetries resulting from any fault. Although potential asymmetries resulting from the framework of the controller, supply circuits, and motor construction have introduced a high source of error in the classification and detection of the fault (Duran & Barrero, 2015; Gonzalez-Prieto et al., 2019; S. Saleh & Ozkop, 2016c; S. A. Saleh, Ozkop, & Aljankawey, 2015; Stojčić et al., 2014). Other applications of automated protection employed in motor drives have been accomplished using online approximations of the motor data specifications, in which the faults are detected and classified on the basis of variation in the magnitude of the approximated data (Gyftakis et al., 2015b). The need for specifying threshold from faultless motor drive complicates the applications of this method in digital based scheme.

The digital protection techniques based on harmonics have pioneered the development of the MCSA approach in motor protection with power electronic converters. In this approach, discrete Fourier transform (DFT) and fast Fourier transformation have been employed to capture selected harmonics originating from voltages and/or currents (Bessous et al., 2018) (Samaga, Vittal, & Systems, 2012). This type of digital protection technique which is based on harmonics has displayed an enhanced performance compared with over-current protection techniques. However, this protection technique has some shortcomings in high-performance drives applications because of the harmonics injected by the power of electronic converts. Furthermore, the nonperiodic and nonstationary features of transient disturbances in motor drives raise some concerns regarding their online applications due to the issue of window size specifications.

The digital protection based on artificial neural network (ANN) is realized and applied in motor drives (induction and permanent magnet). The standard framework of ANN needed, together with the requirement for data mining, to train the ANN for online

deployment has presented a major problem for implementing the artificial intelligence-based protection technique in induction motor drives (Gowthami & Kalaivani, 2019), (Zolfaghari, Noor, Rezazadeh Mehrjou, Marhaban, & Mariun, 2018a). Recently, the MCSA strategy has been achieved by the time-frequency (TF) study. Usually, minimal sensitivities to a slight alteration in the motor specification and control architecture are achieved, and almost independent to window size for online implementation when TF-based digital protection is employed. The applications of wavelet transform such as discrete wavelet transform (DWT), continuous wavelet transform (CWT) (Rangel-Magdaleno et al., 2016), and wavelet packet transform (WPT) in motor drives and power converters protection have received tremendous attention in power system and renewable energy systems.

The fault-tolerance and robustness of multisensory protective strategy in drives, without the need for retrofitting extra hardware, can be referred to as “classical” application. The interswitching ability of motor drives, due to the additional degree-of-freedom offered by more than one control technique has been an intriguing field of study. In this study, a fault-tolerant control approach is performed on a number of induction motor faults. A motor drive utilizing a vector control and equipped with an encoder is the primary control framework. When failure is anticipated from the encoder, the model changes to sensorless control mode. A short or open circuit in the stator winding causes the closed-loop V/f model to take over. If a fault occurs due to low voltage, the paradigm switches to open-loop V/f mode. The faults are diagnosed by the application of the wavelet index function. In case of persistent degradation in the motor performance, the protection circuit comprising the control and the wavelet stops the motor.

The controllers guarantee the efficiency and swift response of each of the four control schemes. The wavelet transform is demonstrated to be an efficacious fault detector. In

addition to that, the system is very flexible as it can revert to the principal controller, in the event that the motor recommences operation in healthy mode, thus guaranteeing its availability at each instant. Furthermore, the need for extra hardware to implement the protection circuit has been eliminated, which contributes to the minimal cost of the IM drive. In addition to that, the sensorless vector control introduces a novel Enhanced Model Reference Adaptive System (EMRAS) to measure the speed. This will obviate the burden of tuning experienced in the case of PI controller implementation.

1.3. Research Objectives

The main aim of this research is to provide protection against damages to the power converters employed in WECS utilizing DFIGs and also in the induction motors. Hence, the objectives that entails this research are;

1. To design a digital crowbar and grid side converter protection scheme, for DFIG based on discrete wavelet transform, (DWT).
2. To enhance the fault-tolerant capability of the DFIG, by incorporating the H_∞ robust control scheme.
3. To develop a wavelet index algorithm based on DWT, that will diagnose the fault occurrence at the stator of the induction motor and trip off the induction motor drive.
4. To design a robust and flexible fault-tolerant control scheme, for the induction motor (IM), based on an enhanced model reference adaptive control technique.

1.4. Scope of the Research

This study is devoted to offering protection to the power electronic converters, employed in the popular topology of wind energy conversion system, utilizing DFIG as well as in the induction motor, mainly in medium and high-powered applications. Thus,

the purview of the research is restricted to ensuring the safety of these converters during fault occurrence in the rotor or stator of the generator. In addition to that, since the topology of the generator is designed in such a way that the stator is directly connected to the grid, and therefore any fault or distortion on the grid will directly affect the stator. Hence, the GSC protection can be extended to islanding occurrence, with the conventional PI regulator being optimized with the H_∞ controller to minimize the grid perturbations during external disturbances. The H_∞ is also observed to mitigate the reactive power absorption, during fault events owing to the crowbar action.

The rotor and stator currents are the parameters utilized for examining and detecting of the fault in the rotor or stator windings respectively. The proposed protection scheme will substantially reduce the downtime of the generating system, due to its ability to trip and reconnect within few μs of the fault clearance time. The major limitation of this study, is that the fault emulation during the experiment, cannot be applied in the rotor or stator of the real generator because it may suffer permanent damages. Therefore, a specially design test rather than the real machine is required. However, during the experimental study the faults were applied at the phases of the rotor and the stator, because this experiment is bereft of test machine. Furthermore, the prime mover coupled to the DFIG was improvised with a DC generator rather than the actual wind turbine.

For the induction motor, model Reference Adaptive Systems (MRAS) are employed to determine parameters by utilizing the adaptive model and reference model. The parameters to be estimated are obtained from the resulting variation of the model pair that drives the adaptive mechanism. A common constant gain linear PI regulator is usually applied by the traditional MRAS to compute the approximate speed of the rotor. The application of the PI controller is exhaustive, resulting from the tuning. This study proposes the substitution of the PI controller with a 'booster or enhancer' that minimizes

the tuning time while still offering a better response. The booster is formulated using a zero-order hold and rate limiter

The deployment of the experimental setup of the FTC control involves the execution of the algorithm associated with fault-tolerant controller with the support of DSP TMS320F28335. Moreover, RS232 is extended to interconnect the PC and the TMS320F28335 DSP. Readings from the outputs were collected via the serial communication interface (SCI). The measurement of the stator current and the speed of the rotor was performed with the aid of ADC, at a sampling rate of 20kHz. The application of the current sensor, which employs the principle of closed-loop hall effect assured the safety appliance of 3-volt maximal to the DSP.

A signal parameterization circuit was utilized to guarantee the regulation of the transmitted signal by the encoder to the 3V F28335 DSP. The circuit was retrofitted and applied to initially receive the signal emanating from the encoder. Both the normal and faulty cases were studied while conducting the experiment. Additionally, open winding, sensor fault, short winding in the stator and minimum voltage were examined. The compilation and implementation of the FTC circuit were performed exclusively by the DSP F28335 controller and MATLAB Simulink, respectively.

1.5. Thesis Outline

This dissertation is compiled in five chapters. **Chapter One** is a general but succinct introduction to the wind energy and the impetus that drives for its harnessing in electrical power generation. The DFIG-based WECS is also introduced as it is the most popular topology in megawatts (MW) applications, where there is possibility of fault occurrence. On the other hand, a new multisensory wavelet-based fault tolerant control for induction motor (IM) is also studied. The latest trend is to make the drive fault tolerant, thereby

improving its robustness, particularly in the industrial application where fault occurrence is economically disastrous.

Chapter Two reviews summarily a few transient faults analysis methods, and the mathematical model design of some of the equipment/components such as the DFIG, IM and power electronics converter are introduced. On the other hand, the transient faults mitigation or protection techniques are reviewed critically to figure out the state-of-the-art technique and improve further on its shortcomings. Although, the literature of wavelets application in fault detection and protection is enough in general electrical power system engineering, there is paucity of it in renewable energy and wind electrical machines. Therefore, the chapter consist of several different types of protection and remedy techniques in WECS and the IM in addition to the methods utilizing wavelets transforms.

Chapter Three, describes the foundation of wavelet transforms, together with its modelling and formulation in relation to the anticipated fault, which is due to be analyzed. Wavelet packet transform, and wavelet analysis are introduced with the detailed mathematical analysis and diagnosis of the current signals for both rotor and stator of generator and the induction motor are carried out. The implementation of the crowbar i.e. RSC protection and also the GSC protection, for the case of DFIG are presented, which is realized with the aid of cyclic convolution and unbiased method. Meanwhile, the protection technique in the induction motor drive, which is embedded with fault tolerant control (FTC) is subsequently introduced. The faults analysis and diagnosis are devised using the traditional wavelet analysis, of Daubechies *db10* wavelet.

Chapter Four has presented the extensive simulation results of the emulated faults and other variations at the rotor and the stator side of the DFIG. This is followed by the wavelets processing of the fault in order to discriminate, whether its actually faults event

or just an ordinary transient event. In similar but separate case, the complete results for the simulation and experiment from the induction motor drives has been presented. It is demonstrated herein that the results from wavelet analysis is capable of accurately detecting the fault.

Lastly, in **Chapter five**, the conclusion and the recommendation that entails the future work, which will offer the best protection techniques for both the doubly-fed induction generator and the induction motor are presented in this chapter. Additionally, the discussion involves how to improve the robustness of the DFIG and the induction motor.

Universiti Malaysia

CHAPTER 2: LITERATURE REVIEW

2.1 Introduction

DFIGs, which are wind turbine generators or systems with variable speed, are regularly used in power-generating systems. The power electronic converter, which supplies the rotor winding, accounts for 30% of the total rated power. The stator winding of the DFIG is typically connected directly to the grid (Z. Chen et al., 2009), and the rotor and the stator of the turbine generator can be cheap sources of transients. The induction generator flux is regulated with the use of open loop control, which manipulates the direct-axis component of the stator current (i_{ds}). However, the rotor flux is mainly fixed at a rated value under standard conditions for fast-transient response. In addition, the vector control technique enables fast-transient response for intelligent control schemes, such as fuzzy logic-based vector control (Simoes & Farret, 2011).

Regarding the fixed-speed wind systems with cage induction generators, the integration of the generator is usually achieved with the use of a third-order (rotor flux transient) dynamic model, based on rotating field theory. The d-q coordinate system is usually applied to model the induction generator (Nunes, Lopes, Zurn, Bezerra, & Almeida, 2004). Transient phenomena in stators are typically faster than rotor transients; therefore, such phenomena are commonly ignored, which is equivalent to neglecting the DC component of the transient current in the stator, thereby allowing the representation of only the fundamental frequency components (Nunes et al., 2004) (Semwal et al., 2019).

The transient stability of a power system is a measure of the extent to which it can retain synchronism when exposed to several interruptions. These interruptions include equipment downtime, load variations and faults that result in large excursions of the machine rotor angles (Kundur, Balu, & Lauby, 1994). The rotor angle of the machine, which is measured according to the reference rotating synchronously, is a variable that

tests the transient stability of a system. The significance of the contingency and trajectory of a system, which result from specific disruptions, can be analysed by the transient stability index (TSI) (Gautam, Vittal, & Harbour, 2009). A commonly-adopted technique for determining the transient stability in a synchronous generator is the critical clearing time (CCT), which is the maximum period of fault occurrence that does not cause any loss of synchronism in a generator (Tajdinian, Seifi, & Allahbakhshi, 2018).

Wind turbine transient stability schemes rely on several factors, such as network variables and fault specifications. Nevertheless, wind speed is assumed constant in simulations of the transient stability of wind turbines (Gautam et al., 2009). Wind energy conversion systems (WECSs) demand generators with extremely high torque capacities owing to the large moment of inertia of the turbine blades. High-speed controllers generate high transients in the mechanical torque, which is reproduced in the general power (Datta, Kalam, & Shi, 2018).

The factors that contribute to transient phenomena in wind power plants (WPPs) are not commonly encountered in traditional power plants and include the extensive application of unconventional generators, turbines and dry-type insulation transformers. The high-frequency interaction of two or more of the equipment in a power scheme results in transients with high stresses and a potential breakdown of the insulation of the essential equipment (Badrzadeh, Gupta, Singh, Petersson, & Max, 2012). The transient-fault detection mechanism must be selective and effective in differentiating the transients that emanate from the usual switching operations of voltage source converters and transients that arise due to fault occurrences. This situation implies that protection systems must not be miscalculated under fast-switching transient conditions, which are unrelated to faults (Geebelen, Leterme, & Van Hertem, 2015).

This review is inspired to develop a control and protection technique that will modify the traditional function of the crowbar in DFIG (i.e., offering protection to the rotor-side converter (RSC) against overcurrent transients) with a new improved version, for mitigating faults in WECS. This objective can be attained by the application of an innovative and user-defined phaselet packet transform to analyse and classify transients occurring in the system as specifically related to fault or non-fault, so as to send a trip signal to the power TRIAC to trip the affected phase, unlike typical protection systems, which failed short of this accuracy, and will trip whether the transient is related to fault or not. Another idea conceived of, regarding the control system, is to propose a space vector pulse width modulation (SVPWM), which will be embedded into the protection scheme.

2.1.1 Transient Models of Associate Components in WECS

Transient modelling techniques of wind power plants were proposed in (Badrzadeh, Gupta, et al., 2012) to expound and validate the basic components of WPPs and thus assess the momentary and transient over-voltages. The simulation of such over-voltages requires the application of low simulation time steps ranging from a few nanoseconds to a few microseconds. Therefore, realization of the overall WPP is a tedious task. A single feeder of a WPP, which consists of WTGs, is often adopted to reduce the simulation time without deviating from the accuracy limit.

2.1.1.1 Wind Turbine Generator Transient Model

A simple model that embodies a DFIG equipped with a wind turbine, shown in Figure 2.1, as a voltage responsible for the transient reactance, was proposed in (Lei, Mullane, Lightbody, & Yacamini, 2006). The DFIG was considered a typical induction generator with a small-magnitude rotor voltage. Neglecting the stator transient per unit electrical equations of the DFIG can be expressed in phasor form as in (Feijóo, Cidrás, & Carrillo,

2000). According to (Z. Chen et al., 2009), the transient recovery of DFIGs is significantly affected by the active power oscillations generated by the shaft dynamics, which depend on the shaft stiffness.

Simplifying and reducing the converter and induction machine model do not substantially change the DFIG transient response. The erratic behaviour exhibited by DFIGs during large disturbances, when the rotor-side converter (RSC) is blocked, has been reported. During the fault ride-through of the DFIG with a crowbar, an electromagnetic torque drops due to the decrease in voltage, which leads to rotor acceleration. The grid voltage falls steeply in magnitude, thereby leading to the generation of high-current transients in the rotor and the stator due to the magnetic coupling between the rotor and the stator (Qiao, Zhou, Aller, & Harley, 2008; Simon & Swarup, 2017). In a previous work, a crowbar was used to short-circuit an RSC to protect it from rotor circuit overcurrent during transient disturbances (Hansen, Jauch, Sørensen, Iov, & Blaabjerg, 2004; W. Li et al., 2018).

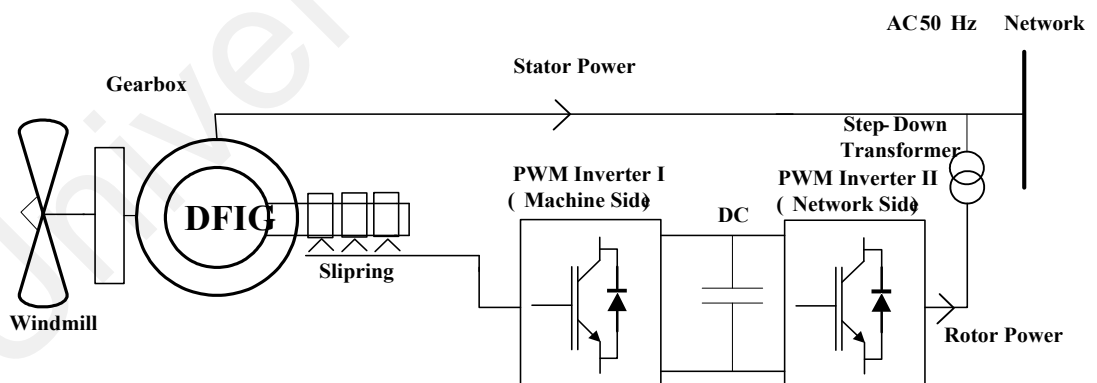


Figure 2.1 DFIG-equipped wind turbine (Lei et al., 2006) .

A similar mathematical model was deduced in (Fernandez, Saenz, & Jurado, 2006); also the permanent magnet synchronous generator (PMSG) depicted as a control current source was presented in (Baroudi, Dinavahi, & Knight, 2007). More recently, a review

on the design consideration of DFIG in wind energy system application was introduced in (Torkaman & Keyhani, 2018).

A reduced order model of DFIG wind turbine (WT) was considered by (Yuan, Yuan, & Hu, 2016), to study the control time scale of the DC voltage dynamics, in the event of severe distortion. The major assumption of the proposed model is to ignore the transient dynamics of the stator flux and the current control. A similar assumption was made by (J. Hu, Yuan, & Yuan, 2017) during which the transient dynamics of the inductor currents, rotor and stator fluxes were ignored, when modelling the DFIG-based WT for small signal stability analysis in the DC-link voltage control (DVC) timescale.

To incorporate the generator models developed above into the standard ones when the latter are used as synchronous generators, an assumption of the idea was adopted by (Hughes, Anaya-Lara, Jenkins, & Strbac, 2005), which showed that the stator transients are fast enough to be considered instantaneous. For the transient and dynamic analyses of mixed generation networks, the models were simplified when integrated into the simulation.

2.1.1.2 Wind Turbine Transient Model

A variable-speed wind turbine model with a DFIG for transient stability analysis was developed by (Ledesma & Usaola, 2005); it includes the mathematical descriptions of mechanical coupling, wind torque, DC link and voltage and speed control systems. The model was assumed based on the current control in both power electronic inverters, which can be perceived as instantaneous from the transient stability perspective. The proposed wind turbine model with a DFIG was incorporated into the transient stability program power system tool. The transient stability of wind turbines equipped with DFIG at an external short circuit fault was discussed by (Muyeen et al., 2006).

2.1.1.3 Circuit Breaker Transient Models

The SF₆ circuit breaker model, which was developed for the transient examination of WPPs, is composed of two resistors connected in series and integrates Cassie's and Mayr's dynamic arc models, as shown in equation (2.1) and (2.2) (CIGRE, 1990).

1. Cassie's transient model:

$$\frac{1}{g_c} \frac{dg_m}{dt} = \frac{1}{\tau_c} \left(\frac{v^2}{V_0^2} - 1 \right) \quad (2.1)$$

Where g_c is the Cassie arc conductance, v is the arc voltage, τ_c is the Cassie time constant and V_0 is the arc voltage coefficient.

2. Mayr's transient model:

$$\frac{1}{g_m} \frac{dg_m}{dt} = \frac{1}{\tau_m} \left(\frac{vi}{P_o} - 1 \right) \quad (2.2)$$

Where g_m is the Mayr arc conductance, v is the arc voltage, i is the arc current, τ_m is the Mayr time constant and P_o represents the steady-state power losses (cooling power). PSCAD/EMTDC simulation case studies were implemented using the test circuit shown in Figure 2.2 to validate the merged models of Cassie and Mayr. The disruption of a short-line fault on a 130-kV Sulphur hexafluoride (SF₆) circuit breaker was simulated using a test setup (Bizjak, Zunko, & Povh, 1995).

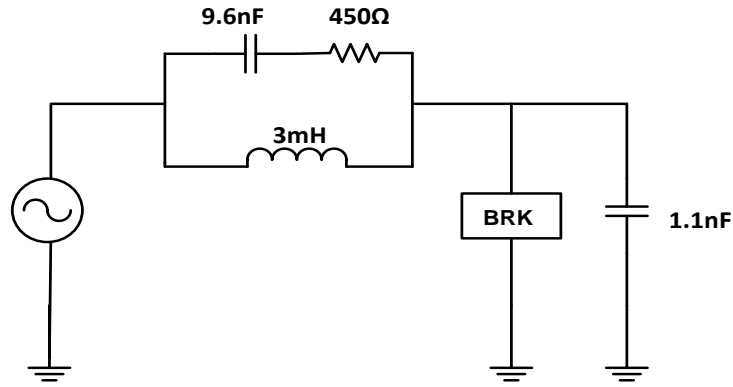


Figure 2.2: Transient model performance during disruption of a short-line fault using the SF₆ test circuit breaker (BRK) (CIGRE, 1990).

In practice, nearly all transient over-voltages are normally deposited on the transformer and not on the machines (Badrzadeh, Gupta, et al., 2012). The individual transient model components treated were the vacuum and SF₆ circuit breakers, three- and quadruple-core cables, turbine generators, power transformers and surge arresters.

2.1.2 Transient Analysis in WECS

An approach to analyse the complex transient trends and dynamic characteristics of a DFIG meticulously during a voltage dip was proposed by (El-Moursi, Bak-Jensen, & Abdel-Rahman, 2010; Lopes, Hatziargyriou, Mutale, Djapic, & Jenkins, 2007) (Kayikci & Milanovic, 2008); this work utilized a built-in DFIG model in which the effect of several prototype parameters and simplifications (for mechanical and electrical subsystems) on the DFIG-based wind power transient responses was demonstrated and investigated.

Transient analysis of a power system with increased DG penetration was studied by (Datta et al., 2018), the beneficial and detrimental impact associated with the increased penetration was observed to be dependent on the location of DG installation and the type. The penetration is characterized with phasing out of the existing traditional generators

and the general effect on the system inertia. The DFIG wind turbine model was introduced by (D. Zhu et al., 2016), and the associated transient electromotive force (EMF) characteristics under grid fault conditions were derived. In a grid fault occurrence, the stator flux usually contains negative-sequence components and transients, which stimulate the large EMF in the rotor circuit. The DFIG equivalent circuit from the rotor side is presented in Figure 2.3.

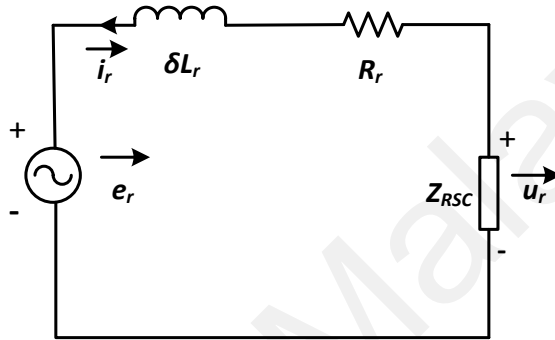


Figure 2.3: Equivalent circuit of DFIG viewed from the rotor side (D. Zhu et al., 2016)

Ignoring stator resistance xR_s , EMF under normal conditions can be expressed as in equation (2.3):

$$\vec{e}_r = \frac{L_m}{L_s} \frac{d}{dt} \vec{\psi}_s^r = \frac{L_m}{L_s} s U_{SN} e^{j\omega_s t} \quad (2.3)$$

where U_{SN} is the rated stator voltage, ω_s is the stator angular frequency, L_m is the magnetizing inductance, L_s is the stator self-inductance and s is the slip. Equation (2.3) further indicates that when a transient fault occurs, the stator flux contains transient components that can be expressed as in equation (2.4):

$$\vec{\psi}_s^s = \frac{(1-p)U_{SN}}{j\omega_s} e^{j\omega_s t} + \frac{pU_{SN}}{j\omega_s} e^{-t/\tau_s} \quad (2.4)$$

where p is the depth of the grid voltage dip, $\tau_s = L_s/R_s$ is the time constant of the stator flux, $\vec{\psi}_s^r$ and $\vec{\psi}_s^s$ are the stator fluxes and the superscripts r and s denote the rotor and stator reference frame.

Additionally, (Flannery & Venkataramanan, 2008) recommended removing the “missing” positive sequence part of the stator flux after conducting a uniform-speed transient evaluation of the overall stator flux and rotor EMF. The transient characteristics of a wind turbine mounted on a DFIG were studied by (L. Wang et al., 2015) through a generic approach, considering the applied voltages due to the RSC at the rotor windings during symmetrical voltage faults.(Abdelemam, El-Rifaie, & Moussa, 2017). The transient state behaviour of DFIG was simulated by(Abdelemam et al., 2017), and its characteristics in symmetrical and asymmetrical short circuit including short circuit within the internal windings.

Conventional Fourier transform is ineffective and inaccurate in fault detection because the DFIG runs predominantly under a transient state, whereas Fourier transform is more indicative in harmonics analysis since the basic functions (the sines and cosines) waveforms are periodic in nature (García, Segundo, Rodríguez-Hernández, Campos-Amezcu, & Jaramillo, 2018). The basic method for exploiting the generator transient response during excitation was presented by (Stojčić et al., 2014). The switching transient of a rotor-side inverter can usually develop a fault detection mechanism for sensing the fault generated by machine asymmetries and estimating the transient leakage inductance.

The authors (Hashemi & Sanaye-Pasand, 2018) addressed the transient stability and the out-of-step (OOS) event in the inverter interface synchronous generators (IISG). The distinction between the development of OOS in IISG and the conventional generators is expounded based on the equal area criterion (EAC). Although, EAC was observed to be

ineffectual in transient stability evaluation of power systems. The detrimental impact associated with the surge in the incursion of PMSG-based wind turbines on power system transient stability was investigated by (Zhongyi Liu, Liu, Li, Liu, & Liu, 2015), and using the extended equal area criterion theory (EEAC), the strong correlation between the power system transient stability and the PMSG integration was also determined.

A complete research on transient and dynamic behaviour of the DFIGs, working under balance and unbalanced grid voltage dips, was presented by (Alsmadi et al., 2018) (J. Liu et al., 2018). The analysis also proved that the DC component generated in the magnetic flux is a result of sudden change in the stator voltage, which is thought to be a transient recovery. The transient performance of a WPP was assessed by (Badrzadeh, Zamastil, et al., 2012) to validate the restrike and prestrike operations of a vacuum circuit breaker (VCB) with a windmill switch gear, as shown in Figure 2.4. Case studies were simulated using the simulation software PSCAD/EMTDC.

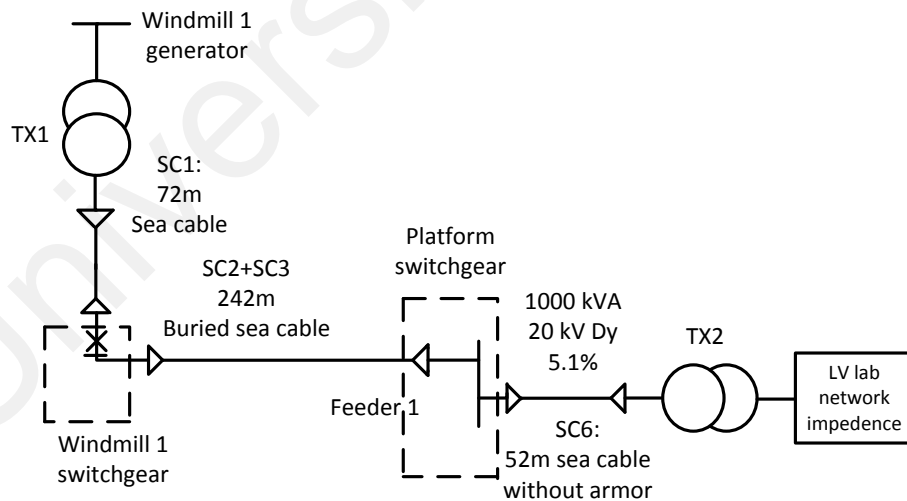


Figure 2.4: Single-line diagram representation of ASEA Brown Boveri (ABB) wind cable laboratory (CIGRE, 1990).

The case study introduced by (Badrzadeh, Gupta, et al., 2012) from the General Swedish Electrical Limited Company (ASEA), analysed several features related to the transient characteristics of the collector grid, which include the following (CIGRE, 1990):

1. maximum voltage,
2. rate at which the voltage rises,
3. oscillation frequencies at each closing of the restrike or prestrike period,
4. breaker maximum current,
5. traveling time of the cables and
6. the relationship of the voltage to the current.

In all the cases, the operational time of the breaker was fine-tuned to obtain and match the equivalent points on the voltage waveform, as demonstrated by (Breder, 2009). The measurement and simulation were qualitatively and quantitatively compared.

A dynamic analysis of an improved transient model of a single-phase induction generator was introduced by (Lamabadu & Rajakaruna, 2017) and fitted for renewable energy conversion. The Runge–Kutta technique was used to calculate the dynamic performance. Given the operational parameters and defined initial values, the nonlinear differential equations were solved using the ode45 function in MATLAB (Version, Company, City, State abbrev if USA or Canada, Country). to obtain the system parameters.

2.1.2.1 Transient Stability Analysis in WECS

TSI is widely used to assess the transient stability in a wind turbine employing the DFIG generators, after the occurrence of disturbance, during which the rotor angle of the machine with respect to a synchronously-rotating reference was used as a variable in evaluating system stability. The TSI was derived from the transient security assessment tool (TSAT) in equation (2.5), which computes the index according to the algorithm of the margin angle (Gautam et al., 2009; D.-Y. Li, Li, Cai, Song, & Chen, 2018), as shown in the following:

$$TSI = \frac{360 - \delta_{max}}{360 + \delta_{max}} \times 10 \quad -100 < TSI < 100 \quad (2.5)$$

where δ_{max} is the maximum angle of departure between two generators, one working concurrently in the system and the other after the fault response. $TSI \leq 0$ and $TSI > 0$ correspond to unstable and stable conditions, respectively.

A substantial number of wind turbine generators is expected to be integrated in existing utility grids in the coming years (Muyeen et al., 2007) Therefore, the transient stability of power systems that are distinctive from wind turbine generator systems (WTGS) should be studied (Muyeen et al., 2006). Furthermore, a wind turbine system that consists of a one-mass or lumped model cannot be used to examine the transient behaviour of a WTGS because of the paucity of detailed technical information.

For an accurate transient analysis of WTGSs, a six-mass drive train model is recommended. During its implementation, unequal torque distribution does not alter the transient stability of the WTGS, which provides an impetus to consider reduced-order three-mass and two-mass models. In the case of the transient stability of a WTGS, simulating every wind turbine is tedious. The stability analysis and energy storage-based solution of wind farm in the event of LVRT was presented by (J. Liu et al., 2018). The electromagnetic transient simulation validates that the frequency of current injected by the wind turbines can be retaining to rated frequency after the voltage dip.

$$J_{\omega t} = \sum_{i=1}^P J_{\omega ti}; J_{gb} = \sum_{i=1}^P J_{gbi}; J_g = \sum_{i=1}^P J_{gi}; K = \sum_{i=1}^P K_i. \quad (2.6)$$

Each wind turbine number is denoted as i_s ; P is the total number of wind turbines; $J_{\omega t}$, J_{gb} and J_g are the wind turbine, gearbox and generator inertial moments. For transient stability assessment, balanced three lines-to-ground faults (3LG) were deliberated. Several non-symmetrical faults, namely double line-to-ground fault (2LG, Lines a and b), double line-to-line fault (2LS, between Lines a and b) and single line-to-

ground fault (1LG, Line a), were also studied. PSCAD/EMTDC was used to implement the simulation. Tables 2.1 and 2.2 summarize the results by considering the damping on the one hand and ignoring it on the other, where S and U denote the steady and unsteady situations of the WTGS, respectively. In all the cases, the two-mass shaft models provided similar transient responses as the three-mass and six-mass drive train models.

Table 2.1: Results of the transient stability of two-mass, three-mass and six-mass models (ignoring all types of damping) (Muyeen et al., 2007). S, steady; U, unsteady.

Induction Generator Power (MW)	1LG Fault			2LS Fault			2LG Fault			3LG Fault		
	2M	3M	6M									
50	S	S	S	S	S	S	U	U	U	U	U	U
44	S	S	S	S	S	S	U	U	U	U	U	U
43	S	S	S	S	S	S	S	S	S	U	U	U
40	S	S	S	S	S	S	S	S	S	U	U	U
39	S	S	S	S	S	S	S	S	S	S	S	S

Table 2.2: Results of the transient stability of two-mass, three-mass and six-mass models (considering all types of damping) (Muyeen et al., 2007).

Induction Generator Power (MW)	1LG Fault			2LS Fault			2LG Fault			3LG Fault		
	2M	3M	6M									
50	S	S	S	S	S	S	S	S	S	S	S	S

A hypothetical assessment of the dynamic and transient characteristics of fixed-speed wind turbine (FSWT), wind speed variations and severe voltage dips was demonstrated by (Rahimi & Parniani, 2009) (Lorenzo-Bonache, Honrubia-Escribano, Jiménez-Buendía, Molina-García, & Gómez-Lázaro, 2017). Modal and sensitivity analyses were employed with the participating factors, and then, eigenvalue tracking was applied to classify and examine the behaviour of transient instability, together with the system variables involved in the trend of instability.

To depict the FSWT's transient performance, analysis was complemented with time simulation, and an eigenvalue tracking technique was implemented by (Potamianakis & Vournas, 2006; Sahni et al., 2012; L. Wang et al., 2015). In this technique, the system was iteratively linearized by the development of the state Jacobian matrix at specific time intervals during the simulation; the eigenvalues were calculated at each snapshot. The single-machine infinite bus (SMIB) system shown in Figure 2.5 was used to study the transient stability with FSWT parameters, where the system investigated the behaviour of transient stability. A balanced three-phase fault was foisted on the infinite bus terminal at 10 s for 200 ms.

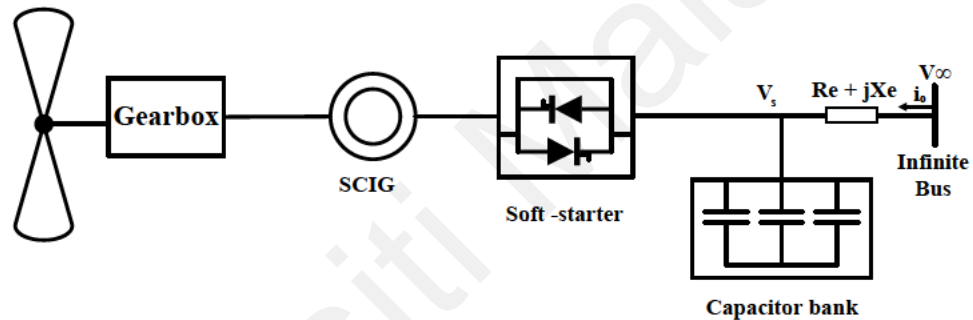


Figure 2.5: Fixed-speed wind turbine (FSWT) attached to the infinite bus (Rahimi & Parniani, 2009).

The simulation result showed that the transient behaviour of the FSWT was unstable. Eigenvalue tracking, and online linearization showed that all electrical modes remained stable after fault clearing, but the FSWT lost its equilibrium when the monotonic mechanical modes approached the unstable state. The observed eigenvalue resembled a monotonic mode. The oscillatory mechanical mode is another critical mode and approaches instability under transient states. (Rahimi & Parniani, 2009).

The obtained result indicated that the multi-mass mechanical dynamics and single-mass model of the WT rotor were the governing kinetics, for dynamic transient analysis in the FSWT. These factors were insufficient because their dynamic and transient

investigation yielded misleading information about stability. However, from the transient stability perspective, the wind turbine drive train must be modelled using two-mass representation to enable the simulation of the torsional oscillations initiated within the drive train system during grid fault (Hansen & Michalke, 2007).

A DFIG-based wind turbine model was designed by (W. Tang, Hu, Chang, Yuan, & Liu, 2018), using the time scale of the rotor speed control, to examine the transient response of the generator. The effect of the unique behaviour on the transient stability of the DFIG-controlled SMIB system was evaluated. To further appreciate the transient response and to test the stability of the DFIG-based WT, the magnitude and phase model of the DFIG-based WT is suggested from the internal voltage vector viewpoint and the application of the rotor speed control time scale. The transient energy function (TEF) of the SMIB system was employed to compare the transient stability of the DFIG-WT, with the conventional synchronous generator (SG).

The penetration of DFIG-based WTG in the utility grid is limited by network transients because it complicates and increases the order of the general model of the system, restricts the size of the scheme and increases computational burden. Therefore, a third-order machine model should be adopted for transient stability analysis because the simplification of the generator model does not significantly alter the DFIG transient response of DFIG. WECS simulation for transient stability analysis in the power system is performed by using the EMT program PSCAD/EMTDC. Table 2.3 summarizes several analysis and modelling methodologies.

Table 2.3: Transient stability evaluations techniques in various WECS applications. IISG, inverter interface synchronous generator.

Subject	Technique/Concept	WECS Part	Ref. No.
Transient Analysis	Single Machine Infinite Bus (SMIB)	DFIG	(W. Tang et al., 2018)
	Transient Stability Index (TSI)	DFIG	(Gautam et al., 2009)
	Transient Security Assessment Tool (TSAT)	DFIG	(D.-Y. Li et al., 2018)
	Critical Clearing Time (CCT)	DFIG	(Tajdinian et al., 2018)
	Eigen Value Tracking	FSWT	(Potamianakis & Vournas, 2006)
	Online approximation		
	Runge Kutta Method	IG	(Lamabadu & Rajakaruna, 2017)
	Equal Area Criterion (EAC) Theory	IISG	(Hashemi & Sanaye-Pasand, 2018)
	Extended Equal Area Criterion Theory (EEAC)	PMSG	(Zhongyi Liu et al., 2015)
	Space Phasor and Asymmetry Phasor Approximation	DFIG	(Stojčić et al., 2014)
Modelling Methodologies	Two-masses or three mass	Windmill	(Muyeen et al., 2007)
	Six-mass drive train model	Windmill	(Muyeen et al., 2006)
	Wound rotor asynchronous machine	DFIG	(Junyent-Ferré, Gomis-Bellmunt, Sumper, Sala, & Mata, 2010)
	Controlled Current Source	PMSG	(Baroudi et al., 2007)
	π or T Network Models	Transmission lines	(Junyent-Ferré et al., 2010)
	IGBT Switches with parasitic capacitance	Converter	(M. Jin & Weiming, 2006)
	SF_6 Cassie's/Mayr's Model	Circuit Breaker	(Bizjak et al., 1995)

2.1.3 Methods for Mitigation and Control of Transients in Wind Turbine Generators

The possibility of damping transients within the power system utility under any disturbance, such as voltage fluctuations, was indicated by (Yassine Amirat, Benbouzid, Al-Ahmar, Bensaker, & Turri, 2009). WTG operations are nearly transient, and a nonstationary method should be applied to recognize faults. A secondary damping controller was embedded in the primary controller of a DFIG for the damping oscillations in the system that result from the rotor oscillations of the generator in various areas (Simon & Swarup, 2017). The sole purpose of the controller was to ensure the suppression of new oscillation modes that might be introduced by the DFIG using a wide area measurement system. The damping control scheme was executed in the software presented by (Rebello, Vanfretti, & Almas, 2015).

A control approach that uses STATCOM for reducing and suppressing distortions in a power system was implemented by (El-Moursi et al., 2010); the method offered substantial improvement in the transient stability margin of a wind park. The latest application of the STATCOM-based mitigation method was introduced by (Mosaad, 2018) by proposing a model reference adaptive controller (MRAC) for facilitating the addition of WECS, when the working condition of the grid was characterized with anomaly and taking into account the low-voltage ride-through (LVRT). In a similar development (Gontijo et al., 2018) presented a robust Model Predictive Rotor Current Control (MPRCC) of a DFIG, driven by a direct matrix converter. The result presented highlight improved performance of the model, during transient moments caused by changes in the wind speed.

2.1.3.1 Transient Control Techniques in WECS

A feed-forward transient compensation (FFTC) control system with a proportional-integral-resonant regulator was introduced by (J. Liang, Howard, Restrepo, & Harley, 2013), and various remedies to satisfy low-voltage ride-through conditions were adopted by implementing the control techniques for RSC. Some of these techniques focus on enhancing the transient response of the control scheme with an equal reference current in the rotor as a typical vector control. For example, FFTC control methods were used to limit transient rotor currents. Transient mitigation terms and parameters are applied on the current, power and input of feed-forward control loops to facilitate transient current control.

The proposed FFTC control framework is depicted in Figure 2.6 in which two functional blocks are inserted in the conventional vector control scheme. d and q transient rotors and back EMF voltages were feed-forward-compensated in the planned FFTC control system. Therefore, the small slowly-varying error in the PLL angle that only affected the decomposition of d-q did not reduce the transient responses. In the study, PLL was designed to block the negative sequence components.

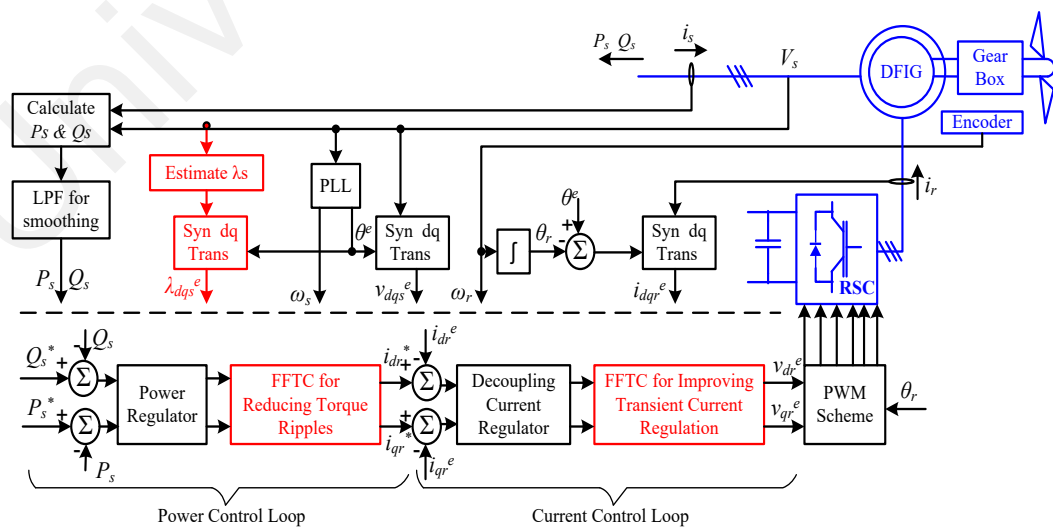


Figure 2.6: Feed-forward transient compensation (FFTC) structural scheme for DFIG with additional computation (in red) for FFTC implementation. RSC, rotor-side converter (J. Liang et al., 2013).

By contrast, (Simoes & Farret, 2007) reported that the feed-forward power signal from an induction generator via the DC voltage loop inhibited the transient spikes of the link voltage. The relationship between the maximum power point-tracking (MPPT) speed and the transient load of a direct-drive PMSG-based variable-speed wind turbine was investigated by (J. Chen, Chen, & Gong, 2014); the higher the MPPT speed, the larger the ripple (produced by the torque and described as transient load) the turbine shaft could receive. The previously mentioned contribution showed that the usual difficulty encountered in settling the transient load and MPPT speed can be resolved by enhancing the bandwidth of the MPPT control scheme, which is shown in Figure 2.7.

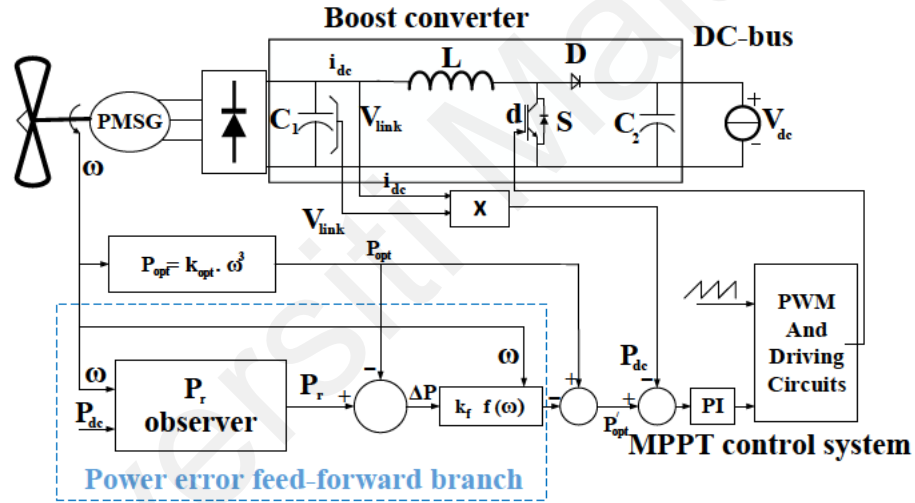


Figure 2.7: Control scheme for direct-drive PMSG-based wind turbine with adaptive-speed (J. Chen et al., 2014).

The application of the closed-loop transfer function by shaft torque in terms of rotor speed is an appropriate method for expressing real transient load. Thus, equation (2.7), which is derived from the equivalent circuit, can be considered a representation of the real transient load. This equation depicts the effect on real transient load.

$$\left| \frac{\delta P_{dc}}{\delta \omega} \right|_q = J\omega Q = \frac{J\lambda_{opt} \ln \varepsilon}{RK_0} = \frac{1}{T_\varepsilon} + \frac{J\lambda_{opt} K_1}{RK_0} \quad (2.7)$$

In addition, the connection between MPPT speed and the transient load acting on the turbine shaft is described using Equation (2.7), where λ_{opt} is the optimal tip speed value of the wind turbine; J is the overall moment of inertia of the scheme in (kg/m^2); P_{dc} is the power generated by WECS in watts; ω is the rotor speed; Q is the steady state point, where $\varepsilon = \frac{\Delta P_\varepsilon}{2|\Delta P_0|}$ and $\Delta P_0 = 3$, $\varepsilon = 5\%$; R is the radius of the turbine in meters; T_ε is the time for convergence in seconds; $T_\varepsilon = \frac{1}{A} \ln(\varepsilon)$ and $K_1 = \frac{-K\omega^2}{JR_s} - \frac{K_t\alpha_0 R^2}{J\lambda_{opt}^2}$, where $\alpha_0 = -0.312$; and K_0 is a constant.

A predictive torque control (PTC) was applied by (Bayhan, Kakosimos, & Rivera, 2018) to achieve very fast transient responses in a brushless doubly-fed induction generator (BDFIG) with a matrix converter. The PTC approach for the combination of BDFIG and the matrix converter was proposed due to its advantage of yielding high power density and being robust to mechanical associated faults. A bridge-type fault current limiter (BFCL) was recently introduced by (Alam & Abido, 2018) for boosting the resistance of the PMSG employed in bulk wind power generation to fault occurrence, while undertaking loads. Another modified version of fault current limiter was proposed by (Firouzi & Gharehpetian, 2017), in which the traditional inductive (BFCL) was replaced with the capacitive (BFCL) to enhance the transient performance of the DFIG-based wind farms during the LVRT. The technique was also characterized with the natural compensation for the required reactive power.

In another case, the power hardware in the loop (PHIL) trial was performed by (Gururaj & Padhy, 2018) to examine the transient characteristics in case of fault occurrence prior to the fault current limiter (FCL), with regard to the DFIG system. The study of fault current of Type-3 WTs was carried out by (Y. Chang, Hu, Tang, & Song, 2018) to estimate the transient and steady-state equivalent circuits of Type-3 WT by

taking in to account the switching sequence of the internal circuits for protection and control in multiple time scales, during LVRT.

Another robust control scheme for a dual three-phase PMSG was adopted by (Abdelsalam, Adam, & Williams, 2016) by introducing a speed controller that commands the generator to operate at the maximum speed, but with the least amount of transients under various wind speed conditions. It was demonstrated by (B. Yang et al., 2018) that passivity-based linear feedback control (PBLFC) enhances the transient responses of PMSG-based WECS. Linear feedback control was applied to ensure the required convergence of error tracking. However, It has been observed by (Geng, Liu, & Li, 2018) that during transient fault in PMSG, the orientation of the phase angle cannot precisely track the angle of the voltage vector. Therefore, better synchronization and reactive power support are required for low-voltage ride-through (LVRT).

An adaptive controller for WECS with undetermined system dynamics was proposed by (Meng et al., 2013), in which transient stability and the steady state were achieved after quantitative examination. The controllers could outline the tracking errors by employing novel error transformation methods to ensure subjective transient and steady-state operation, including steady-state error, convergence rate and maximum overshoot. The wind speed approximation based on a sensor-less control system controlled the WTG under large transient disturbances efficiently and precisely. Another robust adaptive fault-tolerant control methodology was realized by (D.-Y. Li et al., 2018) based on the application of the barrier Lyapunov function to trace the required power signal of each wind turbine with assurance in its transient performance and high immunity to the actuator faults.

A fault-tolerant controller for WECS was designed and developed by (X. Wang & Shen, 2018), using the sliding mode observer (SMO) and by the application of the

multiple fault reconstruction technique. The issue of the fault-tolerant controller arises usually when several faults (transients) are observed in WECS. A grid-voltage-oriented sliding mode control for DFIG was studied by (Villanueva, Rosales, Ponce, & Molina, 2018). This control technique has the advantage of requiring no further modification, able to track torque and stator reactive power even during grid disturbances. Nonetheless, the natural stator flux component may be affected. Hence, a transient demagnetizing reference is needed to be incorporated to the original system, to eliminate the natural flux component. This will facilitate the FRT capability of the controller.

A supervisory controller for developing resistance to fault, owing to lubrication breakdown in the gearbox mechanism of a wind energy system, was composed by (Hosseinzadeh & Rajaei Salmasi, 2016). This control formulation maintains the output power of the wind scheme, at its assumed value, and prevents potential converter failure. In a similar case, an effective fault detection mechanism, in a wind energy system to address the issue of lubricant system failure, was developed by (Hosseinzadeh & Salmasi, 2016). A faulty lubrication system has a negative impact on the transmission efficiency of the gear box and, consequently, could upset the transient stability of the system. The rotation of the wind turbine in a system under transient fault was analysed, in the latest issued grid connection requirement of the Norwegian power system, as wind turbines are required to withstand transient faults. This process should be implemented to avoid substantial generation loss under harmless transient faults. Otherwise, this grid codes should be followed (Jauch, Sørensen, Norheim, & Rasmussen, 2007).

Variable-band vector-based hysteresis current regulators (VBHCR) were developed by (Mohseni & Islam, 2012) to overcome the limitations of several current regulators, such as the sluggish transient response of proportional integral (PI) current regulators, which adversely affects the immunity of DFIGs in the event of fault. To tackle the

shortcomings of PI current regulators, RSC and grid side converter (GSC) were substituted with VBHCR to meet the newly-issued Australian Grid Code requirements for the transient response of large WPPs. The working conditions and execution of this current regulator in a DFIG-based WPP were thoroughly studied by (Mohseni, Islam, & Masoum, 2011). Results from an extensive simulation were also presented, indicating the remarkable transient and steady-state performance of the suggested VBHCR under various regular and fault working conditions.

A schematic representation and realization of the suggested VBHCR in the RSC of DFIG is shown in Figure 2.8. For this current regulator, the tracking errors of the x- and y-components were treated by four- and three-level hysteresis comparators, respectively. D_x and D_y are the digital outputs that are fed to an uncomplicated switching table that decides the RSC output voltage vector at each instant. The proposed current regulator has built-in current-limiting characteristics and rapid transient responses (Kazmierkowski & Malesani, 1998).

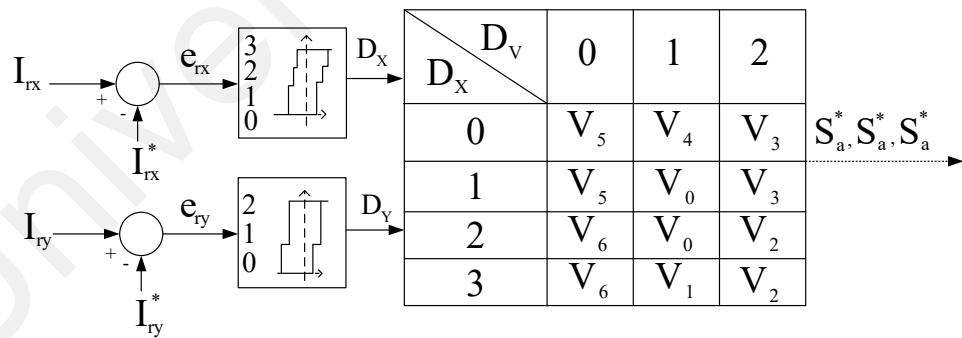


Figure 2.8: Variable-band vector-based hysteresis current regulator (VBHCR) employed in RSC control structure representation (Mohseni et al., 2011)

A control technique for the improvement of transient stability in a system of wind energy employing DFIG was reported by (Zheng, Ouyang, Xiong, Xiao, & Li, 2018) by exploiting the power constraints of the generator. As observed in WECS, the GSC most often runs on the course of the unity power factor and delivers reactive power during the

reactive power, when the orientation of the d-axis is tilting towards the grid voltage as the RSC. The transient power of GSC is expressed in equation (2.8).

$$\begin{cases} P_{Dg} = U_{Ds} i^* D_{gd} \\ Q_{Dg} = -U_{Ds} i^* D_{gq} \end{cases} \quad (2.8)$$

Where $i^* D_{gd}$ is the d-axis reference of the grid current, $i^* D_{gq}$ is the q-axis references of the grid current and U_{Ds} is the magnitude of the stator voltage. The active power from the rotor side drifted to the GSC, then the rotor active power would be equal to the grid active power, that is $P_{Dr} = P_{Dg}$, neglecting the losses in the rotor and stator. The references were applied to manage the transient currents of the DFIG.

A common behavioural methodology for representing the turn-on and turn-off dynamics was studied by (Mohan, Undeland, & Robbins, 2003). A faster and effective control approach in a WECS, employing a full-bridge inverter, was proposed by (E.-C. Chang, 2018) and was observed to enhance the transient and steady-state performance. The proposed control strategy comprises the sliding-mode guidance law (SMGL) and a Fourier nonlinear grey Bernoulli model (FNGBM). In (Duong, Grimaccia, Leva, Mussetta, & Le, 2016), a control method based on fuzzy PI was implemented for controlling the IGBT to facilitate transient stability. The efficiency of a “transistor-based frequency converter employing a reduced order control system” was validated by (May, Sergey, & Ilya), by the use of original transient switches, that is trimming the total number of power supplies in the control scheme.

The researchers (Yang-Wu et al., 2015) discovered that the DFIG regulation capacity of active power is usually uncertain because it strongly depends on its low-voltage ride-through capacity. Thus, a DFIG retrofitted with a super conducting magnetic energy storage has been recommended for voltage frequency support. In this application, the

power reference that enables the speed to track the required speed reference is calculated using Equation (2.9).

$$p_{\omega}^* = k_p(\omega_e^* - \omega_c) + KI \int (\omega_e^* - \omega_c) dt \quad (2.9)$$

Where ω_c is the rotational speed, ω_e^* denotes the reference speed, p_{ω}^* represents the reference power and K_p and K_I are the model constants for the PI controller that must be used to achieve the following:

1. fast recovery
2. speed variation of the transient for a limited period that enables a special type of generator to inject the required amount of active power to remedy the transient frequency deviations.

In other words, the surplus power supplied by the nonconventional/special machine throughout the frequency transient was gained from the stored energy within the inertia of rotating masses analogous to WECS. A recent advancement by (Y. Tang et al., 2017) was presented to expedite the inertial regulation when frequency perturbation occurs by implementing an extended system frequency response. Furthermore, in the latest advancement, the synthetic inertial control method for the DFIG, introduced by (J. Zhu et al., 2018), lithium-ion super capacitors were utilised to strengthen the DC bus in in the event of transient and to upgrade its transient/fault ride-through capability.

Different types of controllers were studied by (Duong, Leva, Mussetta, & Le, 2018) to determine the best in terms of improving the transient stability of DFIGs in the event of large grid distortions. Recently, an adaptive neuro-fuzzy-controlled flywheel storage scheme was studied to facilitate the transient stability in grid-tied wind farms further (Taj, Hasanien, Alolah, & Muyeen, 2015). Although, a hybrid controller employing both PI and a fuzzy logic controllers (FLC) introduced by (Duong, Grimaccia, Leva, Mussetta, &

Le, 2015) was seen to provide a more coherent technique to carry out transient stability on SCIG and has the advantage of requiring no extra equipment.

2.1.3.2 Transient Fault Protection Techniques on WECS

The modern topology of power electronics for wind turbines was investigated by (Z. Chen et al., 2009), where connecting the induction generators to short-lived power system-generated transients with high inrush current was learned. This condition upset the grid and caused high torque spikes in the drive train of the wind turbine, which was directly connected to the induction generator, and restricted the permissible number of wind turbines to be installed due to the level of transient disturbances introduced in the grid. Mechanical switch capacitors (MSC) are among the effective mitigation methods of transient and steady-state voltage control. MSCs are composed of a bank of shunt capacitors that are mechanically switched to supply reactive power compensation. The volume of each capacitor should be down-sized to prevent large transients of voltage.

Induction generators driven by wind are frequently exposed to power system transients during their working. Impulsive mechanical input power, which is mostly due to wind gusts, is considered one of the frequent occurrences of transients. This abrupt shift in input power can be represented as an incremental step in the input power. Voltage sag and short circuit are two common transients to which DFIG is susceptible. The transients of a DFIG due to external short circuit faults were evaluated by (Mohan et al., 2003). Voltage sag usually occurs due to short circuit in a remote bus or other generator terminals in a wind farm. The generator transient performance under the aforementioned conditions should be exactly forecasted for the appropriate selection, modelling and coordination of protective devices and for stability analysis (Jabr & Kar, 2007).

The authors (Shuai, He, Xiong, Lei, & Shen, 2018) surveyed the behaviour of the short-circuit fault of voltage source converter-based DC distribution systems, with

various dispersed generators. It was observed that, in the event of short-circuit fault, the bidirectional DC/DC converter and the DC link capacitors discharge a high transient current. The assessment was carried out by taking the three-phase short circuit measurement of the PMSG. For the ease of calculation, the d-axis sub-transient reactance was assumed equal to the q-axis sub-transient reactance, viz. $X_d = X_q$. The results obtained from (S. A. J. I. T. o. I. A. Saleh, 2017) demonstrated that in PMG the ω_r encountered transients, as a result of the capacitor step changes. It was observed that the reduction of C induces transients in ω_r , which created changes in the torque T_e .

In another case, the similarity of transient current was applied by (K. Jia et al., 2018) to formulate a protection scheme in wind farm transmission lines and also applied the indices of the correlation coefficient to compare the signals of the transient current on either end of the line span. Recently, (Liao, Zhu, & Wang, 2019) proposes a transient fault current similarity-based differential protection DP, in the interconnection of transformers employed in wind farms. This is because the conventional transformer DP protection misconstrue the internal faults as magnetizing currents, owing to the peculiarities of faults introduced by the LVRT techniques of DFIG-based wind farms. However, (W. Jin et al., 2019) enhances the protection system by applying a blocking scheme for collector power line using the amplitude ratio and phase difference.

The transient process of a WECS that simultaneously operates as a power generator and an active filter (AF) was explained by (Todeschini & Emanuel, 2011). The research was put forward to resolve the system response to two types of transient phenomena: wind variations (slow transients) and voltage dips (fast transients). The transient response of a WECS that executes the function of an AF operation under voltage dips or wind speed variations was investigated. The result of the experiment conducted on a DFIG system, as shown in Figure 2.9, was regarded as the first step to studying the transient response

of a WECS when employed as an AF. The stator terminals of the DFIG are coupled with the PCC via a feeder, which was modelled as equivalent resistance R_C and inductance L_C .

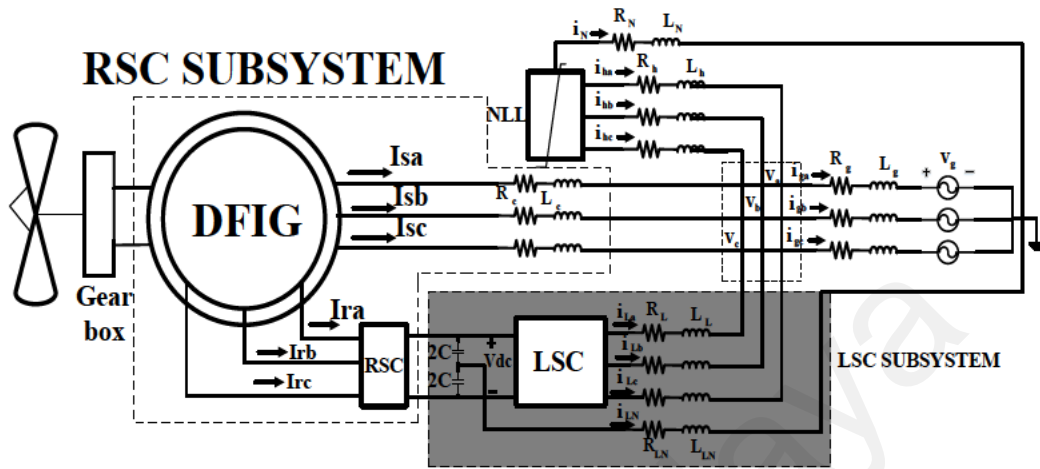


Figure 2.9: System configuration (Todeschini & Emanuel, 2011)

The applications of digital signal processing for detecting and diagnosing transient faults, in electrical power and renewable energy systems, was presented by (W. Liu, Zhang, Han, & Wang, 2012) using local mean decomposition and by (Taj et al., 2015) using the Morlet wavelet. However, Morlet wavelets finds application in sensing high-impedance fault (HIF) during transient disturbance and to discriminate (HIF) from ordinary switching transient due to non-fault events (S.-J. Huang & Hsieh, 1999). Artificial intelligence-based relays such as the ANN and fuzzy logic systems proposed by (Silva, Souza, & Brito, 2006), (De Souza, Meza, Schilling, & Do Coutto Filho, 2004), respectively. The application of artificial intelligence in the classification and detection of transient faults, in distributed generation, required the training of data and huge computational task, these factors are considered as drawbacks for their online implementation.

The wavelet transform breaks down the signal into only the low-pass components that constitute the approximations of the signal transform, while the wavelet packet transform (WPT) breaks down the transient signal into both the low-and high-pass components,

which constitute the details of the signal transform (Samantaray & Dash, 2007). The most efficacious diagnostic method in digital protection was discovered on the basis of sensing and categorizing the transient disruption that frequently occurs in distributed generation units (DGUs), that is the application of the phaselet packet transform, which was established and proposed by (S. A. Saleh, Ahshan, Abu-Khaizaran, Alsayid, & Rahman, 2014; S. A. Saleh et al., 2016). The method developed for sensing and categorizing transient disruptions determined the phases and magnitudes of the high-frequency content of the sub-band components presented in the d-q axis of the PCC currents.

A novel strategy for fault diagnostic and isolation (FDI) for wind turbines was introduced by (M. Li et al., 2018), using the deep long short-term memory (DLSTM), and the planned technique was observed to possess superior diagnostic performance, when compared with the conventional wind turbine FDI techniques. The DLSTM was implemented on the basis of the data-driven residual-based approach. This method can be applied to all types of wind turbines. In (T. Zhang, Wang, & Fu, 2018), three-channel filters were designed to tackle the difficulties encountered in FDI for the redundant inertial measurement unit. The presumed concept offered the ideal situation to facilitate the operation of the FDI system. This can find potential application in the aerodynamics of wind turbines.

A schematic of the laboratory configuration of (DFIG-based WECS) was employed in (S. Saleh, Meng, & Meng, 2016). The PCC current components of the d-q axis (adopted by the principal controller of each DGU) were applied on the inputs of the phaselet frame-based digital protection (S. A. Saleh, Richard, Onge, Meng, & Castillo-Guerra, 2018), and the output was a trip signal that retained a voltage of approximately 10 V in non-fault events. The trip signal was derived via a three-conduit opto-coupler driver circuit before it was guided through three TRIAC switches (S. A. Saleh et al., 2014). A new approach

for accurate fault classification in distributed generations was introduced by (Abdelgayed, Morsi, & Sidhu, 2017). In which optimal wavelet functions matching pursuit (OWFMP), based on particle swarm optimization technique was applied to identify the best wavelet function combination.

Some faults initiate high-frequency components in which transient phases generate nonzero output in one or more high-pass filters. A fault on opposite sides of the PCC can be sensed and classified as fault and non-fault events denoted by the relation in (2.10) (S. A. Saleh et al., 2018).

$$D_{dq}[f] = \begin{cases} 0 & \text{Nonfault} \\ \tau & \text{Fault} \end{cases} \quad (2.10)$$

Where $r \in R(\tau \neq 0)$, and vector $D_{dq}[f]$ is defined by Equation (2.11) as follows:

$$D_{dq}[f] = D_0[f] + D_1[f] + D_2[f] + D_3[f] + D_4[f] + D_5[f] \quad (2.11)$$

Another recent advancement in transient fault detection and diagnosis was introduced by (Yang-Wu et al., 2015) by applying a space vector-based index in a wound-rotor induction machine. The diagnosis was achieved by extracting signature information obtained from the product of the rotor current and rotor voltage space vectors, termed as diagnostic space vector \bar{D}_{SV} , which is a tool for diagnosing the rotor electrical fault operating under transient speed.

Table 2.4 summarizes various remedy approach in wind energy technology. In PMSG schemes, there is no transient power-angle features as in the typical synchronous generator or manifest any inertial tendencies toward the grid, i.e., inertia remain constant.

Table 2.4: Summary of various Control/Protection Techniques for Mitigating Transient Faults

Subject	Remedy Approach	Concept	Generator	Ref. No.
Control Scheme	Conventional Vector abc-dq Control	DSP/FCGA	DFIG/PMSG	(Kramer, Chakraborty, Kroposki, & Thomas, 2008)
	Variable band Vector-based Hysteresis Control	Tracking of Errors	DFIG	(Mohseni & Islam, 2012)
	Novel RSC Vector Control	Stator flux (d-q)	DFIG	(Alsmadi et al., 2018)
	NN Adaptive Controller	Novel error transformation	WT	(Meng et al., 2013)
	Adaptive Neuro-Fuzzy fly-wheel Controller	Fly-wheel storage	DFIG	(Taj et al., 2015)
	Modal Reference Adaptive Controller (MRAC)	SPWM	SEIG	(Mosaad, 2018)
	Adaptive fault-tolerant Controller	Barrier Lyapunov Function	WT	(D.-Y. Li et al., 2018)
	Fault-tolerant controller	Sliding mode observer (SMO)	DFIG	(X. Wang & Shen, 2018)
	Proportional & Inertial Control	Extended frequency response	DFIG	(Y. Tang et al., 2017)
	Hybrid (PI/Fuzzy) Controllers	Fuzzy logic technique	SCIG	(Duong et al., 2015)
	Sliding Mode Guidance Law Controller	Fourier nonlinear grey Bernoulli method	PMSG	(E.-C. Chang, 2018)
	Speed Controller		PMSG	(Abdelsalam et al., 2016)
	Passivity Based Linear Feedback Control (PBLFC)	Passivity Theory/FLC	PMSG	(B. Yang et al., 2018)
	Feed Forward Transient Compensation	Back E.M.F & Resonant Regulator	DFIG	(J. Liang et al., 2013)
	Secondary Damping Controller	Wide Area Measurement System (WAM)	DFIG	(Simon & Swarup, 2017)
	Predictive Torque Control (PTC)	Matrix Converter	BDFIG	(Bayhan et al., 2018)
	MPPT Control	Transient Load & Bandwidth	PMSG	(J. Chen et al., 2014)
	Bridge-type Fault Current Limiter	Real Time Hardware in Loop (RTHIL)	DFIG	(Alam & Abido, 2018)
	Supervisory Controller	Gearbox elements	All Except SG	(Hosseinzadeh & Salmasi, 2016)
Protection Measures	Mechanical Switch Capacitors	Bank of Shunt Capacitors	DFIG	(Z. Chen et al., 2009)

	Active Power Filtering	RLC	DFIG	(Todeschini & Emanuel, 2011)
	Three Channel Filters	Quantization		(T. Zhang et al., 2018)
	Digital Signal Processing (DSP) Relays	PPT, WPT, Travelling Wave Fault Locators (TWFL),	DGU interconnections & HVDC	(S. A. Saleh et al., 2014; S. A. Saleh et al., 2016) (Soeth, de Souza, Custódio, & Voloh, 2018)
	Artificial Intelligent-based relays	ANN & Fuzzy logic relays	DGU Interconnections	(Datta et al., 2018; Silva et al., 2006)
	Deep Long Short-Term Memory (DLSTM)	Residual Data-driven Method	Wind Turbines Generally	(M. Li et al., 2018)

2.2 Methods for Control and Detection of Faults in the Induction Motor Drives

Several faults in an induction motor can be anticipated during its healthy operational hours. Different types of faults, such as stator open or short winding, unbalanced stator, rotor eccentricities and broken rotor bars could lead to the grounding of the motor, if the fault is not detected beforehand. The parameters of the machine that are frequently been observed, are mostly the line current, vibration and leakage flux. However, line current is the most common and accessible parameter to be exploited for the fault occurrence assessment, especially in the industrial application of the induction motor. Recently, many researchers have put forward the prognosis and diagnosis techniques of an induction motor drives. Several algorithms and mathematical procedure have been proposed for the IM fault detection and localization.

Induction motors drives are extensively employed for industrial deployment owing to their robustness, occupying less space, low cost and maintenance. Vector control or field-oriented control of induction motor usually attained outstanding performance, thus it becomes the standard bearer of the industry. The latest trend in the research is to transform the motor to a fault tolerant drive. This has stirred a motivation in the study of more

sophisticated techniques of fault diagnosis in induction motors. The machine dysfunctional operation can be attributed to a fault in the motor such as stator interturn faults. The overall fault conditions in the scheme can be outlined as in Figure 2.10.

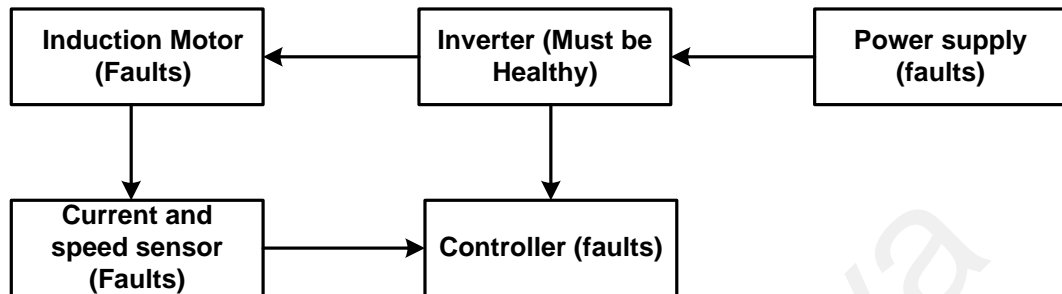


Figure 2.10 Fault-tolerant inverter-fed motor drives and the fault modes.

There are two types of fault diagnosis which are; cause effect diagnosis and effect cause diagnosis. The cause effect diagnosis is also termed as the dictionary-based diagnosis as it stores all the pre-evaluated failing responses of all the designs in a dictionary. An adaptive dictionary matching orthogonal matching pursuit was developed by (W. Huang, Sun, Luo, Wang, & Processing, 2019) for incipient fault feature extraction of the rolling elements in a bearing.

2.2.1 Induction Motor Faults

The squirrel cage type is used in more than 97% of the IMs (Y. Liu & Bazzi, 2017), while 3% of the IMs are wound rotor type. As explained ahead, there are various types of faults that may occur during the operation of the IM. In this work, the survey will be divided in two sections:

1. IM faults detection with the wavelet and
2. Fault tolerant control survey for inverter-fed motors.

Some of the inverter faults are listed here after.

2.2.1.1 Stator Opening, Shorting Phase Winding

The following are the frequencies of the stator faults: The fault diagnosis of the stator and the alternator inter turn in the electric machines was presented by (Salomon et al., 2019). The detection of the stator winding inter-turn shorts was presented by (J. Zhao, Guan, Li, Mou, & Chen, 2020). A unique diagnostic system was presented by (S. Wang, Xiang, Zhong, & Zhou, 2018), which was based on the hidden Markov models to detect the short circuit fault of the IM. The fault diagnosis was studied by (El Menzhi & Saad, 2013) (Glowacz & Glowacz, 2016), associated with the auxiliary winding using the spectral analysis. A neural network for the detection of online stator and rotor resistance in the sensorless vector control was presented by (Tarvirdilu-Asl et al., 2020) and (Omari et al., 2019). An analytical study of the negative effects on the stator winding faults was presented by (Dybkowski & Bednarz, 2019).

To detect the abnormal connection faults in the stator of the IM, the abilities of the signature graphical tools were demonstrated by (Cabal-Yepe, Fernandez-Jaramillo, Garcia-Perez, Romero-Troncoso, & Lozano-Garcia, 2015). The vibration faults were studied by (H. Liang, Chen, Liang, & Wang, 2018) in the stator winding based EMAM. In addition, a model of dual stator winding of induction machines was presented by (J. Tang, Chen, et al., 2020) for the stator and rotor faults diagnosis. A diagnosis of the inverter fed IMs was presented by (J. Tang, Yang, Chen, Qiu, & Liu, 2020) for the mechanical faults in the stator and rotor windings.

2.2.1.2 Shorted Rotor Winding

One of the best modeling techniques for the rotor faults occurring in the IM was introduced by (J. Tang, Chen, et al., 2020) and modelled the rotor faults based on the methodology of the winding function. Also revealed that rotor faults usually stem from congenital defects, owing to mechanical and thermal stresses are up to 10%. The

occurrence of rotor turn-to-turn faults in synchronous motors was studied by (Afrandideh, Haghjoo, Cruz, & Milasi, 2020) and noted that the shorted turns are mostly shunted, which eventually resulted in the diminishing number of the effective turns of the starting windings. Thus, a rotor turn-to-turn fault (RTTF) causes the starting current to build up and the consequence decrease of the reactive power at the output of the machine.

2.2.1.3 Broken Rotor Bar and Crack End Ring

These faults are caused by various factors such as vibrations and electromagnetic distortions created by the mechanical or magnetic effects. These may vary from thermal effects in some parts to fatigue (Yetgin, 2019).

(Delgado-Arredondo et al., 2015), conducted a comparative study between the internal diagnosis method based on the time-frequency decomposition technique, derived from the analytical studies and the external studies of the IM model such as, vibration analysis of stator current with a broken rotor bar fault. The impacts of the inter bars current were studied by (Gyftakis et al., 2015a), as it is the contributing factor behind the broken rotor bar faults. Axial stray sensor for the process monitoring of three-phase IM by means of orbital analysis was proposed by (Lamim Filho, Santos, Batista, & Baccarini, 2020), while a global online fault index was used by (Sun, Liu, Zheng, & Li, 2019) to do the fault diagnosis of the broken bars. Single and multi-fault diagnosis of variable frequency drive-fed IM, was introduced by (Ali, Shabbir, Zaman, & Liang, 2020). The broken bar diagnosis was presented by (Abd-el-Malek, Abdelsalam, Hassan, & Processing, 2017) by using the starting current analysis and Hilbert transform.

The voltage analysis modulation with the motor square current was used by (G. Singh, Naikan, & Processing, 2018) to detect the fault in the rotor bar. A new approach of using the multi-layer perceptron neural network for the detection broken bar was adopted by (Zolfaghari et al., 2018a) in accordance with the wavelet analysis and FFT application.

While (Monfared, Doroudi, Darvishi, electrical, & engineering, 2019) used the continuous wavelet transform for the identification of the broken rotor bar of squirrel cage IM. The stator current envelope effect was used by (Abd-el-Malek et al., 2017) to detect the faults in the broken bar and stator short circuit. A fast and accurate of the online detection of broken bars of squirrel cage IM, using the stator current spectrum were investigated by (Samanta, Naha, Routray, Deb, & Processing, 2018).

2.2.2 Wavelet-Based Faults Diagnosis

In this section the methods of faults detection and diagnosis of the IM with wavelet will be discussed. The different faults including, air gap eccentricity, gear box and bearing faults, stator opening or shorting phase winding, shorted rotor field winding, broken rotor bar and shaft bent are considered.

The fault diagnosis using the wavelet technique is an active area in this field. These techniques allow the extraction of data within the time and frequency domain. A review of the machine diagnosis with conditions based on the prognostic maintenance approach was presented by (S. Kumar et al., 2019). There are two main levels in the fault diagnosis:

1. Classic control-based fault diagnosis.
2. Measurement based fault diagnosis.

Figure 2.11 shows the percentages of different faults in an IM such as bearing, stator winding, miscellaneous, rotor faults respectively. The wavelet-based fault diagnosis consists of; wavelet feature extraction module, fault decision module and feature cluster module. Faults are best indicated by a negative sequence current and impedance. The stator short circuit faults were detected through the Park's vector and MCSA.

The wavelet, however, has emerged as an attractive option through its multi resolution analysis and good time localization, which is able to counter the drawbacks such as; the assumption undertaken that the values of load, motor speed and stator fundamental frequency are constant, as done in the FFT technique.



Figure 2.11 IM faults percentages according to IEEE

Among different wavelet technique, the discrete wavelet transform is a favorable option, in which the mother wavelet is scaled to the power of 2 (S. Saleh & Ozkop, 2016b). The resolution issue apparent in this method were attempted to be solved by (G Strang & Truong Nguyen, 1996) through the CWT.

2.2.2.1 Gear Box and Bearing Faults

A novel fault diagnostic technique based on a signal processing technique called the empirical wavelet transform (EWT) was applied by (Deng, Zhang, Zhao, & Yang, 2018) to diagnose the bearing fault of a motor, which include the normal signal, outer race fault signal, inner race fault signal and rolling element fault signal. This technique shows better result when incorporated with Fuzzy entropy. A new time-frequency method for the detection and classification of ball bearing fault in induction motors was introduced by (Attoui et al., 2017). The bearing defect of induction motor was detected by (Y Amirat,

Benbouzid, Wang, Bacha, & Feld, 2018) based on the ensemble empirical mode decomposition approach in conjunction with a statistical tool.

A probabilistic frequency-domain discrete wavelet transform for improved identification of bearing faults in an induction motor was developed by (Ghods & Lee, 2016) . The authors developed their previously introduced method, frequency-domain discrete wavelet transform (FD-DWT), into a stochastic model. An approach to detects the incipient state bearing fault was presented by (Kompella, Mannam, Rayapudi, & Technology, 2016) during which stator current signature analysis was used with the aid of noise cancellation and DWT decomposition.

The severity of the fault was estimated by computing fault indexing parameter. (Roy, Mohanty, & Kumar, 2015), studied the multistage transmission gearbox in the place of conventional vibration monitoring done with frequency modulated signal.. A support vector machine (SVM) and Stockwell transform was presented by (M. Singh & Shaik, 2019) as a classifier to capture several features in both time and frequency domain. This was used in the diagnosis of the faulty rolling bearing of a three-phase induction motor.

A novel technique based on the combination of the wavelet and frequency spectral subtraction techniques was introduced by (Kompella, Rao, & Rao, 2018) for the detection of the bearing defect through the indexing of the fault factors in three-phase induction motor. The compound fault diagnosis of gearbox was tackled by (P. Liang et al., 2019) through the multi-label convolutional neural network wavelet transform. This technique offers the best feature extraction by the wavelet transform. An accurate classification of bearing fault in an induction motor was realized by (Shao et al., 2019) based on the multi-signal model of fault diagnosis with the aid of convolutional neural network, in which both the vibration and current signal were used. A timely bearing and

stator fault diagnostic procedure of a single-phase induction motor was put forward by (Glowacz, Glowacz, Glowacz, & Kozik, 2018) by the application of acoustic signal.

The authors employed an exclusive technique coded MSAF-20-MULTIEXPANDED, the adopted strategy was found to be affordable and non-invasive. However, the methodology was observed to be prone to the ambient noises. To manage the issue of timely rolling bearing fault diagnostic under intense environmental noise, a fault diagnostic technique was developed by (B. Chen et al., 2019) on the basis incorporation of Resonance-based sparse signal decomposition (RSSD) and wavelet transform (WT).

2.2.2.2 Stator Open and Short Winding Faults

An approach for conditioning monitoring of an induction motor, with finite element accuracy using hardware in loop system was devoted by (Sapena-Bañó et al., 2019) the technique was demonstrated using the static eccentricity fault but the same procedure can be applied to deduce the inductance matrix for other type of fault such as stator short-circuits. (H. Liang et al., 2018) conducted the software diagnosis and detection of the short inter turn and the open circuit of the stator winding in a sort of a three-phase PMSM using enhanced wavelet packet transform by employing both vibration and stator current signal.

A more efficient technique of capturing essential information from PMSM during stator short-circuit faults was demonstrated by (Minaz, 2020), using the one dimensional local binary patterns (1D-LBP) strategy, rather than the time-frequency analysis or frequency spectrum analysis . The phaselet-based technique was used by (S. Saleh & Ozkop, 2016c) in the detection of stator faults with wavelet. The d-q components were used in this paper for the line-to-line faults in the stator windings. The MCSA was used by (Guo & Liu, 2018) and (Yin & Hou, 2016) for the fault diagnosis of IM in a complex

industrial process, where the stator faults were classified with WT using the SVM. A stator fault analysis of three-phase induction motor based on information gathering and artificial neural network was presented by (Bazan et al., 2017).

2.2.2.3 Shorted Rotor Field Winding

The signature analysis of wavelet packets in conjunction with Fourier transform was employed by (Zolfaghari et al., 2018a) for the detection broken rotor bar faults in the IM's. A new technique was presented by (Ameid, Menacer, Talhaoui, & Azzoug, 2018), based on the DWT and energy eigen value in the detection and diagnosis of the broken rotor bar faults of a field oriented control of induction motor drive.

2.2.2.4 Broken Rotor Bar and Crack Ring

A new strategy for the identification of broken rotor bar fault, in induction motor using the duo of stationary wavelet packet transform (SWPT) and multiclass wavelet support vector machines (MWSVM), was proposed by (Keskes, Braham, & Lachiri, 2013). Although, the diagnostic procedure was achieved at a lower sampling rate, the SWPT shows good extraction performance of signature information. Various MSVM techniques were compared with a number of Kernel functions with respect to training, testing complexities. The classification outcome demonstrated that the wavelet Kernel function detects the fault with a higher accuracy. An enhanced cyclic modulation spectral analysis based on the continuous wavelet transform (CWT) was applied by (Zhen et al., 2019) for the diagnosis of broken rotor bar fault in an induction motor.

A novel algorithm based on the continuous Gaussian wavelet transform (CGWT) was proposed by (Monfared et al., 2019) to diagnose broken bar of an induction motor rotor, the approach proposes a supplementary index to suppress the spectral leakage effects and noises. (Luong & Wang, 2020) explored and developed a new synergistic analysis

technique to capture essential information from the vibration and current data to detect a broken rotor bar fault in an induction motor. The WPT decomposition and convolutional neural network was used by (G. Li, Deng, Wu, Chen, & Xu, 2020) in the detection of the bearing fault of the IM.

As an indicator of faults, which was used to obtain 1-D time-frequency coefficients from the vibrational signal. The continuous wavelet transform (CWT) and Hilbert Transform (HT) were applied by (Konar & Chattopadhyay, 2015) as signal processing tools for capturing essential information from vibrational signals as an approach for a multi-class fault diagnostic technique in induction motors. In a similar case (Zepeng Liu, Zhang, & Carrasco, 2020) used empirical wavelet thresholding technique to detect bearing fault in the blade of a wind turbine by analyzing the vibration signal.

Many researchers have studied the drawbacks that accompany the FFT when used for the detection of the broken rotor bars through the db40 as a mother function (da Costa, Kashiwagi, Mathias, & Processing, 2015). This prevented the low overlapping with the adjacent bands. A machine learning algorithm is proposed by (Arabaci & Mohamed, 2020) to detect and clarify a fault in the broken rotor bar of induction motor by eliminating high frequency component followed by the amplification of the single-phase current. The signature was then captured using FFT and principal component analysis. The detection of the exact location of a fault in the broken rotor bar of squirrel cage induction motor was considered by (Abd-el-Malek et al., 2017). The proposed technique was based on the application of Hilbert transform and statistical analysis of the envelope of the stator current. The detection of the broken rotor bar in the transient region was done by (Burriel-Valencia, Puche-Panadero, Martinez-Roman, Sapena-Bano, & Pineda-Sanchez, 2018), using current sensors, with optimized Slepian window for applying the short time Fourier transform (STFT) on the stator current signal.

A technique based on the signal and image processing was developed by (De Santiago-Perez et al., 2018), to automatically detect broken rotor bar faults in IMs. For the former a low pass filtering and STFT were applied to the current signal. Whereas the latter an image processing algorithm was performed. An algorithm founded on the spectral subtraction analysis was developed by (Iglesias-Martínez, de Córdoba, Antonino-Daviu, & Conejero, 2019) and applied to detect breakage of a rotor bar in induction motors, which was independent of the position of the broken rotor. The Pearson correlation was subsequently performed on the stray flux signals. An improved FFT-based technique for the detection of broken rotor bar in induction motors was proposed by (Rivera-Guillen, De Santiago-Perez, Amezcua-Sanchez, Valtierra-Rodriguez, & Romero-Troncoso, 2018). The employed a new FFT-based method called Toot-FFT for detecting changes in both frequency and amplitude. Table 2.5 shows the frequency characteristics for a healthy and faulty IM.

Table 2.5: Induction Motor frequency characteristics formulas

Air gap eccentricity fault	$f_{ecc} = f_s(1 \pm \frac{k(1-s)}{p})$
Broken bar	$f_{brk} = f_s(1 \pm 2ks) \& f_{brk} = k/p(1-s) \pm s)f_s$
Healthy machine harmonic	$f_{psh} = [\frac{kR}{p(1-s)} \pm v]f_s$
Inter turns short-circuit of stator winding	$f_{st1} = (3-2s)f_s \& (f_{st2} = (5-4s)f_s$
Fault frequency component of bearing inner ring	$f_{bri} = N/2f_r(1 + \frac{D_b}{D_c \cos(\alpha)})$

2.3 Fault Tolerant Control (FTC) Survey

The FTC systems have been studied by many researchers in the control community. The global online studies of fault tolerance control technique were done by (Sun et al., 2019), the technique was based on optimization algorithm of the online current. The

method permits the computation of the current references with the least losses in the stator winding in the event of the open phase fault. In an attempt. To enhance the performance efficiency of the motor (Zhou, Sun, Li, Lu, & Zeng, 2019) developed a new different tolerance strategy on the basis of four-leg inverter, which is stronger and does not require the reconfiguration of the controller aftermath of the open-phase fault. Hardware redundancies have inflicted the FTC in most of the real industrial systems. The redundant sensors are used in majority of the voting schemes to deal with the sensor faults. Since the last two decades, limitations such as hardware redundancies, high cost and occupying large spaces, solutions based on analytical redundancies have been studied.

The analytical redundancies are applied through two various approaches:

1. Passive approaches as a type of classical control
2. Active approaches as a type of adaptive control

The FTC systems only deal with the major faults that therefore do not test the full potential of the system and thus its robustness is not challenged. If it were to incorporate small faults that are hard to detect, then the case would have been different, and the system would be put against a realistic challenge. The fault tolerant controls are often used with the remote diagnosis. Another FTC classification is as:

1. There is unlimited computing power in the off-board component, but it still has to deal with the limited and biased measurement data.
2. Restricted computing power is granted to the on-board components, which limits the algorithm complexity of the task to be performed.

A new fault-tolerant doubly-fed flux motor reversal with the armature windings wound on both rotor and stator teeth is proposed by (Wu, Zheng, Fang, & Huang, 2020)

to facilitates the fault tolerance capability of the machine. The model DF-FRM can work alternatively with armature windings in the event of fault occurrence. This endows the machine with high fault tolerance capability. A dual-stator structure-parallel fault-tolerant machine (DSSPFTM) was design and manufactured by (Y. Zhao, Huang, Jiang, Lin, & Dong, 2020), during which its fault tolerant design was streamlined. In the permanent magnet machine, the radial-flux dual-stator design with higher mass-volume relations are nominated for the fault-tolerant scheme, for resilience performance, while operating under fault condition.

A unified approach to offer a conclusive analysis on a six-phase induction motor drive about the FTC capability, in aftermath a fault with the symmetrical, asymmetrical and dual three-phase configurations was offered by (Munim et al., 2016) with the derating in the post-fault scenario. (González-Prieto, Duran, & Barrero, 2016), improve the braking process of a six-phase induction motor drives. The techniques employ the maximum torque and minimum loses principle to achieve proper injection of current, for minimal derating.

The impact of IGBT-Gating failure on a fault-tolerant and current-controlled five-phase induction motor drive was studied by (Guzman, Barrero, & Duran, 2014)., in which the working of the five-phased fault was analyzed aftermath the fault occurrence, when the freewheeling diodes of the affected phase are still switched on. A new technique of fault diagnosis using current sensor and tolerant control of induction motor was proposed by (Yu, Zhao, Wang, Huang, & Xu, 2017). The proposed method is favorable where safety is highly considered.

The issue of designing the fault tolerant system for the 5-phase IPM synchronous motor drive was considered by (L. Zhang, Zhu, Gao, & Mao, 2019), using the new criteria of flux- intensification, fault-tolerant, interior permanent magnet (FIFT-IPM)

motor, for sensorless operation and robustness. In a similar case a fault-tolerant control technique for a 12-phase PMSM model was developed by (Gao, Zhang, Wang, & Chen, 2019) in the static coordinate system to retained its robustness in the event of fault. A sensorless fault tolerant control (SFTC) technique was proposed by (Zafari & Shoja-Majidabad, 2020) to detect and persevere faulty condition in five-phase IPMSM, using the model reference adaptive system. A simple fault-tolerant control based on model predictive control design was considered by (Tao, Zhao, Du, Cheng, & Zhu, 2019) for a five-phase permanent-magnet motor the design offered a classical control model, with minimal computational complexities, aided by the virtual voltage vectors. A promising fault tolerant control technique based on the principle of nonlinear sliding mode controller was presented by (Layadi et al., 2020), in order to mitigate the impact fault occurrence in two-star induction machine.

A study to compare the resonance and predictive controllers of a five-phase fault-tolerance controlled induction motor was put forward by (Guzman et al., 2015). The comparison was carried out experimentally on the original and physical induction machine. An adaptive fuzzy control of stochastic nonlinear parameters system, based on command filtering was presented by (Z. Zhao, Yu, Zhao, Yu, & Lin, 2018). The designed was made to tackle the unknown functions and multiple complex problem in the induction motors.

The diagnosis of fault and the resilience of multi-motor control scheme on the basis of dynamical complex and consistent matrix was developed by (Mao, Li, Feng, & Zhang, 2020), in order to mitigate the malfunctioning of sensors during the synchronous control of multi-motor system. The fault tolerance scheme for handling the vector control of an induction motor on a global scale was proposed by (Gouichiche, Safa, Chibani, & Tadjine, 2020). This technique utilizes the principle of sliding mode

observer and spectral analysis to detect and localized, any fault the may emanate from the stator winding or broken rotor bar. In addition to that, sensors failures, such as current and speed sensors was tackled by this approach.

A combined fault diagnostic and fault-tolerant techniques on the basis of synchronizing complex network was introduced by (Mao et al., 2020) to cushion the impact of sensor fault issues in a multi-motor synchronous regulation based on the principle of distancing . The idea was conceived from the coupling matrix in the synchronization of complex network, during which a consistent matrix was derived in such a way to mimic the similarity of various sensor from the resulting data. The reliability and the availability characteristic will define a fault tolerance of any system. By reliability we refer to the system's ability to continue its operation under damaging conditions. Availability refers to the system's readiness to attempt a correct action. The addition or a spare available in a system to replace the unit that fails to perform in a manner that the system is able to continue with its operation in spite of the failure, is referred to as the redundancy of a system. An asymmetry is created between the three phases due to the faults in the stator winding of an induction machine, which results in a negative sequence component in the line currents (Zicheng Liu, Sun, Zheng, Jiang, & Li, 2019). A combination of various stresses acting on the stator is the reason behind the majority of the faults. These stresses can be thermal, mechanical, electrical and environmental (Mróz & Poprawski, 2019).

2.3.1 Stator Winding Fault Tolerant

The failure of the motor windings is almost 38% of all the motor faults. The stator winding faults can be classified as (Godoy, da Silva, Goedel, & Palácios, 2015), during which three different methods that is fuzzy ARTMAP network, (FAM), multilayer

perceptron network (MPN) and support vector machine (SVM) of machine learning were compared.

1. Open circuit faults
2. Short between any turns in the winding
3. Short-circuit between line to ground

In (Ali et al., 2020) are various fault diagnosis methods for the detection of stator winding faults mentioned in the literature. Developments are still required in the detection methods of delay times between two turn faults and its intensity. Dangerous effects can be prevented if the stator winding faults are detected as early as possible and will give enough time to plan an action to maintain the required performance. During the short turn fault, a large circulating current will be induced which creates excessive heat. Majority of the stator winding fault detection methods proposed are revolving around the perturbation in the motor parameters through the second order harmonic in the air gap torque (Mossa, Echeikh, Iqbal, Duc Do, & Al-Sumaiti, 2020) and (Xie, Pi, & Li, 2019). The AI techniques, the wavelet and negative sequence approaches (Chicco & Mazza, 2019) the action of the controller does not influence these methods, but they need the voltage sensors in the circuit.

2.3.2 Design Methodologies

(Sobanski, Orłowska-Kowalska, & Simulation, 2017), presented a cheaper topology of fault tolerant control as shown in Figure 2.12. Actuator saturation is serious problem in this method which is needed to change the input/output controller parameters and structure of the controller.

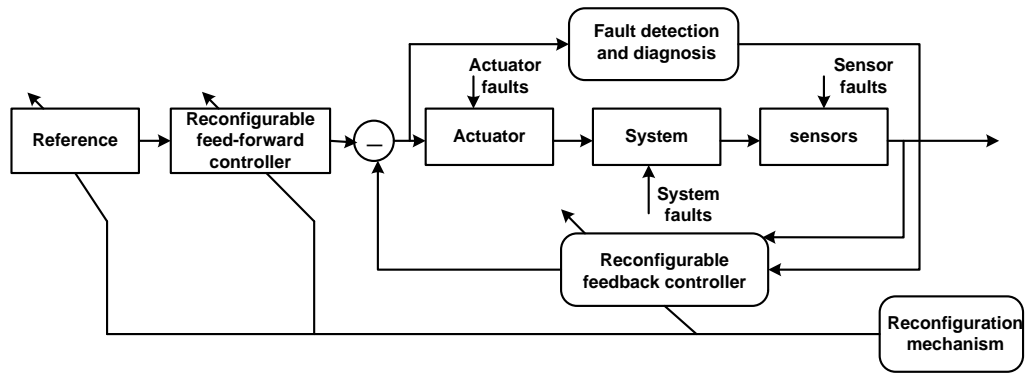


Figure 2.12 Basic block diagram of the FTC scheme

In the case of an induction motor being subjected to inter-turn short circuit faults (Guezmil et al., 2019) introduced a higher order sliding-mode fault tolerant controller based on backstepping algorithm to achieve a robust IMD, which was validated using the Lyapunov theory. Temperature variations and sensor faults cause these faults. The internal and the external factors were dealt with the help of the passive FTC and active FTC strategies. A dual-winding fault-tolerant permanent magnet (DFPM) motor having 3-phase and with four-leg inverter was suggested and developed by (X. Jiang, Huang, Cao, Hao, & Jiang, 2016), This design gain popularity, because of its ability to minimize the total number of power switches as well as improving the efficiency, with high reliability. The block diagram of the FTC techniques is illustrated in Figure 2.13. A power density of higher magnitude was also observed.

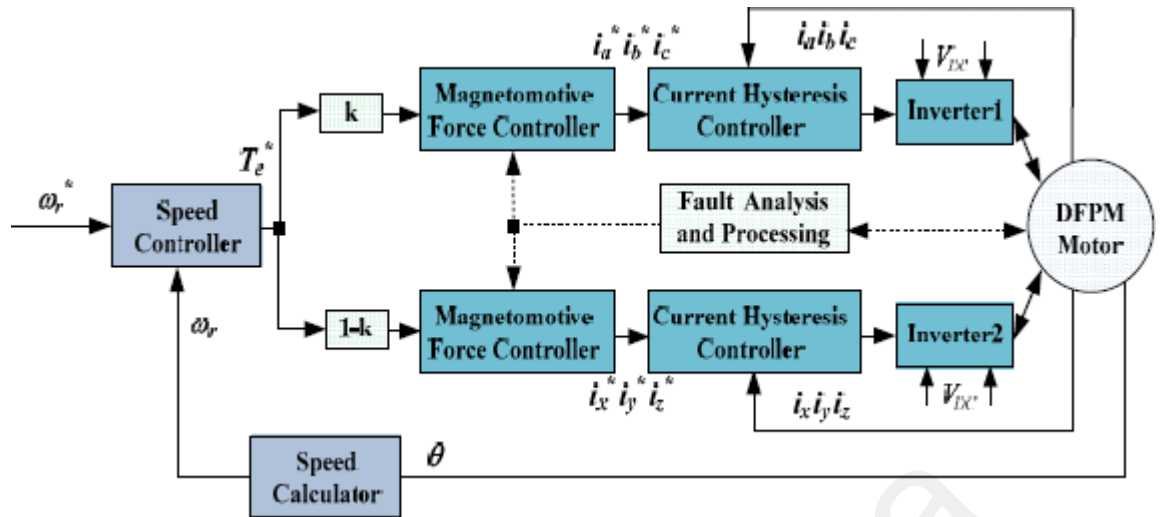


Figure 2.13 Proposed FTC technique with 3-phase four-leg inverter (X. Jiang et al., 2016)

A novel fault-tolerant control for a linear permanent magnet Vernier (LPMV) motor fed by dual converter with a floating capacitor was developed by (W. Zhao, Chen, Xu, Ji, & Zhao, 2018). The combination of control technique based on unity power factor together with fault-tolerant control strategy was applied to maintain the operation of the central inverter, at a unity power factor capacity with better optimization of the dc-link voltage, by constantly replenishing the reactive power of the scheme. This duo of fault tolerance and unity power factor was also found to retain the range of the highest modulation as wide as prior to the fault occurrence.

The effect of DC-link voltage of the passive cells on the fault-tolerance capacity of a cascaded H-Bridge converter for motor drives was investigated by (Bisht, Das, & Electronics, 2020), in which multiple fault-tolerant circuitry of the CHB for the drives. The proposed topology was observed to withstand several faulty cells. Prior to that, a fault-tolerant dc-ac converter-fed induction motor drive, with faulty-switching was introduced by (Farhadi, Fard, Abapour, & Hagh, 2017), where the basics of fault detection and isolation strategies were offered. In addition to the novel Joule-integrated-based technique for the appropriate selection of fuse rating, for the reliable fault isolation,

two control techniques viz-a-viz predictive control and voltage mode-controlled PWM, was presented, for two stages of the converter.

Fault diagnosis technique and a fault tolerance control was applied by (K. Hu, Liu, Tasiu, & Chen, 2020) to remedy the IGBT open switch faults in voltage-source inverter-based field-oriented control of induction motor drives, during the diagnostic procedure, the phase voltages were regenerated from the control scheme parameters, in such a way to avoid extra sensors. A sensorless control approach was adopted by (Khadar, Kouzou, Rezzaoui, Hafaifa, & Science, 2020), in which backstepping control technique was applied to the open-end winding of five- phase induction motor. The outcome reveals that the suggested backstepping technique has the high capacity to withstand the impacts stator faults owing to the short-circuit faults between coils.

The combination of fault detection based on signal analysis of the voltage from the power inverter and the approach based on the sliding mode was executed by (Khlaief, Saadaoui, Abassi, Chaari, & Boussak, 2020) in a pursuit to yield a fault-tolerance control (FTC), for a permanent magnet synchronous (PMS), with a sensorless speed mechanism. The back-emf and sliding mode observer was employed to rotor position, stator current measurements and the concurrent fault diagnosis of motor control unit system (MCUS).

The enhancement of model predictive torque control (MPTC) of a five-phase, fault-tolerant permanent magnet synchronous motor, with harmonic suppression and pre-selective voltage was investigated by (W. Huang, Hua, Chen, & Zhu, 2019). The main contribution was to facilitates the system of MPTC for a five-phase flux-switching permanent magnet (FSPM) motor drive working under open circuit fault scenario, after which the efficiency of the system drive can be improved, in such a way that the control of both harmonic and fundamental subspaces can be achieved via a simple computation.

The study of constant switching frequency and predictive control of an asymmetric source dual inverter scheme was put forward by (Chowdhury, Wheeler, Huang, Rivera, & Gerada, 2018), using a floating bridge for multiple level of operation. The study hypothesizes a modified modulated model predictive control (MMPC) strategy to control an open-ended winding induction motor drive, the proposed MMPC scheme improve the efficiency, when compared with the typical scheme of model predictive control.

A methodology based on signal analysis of an open-ended wound induction motor (OEWIM) was proposed and implemented by (S. Yang, Sun, Ma, Zhang, & Chang, 2019), in order to detect the occurrence of open-circuit fault in a switch, in addition to the accurate identification of the faulty switch. This technique was observed to be highly beneficial to the enhancement of fault-tolerant algorithm of the dual-inverter fed drive.

Table 2.6 shows the summary properties of the fault diagnosis methods of the IM.

Table 2.6: Common Procedures for Diagnostic Techniques of IM

	Concept	Applications	Disadvantages	Reference
Signal Processing	Time-domain, which are based on measuring zero sequence components of currents & voltages.	Capturing, signature information from faulty current or voltage signals from the stator or rotor	Inaccurate because it identifies faults, during starting and load changes transients as faults	(Henaio et al., 2014)
	Frequency domain this is developed on the basis of harmonics components, which are ushered in by faults	Frequency domain techniques are founded to analyze signals, which are periodic and stationary	Misidentification of transients as faults during high impedance faults. Therefore, their accuracy is compromised when employed in industrial based IMs	(Riera-Guasp, Antonino-Daviu, & Capolino, 2014)
	Time- frequency employs the MCSA, by considering the facts that current taken by the IM contains essential information with	Time-frequency techniques are implemented using the short-time Fourier transform, adaptive transform and Hilbert transform	Shows some improve accuracy regarding fault types reduced sensitivity to loading	(S. B. Lee et al., 2015)

	regard to the fault	(Harmonic based digital protection).		
Artificial Intelligence (AI)	This method (ANN) is designing to identify set of characteristics usually by heuristic technique, shows good performance in detecting fault.	Artificial neural networks (ANN), which employs optimized networks and statistical data	The online execution of ANN remains a challenge, due to the requirement for training data.	(Skowron, Wolkiewicz, Kowalski, & Orłowska-Kowalska, 2019)
	Algorithm techniques, at the initial stages shows good fault detection capabilities.	These algorithms are achieved by the application of support vector machine (SVM), principle component analysis and Kernel density estimation.	The applications of these algorithms in IMs, is still uncertain	(Gowthami & Kalaivani, 2019)
Alternative quantities	This technique is developed to offer noninvasive detection of faults, which proved to be difficult to other techniques	This method includes thermal imaging, finite element models and d-q axis formulations	This technique is still in its nascent stage and therefore under study.	(Riera-Guasp et al., 2014)
Detecting insulation failures in IM's winding	MCSA techniques	Due to changes caused by interturn faults, which may initiate harmonics in the line current of the affected winding	The MCSA harmonic based technique is sensitive to other source of harmonics other than that of interturn fault	(Ojaghi, Sabouri, & Faiz, 2014)
	Negative Sequence current	These is developed on the basis that interturn faults changes the impedance of the affected windings, thereby resulting in the flow of unbalanced 3-phase current in the stator of the IM.	sequence components show some shortcomings, in discriminating the faulty sequence component source, that could be due to unbalanced voltage supply	(Han et al., 2019)
	Stray Flux	This is based on processing the stray flux, in order to sense faults in the winding's insulation. This nonintrusive setup offers signature information for detecting faulty windings.	Other sources of magnetic flux were observing to be sensitive during the application of this technique, which will cause uncertainty in precisely identifying the fault.	(Riera-Guasp et al., 2014)

2.4 Inverter Faults

The three-phase inverter consists of three legs with two transistors in each leg. IGBT transistors in the normal power level or the GTO thyristors types employing online data-driven techniques in the induction motor drives have been studied by (Gou, Xu, Xia, Deng, & Ge, 2020). The inverter can provide the three-phase voltage supplied to the IM, that is supplied by a voltage source comprising of a diode rectifier and a capacitor filter C to serve the dc-link (Adapa, Bhowmick, & John, 2020). To obtain low impedance for the AC component in the dc-link, the C value of 3300 μ F is used in this thesis.

The voltage source inverter (VSI) can provide high performance (Maamouri, Trabelsi, Boussak, M'Sahli, & Systems, 2018) The inverter diagnostic method is classified here as signal based approach. Faults such as, the IGBT open circuit fault in one or more transistor in the same or different leg can occur (Trabelsi, Boussak, & Benbouzid, 2017). These faults can be highly damaging specially in the case of the complementary IGBT being turned on and an open circuit in one or more leg. The proposed diagnostic technique utilizes the similarity test algorithm between the regular and approximate to determine the fault detection index (FDI) in the inverter. The stability of the system was maintained through the evaluation of the stator flux at zero voltage and the frequency at minimum through an ANN, by using a simple open loop inverter (PWM_VSI) fed IM (Bana, Panda, Naayagi, Siano, & Panda, 2019).

The path linking the uncontrolled rectifier of a variable V/F control IM drive was studied by (Dekate & Bhargava, 2018). (Bisht et al., 2020) studied and analyzed a robust cascade H-Bridge topology and examined the effect of DC-link voltage of a redundant cell on the resilient capability of the proposed converter. A novel clamping methodology was also scheduled to be implemented. In another case, a nonredundant robust topology

was studied for two-leg fault on a back-to-back converter -fed IMD. A scheme based on finite control set and model predictive control was introduced for independent control of the converter.

The motor operations are affected by these faults; therefore, the fault diagnostic is an important step as it will allow early detection and control. This work will however assume that the inverter is healthy in all the operations, as we will not discuss the faults associated with the inverter. Figure 2.14 shows the percentage of component failures in the adjustable speed drives according Pareto chart. The control circuit faults are higher than the power electronics and external auxiliaries' faults.

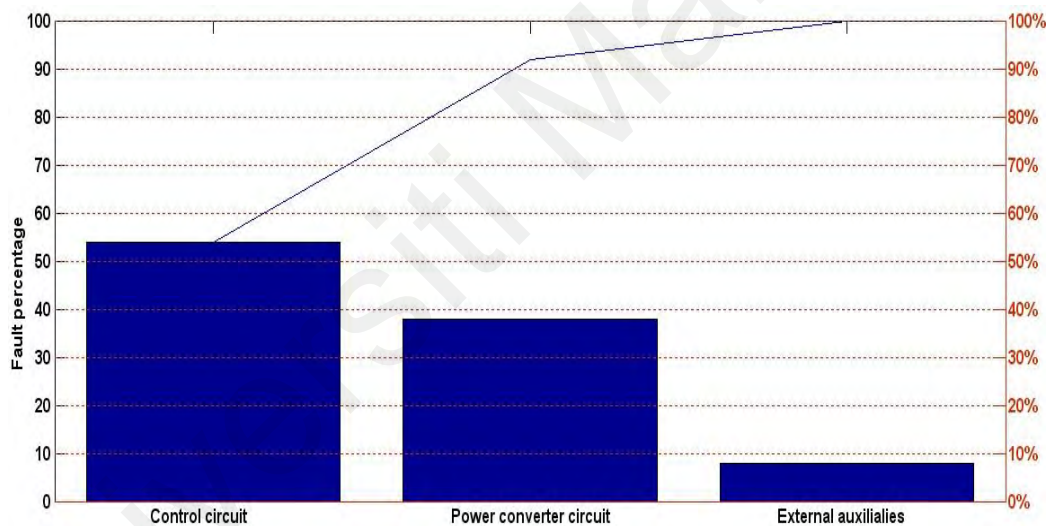


Figure 2.14 Percentage of component failures in ASD

Figure 2.15 shows the percentage of component failures in the switch power supply. In this figure more than 60% of switch mode power supply faults are DC link capacitor, 32% is power transistor and 8% is diodes and other faults.

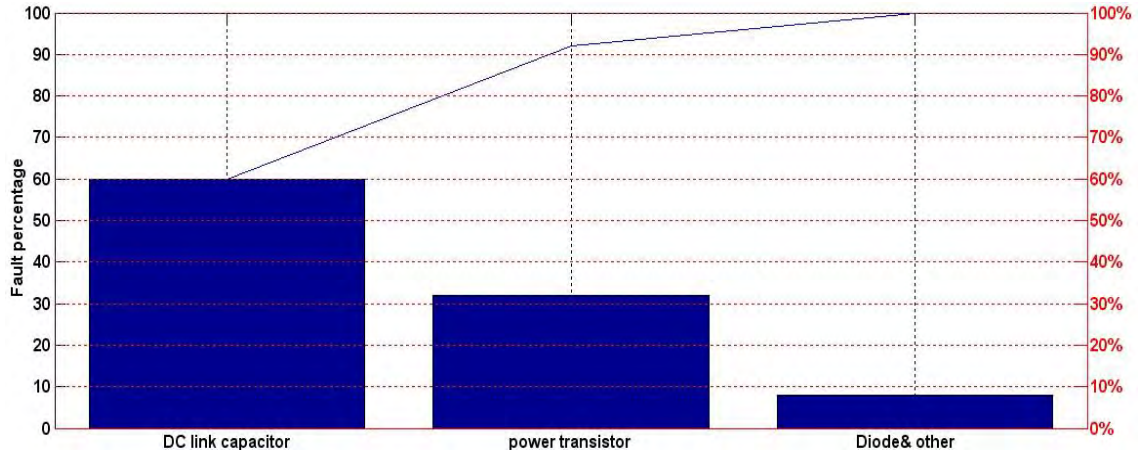


Figure 2.15 Percentage of component failures in switch mode power supply

(Hmidet & Boubaker, 2020), introduced the VSI open circuit and short circuit faults with V/F control strategy. The prospective control architecture was supported by a solid ant windup PI controller and robustified by the combination of the STM32F4-Waijung block set. A new open circuit fault diagnostic technique for voltage source inverters is suggested by (F. Wu et al., 2020), in which a real time , easily executed, basic Fourier series algorithm for low frequency with data regeneration to detect twenty-one transistor open circuit was realized.

As expressed by (Y. Zhang, Roes, Hendrix, Duarte, & Systems, 2020), the Fourier series of the phase voltage obtained from a 3- Φ inverter can be written as in equation (2.12).

$$U_A = \frac{2}{\pi U_{dc} \sum_{n=1}^{\infty} \frac{1}{n} \sin(nwt)} = U_{m(n)} \sum_{n=1}^{\infty} \sin(nwt) \quad (2.12)$$

Where $U_{m(n)} = \frac{2}{n\pi} U_{dc}$ is the peak value of the nth harmonic. $n = 1 + 6k, k = 0, \pm 1, \pm 2$

The wavelet transformation tool algorithm for the diagnosis of a multilevel inverter was presented by (Garapati, Jegathesan, & Veerasamy, 2018), during which the power dissipation in the cascaded H-bridge multilevel inverter was significantly reduced.

Several sources constitute the DC-link voltage pulsation such as, pulsation components in the diode rectifier circuit and asymmetrical AC voltage (G. K. Kumar & Elangovan, 2019). For the healthy inverter case, the DC voltage was 362 V and it reduced until 150V in the faulty inverter which is good observation of inverter fault.

The rapid detection of fault in a power converter, involves the development of fast diagnostic algorithm and fault-tolerant technique. Therefore, it becomes necessary in the DC-DC converter to be embedded with fast fault detection mechanism for safe operation. With regard to the essential and smooth operation of power converters in safety-critical applications, such induction motor drive (Sukumar, Jithendranath, Saranu, & Systems, 2014) introduce a neuro-fuzzy based space vector modulation approach for a three-level inverter fed IMD. The approach employs the integrated learning algorithm, to train the data with respect to the input/output relationship. An optimized space vector pulse width modulation (SVPWM) was proposed by (Reddy, Keerthipati, & Iqbal, 2020), in order to phase out the common-mode voltage (Nian, Zhou, & Zeng, 2015). The idea of 180° decoupled SVPWM was proposed by (Reddy & Keerthipati, 2017) during which the enhancement of modulation range of the suggested configuration was achieved by the injection of third harmonic SVPWM. The design and performance comparison of active zero vector pulse width modulation (AZPWM) and space vector pulse width modulation was carried out by (Jayaraman & Kumar, 2019). The effect of both the SVPWM and AZPWM on the passive common mode (CM) attenuation to minimize CM current in the inverter-fed $\frac{v}{f}$ controlled induction motor drive.

A direct power regulation, which is recognized with space vector modulation for a shunt active power filter (SAPF), was suggested by (Ouchen et al., 2020) in order to tackle the shortcomings of the traditional DPC, in which the SVM can minimize the high active and reactive power ripples and retaining constantly the ON and OFF switching.

(Akhtar, Behera, & Electronics, 2020) presented three single-phase H-bridge inverters fed open-ended wound induction motor (OEWIM) drive that minimizes the parallel topology of the battery in an electric vehicle application. Space vector modulation were evolved by the vectors of intermediate and large quantity. These SVMs are divided according to four PWM strategies, during which their performance was compared on the basis of common mode voltage (CMV), zero sequence voltage (ZSV) and the utilization of DC-bus.

In order to reduce the voltage ripple and power losses in the submodule of multi-modular converter (MMC), the traditional multi-modular converter (MMC) was upgraded by retrofitting the conventional topology with active power filter (APF) circuitry the concept employed a dual submodule at the center, in order to redirect the ripple powers of the phase through the capacitors (G. Jia, Chen, Tang, Zhang, & Zhao, 2020).

The voltage source inverter is said to be primarily based on the pulse width modulation and the instantaneous power theory. It is important to consider the vested voltage or the current in the PWM techniques. The utilization rate of the DC voltage, obtained after the selection of the proper switching mode to decrease the harmonic content, is 78.5% which is much less than the 100% of the six-step wave. Thus, studies have been focused on the improvement of the DC voltage rate (Farzan Moghaddam & Van den Bossche, 2020).

2.5 Summary

A comprehensive review of the transient phenomena that evolve from the applications of wind energy technology is elaborated in this chapter. The equations and techniques used in the analysis of transients due to the rotating parts of WTG and those of the protection of rotor and grid converters are introduced. Additionally, models of transients

that originate from the stators and rotors of WTGs are discussed. Furthermore, various control and protection systems that are used in the remedy and mitigation of transients were clarified. In this thesis a new protection scheme is proposed to safeguard the rotor side converter in a popular topology employing DFIG. In a similar case, a multisensory technique for fault-tolerance induction motor was used to protect the inverters by mitigating the effect of the fault, mainly caused short-circuit in the stator or broken rotor bars.

Universiti Malaya

CHAPTER 3: RESEARCH METHODOLOGY

3.1 Introduction

This chapter presents the modelling methodologies, and conditioning of the rotor and stator current signals of the DFIG, to determine whether the transient event is related to fault or not. The method developed for sensing and categorizing transient disruptions determined the phases and magnitude of the high-frequency content of the sub-band components presented in the d-q axis of the crowbar/rotor currents. Wavelet Packet Transform (WPT) will be adopted for analyzing and categorizing the transient events as fault or non-fault events. Subsequently, the formulation of the faulty stator and rotor current signal of the induction motor follows. This involves modelling of the fault and the range or argument over which only the fault is considered to have occurred. Similarly, wavelet analysis based on Shannon entropy is used to analyze the fault for the IM. Furthermore, H_∞ controller and fault tolerance control strategy are employed for the robustification of the DFIG and the induction motor respectively.

3.1.1 Proposed Protection Scheme for RSC and GSC

The protection scheme can be implemented by embedding it within the controller of the generator, which could require no additional or separate control block that could complicate the system further. Additionally, the implementation is simple as the DFIG-based WECS is realized in MATLAB machine tool box. Similarly, the development of d-q phaselet-based digital relay is achieved by writing MATLAB codes to read the 3-phase current data. The algorithm computes the I_d and I_q for the rotor and the grid, half-band digital high-pass filter HPF $h[n]$ is applied to extract Y_{dq} , by cyclic convolution in wavelet toolbox. The same procedure is applied at the stator of the generator for GSC protection.

3.1.1.1 Implementation of the Wavelet-Based Digital Crowbar

The preceding section reviewed the framework of the d-q phaselet-based digital protection, during which a fault can be identified and classified upon the application of the d-q wavelets embedded in the HPF. For the scheme of digital protection for the rotor side converter (RSC) in DFIG, the half-band digital filter is directed to the d-q axis units of the three-phase currents taken by the crowbar. Figure 3.1 depicts the prospective digital crowbar in the commonly known DFIG topology employed at the distribution stage, of the power system.

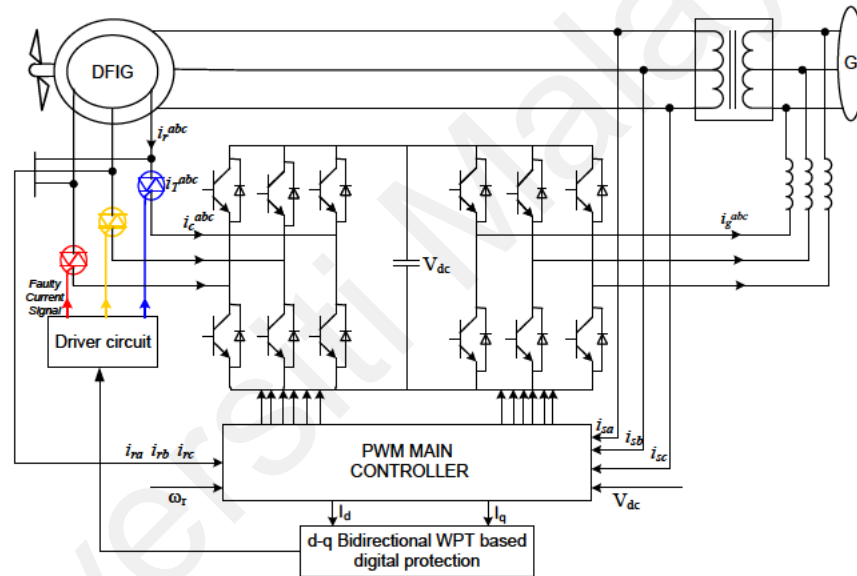


Figure 3.1: Digital Crowbar Implementation Topology

The operation of the half-band digital HPF generates the first level of the phaselet details (the high frequency sub-band), i.e. components of the d-q axis, Y_{dq} . The finding of Y_{dq} can be achieved using the convolution notation $Y = h * x$, (Martucci, 1994; Wickerhauser, 1996) which could further be mathematically expressed in (3.1) for finite signals or periodic signals (much as the Fourier series) (S. Saleh, Aktaibi, Ahshan, & Rahman, 2012).

$$Y_{dq}[n] = \sum_{l=0}^{N-1} X_{dq}[l]h_4[n-l]; l \in \mathbb{Z} \quad (3.1)$$

Hence h_4 is given as cyclic convolution in a matrix expressed in (3.2) based on db_4 coefficients.

$$h_4 = \begin{bmatrix} h(0) & h(3) & h(2) & h(1) \\ h(1) & h(0) & h(3) & h(2) \\ h(2) & h(1) & h(0) & h(3) \\ h(3) & h(2) & h(1) & h(0) \end{bmatrix} \quad (3.2)$$

Where the vector X_{dq} is derived using the unbiased technique in expression (3.3) as in (S. A. Saleh et al., 2011) and (Gopinath, 2005).

$$X_{dq}[n] = (I_{dr}[n])^2 + (I_{qr}[n])^2 \quad (3.3)$$

Where $I_{dr}[n]$ and $I_{qr}[n]$ are the d-q-axis components of the three-phase current taken by the DFIG and are derived from the controller of the rotor side of the generator.

Even though, the d-q phaselet-based digital protection is designing to be integrated within the rotor side controller, it can be redesigning to function as a distinct system. In case of applying the d-q phaselet-based digital crowbar as a separate scheme, its input will be components of the three-phase currents taken by the rotor. These components of three-phase currents are transformed into their d-q-axis elements by equations (3.4) and (3.5) respectively;

$$I_{dr}[n] = \sqrt{\frac{2}{3}} \left(I_a[n] \cos(\theta_r) + I_b[n] \cos\left(\theta_r - \frac{2\pi}{3}\right) + I_c[n] \cos\left(\theta_r + \frac{2\pi}{3}\right) \right) \quad (3.4)$$

$$I_{qr}[n] = \sqrt{\frac{2}{3}} \left(I_a[n] \sin(\theta_r) + I_b[n] \sin\left(\theta_r - \frac{2\pi}{3}\right) + I_c[n] \sin\left(\theta_r + \frac{2\pi}{3}\right) \right) \quad (3.5)$$

The frequency components of the rotor currents can be repositioned to expedite the extraction of the high frequency sub-bands. The extraction of frequency contents sparked due to the faults occurrence can be streamlined by the repositioning of nonstationary components in order to be precisely extracted by the four HPFs (S. Saleh, Ahshan, & Rahman, 2013).

As seen from Figure 3.2, encircled is the conventional crowbar that is employed in DFIG scheme, to provide the conservative protection to the rotor side converter (RSC). The crowbar is fitted at the rotor terminals of the DFIG, to divert high inrush flow of rotor current during faults. It is usually activated by switching off the rotor converter. The switching off of the converter causes the absorption of grid reactive power, which is undesirable to the DFIG operation. The classical crowbar is devised with resistance, rectifier and controlled switch.

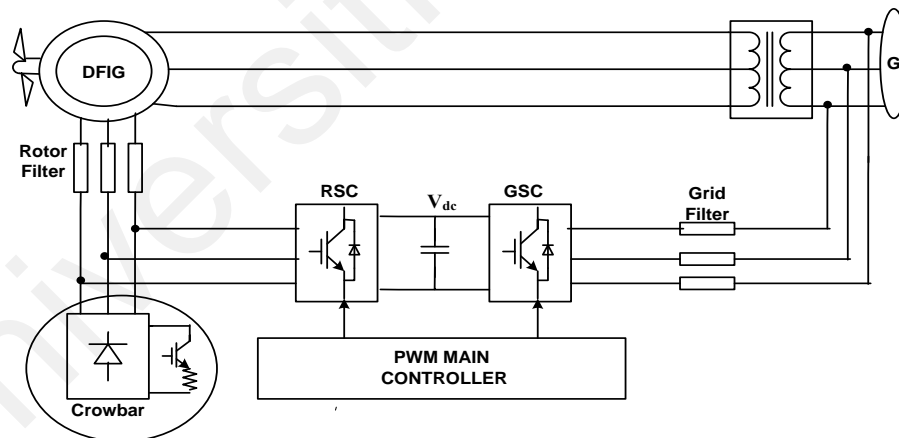


Figure 3.2: Conventional Crowbar Implementation Topology

3.1.1.2 Implementation of the Wavelet-Based Digital Protection for GSC

A similar topology to offer protection for the GSC during grid faults is shown in Figure 3.3, which is designed by simply changing the position of the digital relays from the rotor circuit to the grid circuit. This type of design can also help prevent the GSC from damages

during islanding as applied and implemented in (S. Saleh et al., 2017a). Although, in this case the stator or the grid current is required to be analyzed and convoluted using the unbiased technique and cyclic convolution equation respectively.

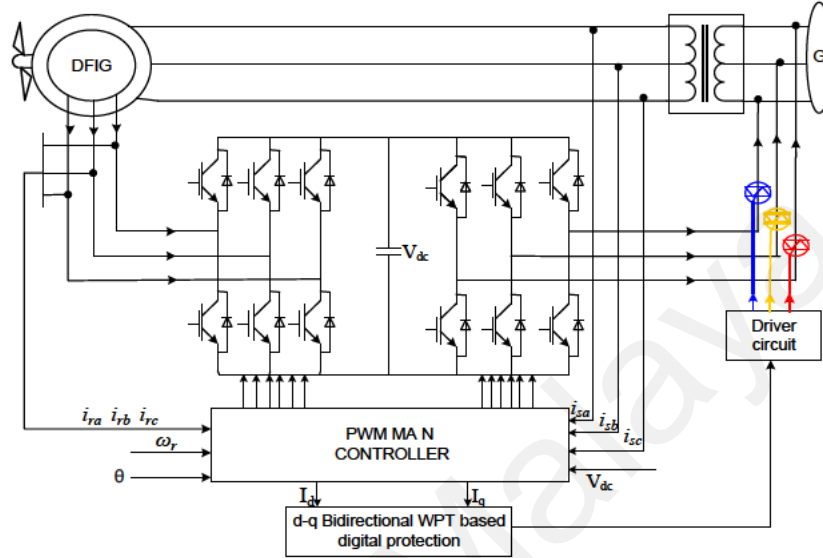


Figure 3.3: Digital Protection Topology for GSC

3.1.2 d-q Axis wavelet transform applications

The dq0 frame, generated by the $abc - to - dq0$ coordinate transformations, is widely applied in the design and implementation of controllers employed in three-phase systems. More especially the three-phase power electronic converters. Such controllers are often used in renewable energy systems, power system control and motor drives. The $abc - to - dq0$ transformation is described mathematically in vector expression (3.6) by (S. Saleh et al., 2012; S. A. Saleh, Ahshan, Abu-Khaizaran, Alsayid, & Rahman, 2013).

$$\begin{bmatrix} \beta_a(t) \\ \beta_q(t) \\ \beta_0(t) \end{bmatrix} = \Delta(\beta_a(t), \beta_b(t), \beta_c(t)) = T \begin{bmatrix} \beta_a(t) \\ \beta_b(t) \\ \beta_c(t) \end{bmatrix} \quad (3.6)$$

Where $\beta_a(t)$, $\beta_b(t)$, and $\beta_c(t)$ are the time functions of the three-phase quantities (rotor currents), and the matrix of transformation T is given by expression of (3.7)

$$T = \sqrt{\frac{2}{3}} \begin{bmatrix} \cos(\theta_r) & \cos\left(\theta_r - \frac{2\pi}{3}\right) & \cos\left(\theta_r + \frac{2\pi}{3}\right) \\ \sin(\theta_r) & \sin\left(\theta_r - \frac{2\pi}{3}\right) & \sin\left(\theta_r + \frac{2\pi}{3}\right) \\ \frac{1}{\sqrt{2}} & \frac{1}{\sqrt{2}} & \frac{1}{\sqrt{2}} \end{bmatrix} \quad (3.7)$$

Where $\theta = 2\pi f_s t$, and f_s is the fundamental frequency in $\beta_a(t)$, $\beta_b(t)$ and $\beta_c(t)$.

The shifted frequencies in $\beta_a(t)$, $\beta_b(t)$ and $\beta_c(t)$, are considered one of the essential features offered by $abc - to - dq0$ transformation. The shifting of frequency can be demonstrated by considering two frequencies f_1 and f_2 , in such a way that $f_1 < f_s$ and $f_2 > f_s$. These frequencies will be shifted by the $abc - to - dq0$ transformation as shown by equations (3.8-3.10) in (S. Saleh et al., 2012).

$$f_s \overset{\Delta}{\leftrightarrow} [0 = |f_s - f_s|] \quad (3.8)$$

$$f_1 \overset{\Delta}{\leftrightarrow} \begin{bmatrix} f_{1l} = |f_1 - f_s| \\ f_{1h} = |f_1 + f_s| \end{bmatrix} \quad (3.9)$$

$$f_2 \overset{\Delta}{\leftrightarrow} \begin{bmatrix} f_{2l} = |f_2 - f_s| \\ f_{2h} = |f_2 + f_s| \end{bmatrix} \quad (3.10)$$

Generally, the abc -to- $dq0$ transformation is performed by microprocessor or digital circuitries that demand the sampling and digitization of the three-phase quantities (voltages or currents) as a preprocessing step. Such demands entail that the frequency shifting as in the three equations of (3.8 to 3.10), are advanced by mapping continuous frequencies into discrete ones. This frequency mapping depends on the sampling frequency f_d , which can be represented by equation (3.11) as in (S. Saleh et al., 2012; S. A. Saleh et al., 2014).

$$\omega = \frac{2\pi f}{f_d}; \text{ such that } \omega \in [0, \pi] \quad (3.11)$$

Where ω is a discrete frequency, and f is a continuous frequency existing in $\beta_a(t), \beta_b(t)$ and $\beta_c(t)$.

It has been described in (S. Saleh et al., 2012), that the frequency alignments and shifting, owing to the digital implementation abc-to-dq0 transformation, relocates the frequencies that are present in three-phase quantities into low-and high-frequency bands as

- Frequencies associated with the only the momentarily transients are relocated to the low frequency band X_l . This low-frequency band is classified as in equation (3.12).

$$X_l: 0 \leq \omega < \frac{\pi}{2} \quad (3.12)$$

- The frequencies due to the actual fault occurrence are moved to a high frequency band X_h . This high-frequency band is classified as in expression (3.13).

$$X_h: \frac{\pi}{2} \leq \omega < \pi \quad (3.13)$$

The above analysis on frequency alignments and shifting offers that an HPF can be utilized to capture the frequency contents that are associated with the actual occurrence of fault. In addition to that, considering that the frequency contents recognized with the fault occurrence, are of nonperiodic and nonstationary fashion, the application of HPF is required to offer the time localization of the captured frequency contents (Lu & Sharma, 2009) (Seshadrinath, Singh, & Panigrahi, 2012) (Khan, Radwan, & Rahman, 2007). These criteria can be fulfilled by the phaselet frames that are generated by the application of four half-band digital HPFs. The scaling function $\Phi(t)$ and its associates wavelet function $\psi(t)$ are used to decide the parameters of such filter (S. Saleh et al., 2012; S. Saleh, R. Meng, et al., 2016). Several techniques exist, for determining the best scaling functions $\Phi(t)$ with its companion wavelet function $\psi(t)$ and for different types of

applications. In this research work, the Daubechies $db4$ scaling function $\Phi_{db4}(t)$ and wavelet function are observed to be efficacious for diagnosing fault currents in power systems and renewable energy. The half-band digital HPF accompanying the $\Phi_{db4}(t)$ and $\psi_{db4}(t)$ is $h[n]$, and its parameters are provided in (Burrus, Gopinath, Guo, Odegard, & Selesnick, 1998).

The low-pass and high-pass operators $(Hs)_k$ and $(Gs)_k$ will be applying to analyze the rotor current signals. For wavelets based on D_4 , the values of the coefficients in the filter were deduced by the division of $\sqrt{2}$ throughout the coefficients in equation (3.14) thereby yielding;

$$h_0 = \frac{1+\sqrt{3}}{4\sqrt{2}} \approx 0.48296, h_1 = \frac{3+\sqrt{3}}{4\sqrt{2}} \approx 0.83652$$

$$h_2 = \frac{3-\sqrt{3}}{4\sqrt{2}} \approx 0.22414, h_3 = \frac{1-\sqrt{3}}{4\sqrt{2}} \approx -0.12941$$

Thus Daubechies-4 coefficients have a particularly pure form of equation (3.14) (Daubechies, 1996).

$$h_{D4} = \left\{ \frac{1 + \sqrt{3}}{4\sqrt{2}}, \frac{3 + \sqrt{3}}{4\sqrt{2}}, \frac{3 - \sqrt{3}}{4\sqrt{2}}, \frac{1 - \sqrt{3}}{4\sqrt{2}} \right\} \quad (3.14)$$

3.1.3 H_∞ Controller Design for the DFIG

Doubly fed induction generator (DFIG) based WTs outperform many of the generators employed in the WECS, owing to the number of its advantages, such as smaller size, reduced power electronics topology (Muller, Deicke, & De Doncker, 2002). However, the DFIG is more vulnerable to grid voltage distortions and have severe impact on its operation (Y. Wang, Wu, Gong, & Gryning, 2016). When there is voltage sag in the grid, the transient constituents in stator flux will result in a high rating current to flow in the

manages the bandwidth of the controller and stability of the system robustness by manipulating KS. The tracking performance of the external disturbance is devised by the matching of W_p to v . Meanwhile, W_u can be taken as unvarying gain. In case of standardize system, an acceptable span of the W_u should be within the range of $W_p \leq 1$.

The input and the output of the controller K , designated as v and u respectively, are so designed to follow the two weighting functions, referred to as W_u and W_p . The output, which is measured and controlled is denoted as $z = [z_1, z_2]$. The block together with the weighting functions and controlled system is known as the shaped generalized plant model, denoted as P . The interconnection of K and P block form the scheme of the closed-loop, represented as N . The state space formation of P can be realized as in equation (3.15).

$$\begin{bmatrix} y\Delta \\ z \\ v \end{bmatrix} = P(s) \begin{bmatrix} u\Delta \\ w \\ u \end{bmatrix} = \begin{bmatrix} P_{11}(s) & P_{12}(s) \\ P_{21}(s) & P_{22}(s) \end{bmatrix} \begin{bmatrix} u\Delta \\ w \\ u \end{bmatrix} \quad (3.15)$$

The block N is represented as $z = N(s)w$. $N(s)$ is the closed-loop transfer function. $N(s)$ can be derived based on equation (3.15) by applying linear fractional transformation (LFT) between P and K . Considering equation (3.15) and by defining the system functional sensitivity as $S = (I + G_s K)^{-1}$. Where $N(s)$ is expressed in (3.16). Additionally, it is observed from equation (3.16) that KS is streamlined by W_u , in which the KS represents the transfer function between the control signals and d , and the measure of controller stability.

$$\begin{aligned}
N(s) &= \begin{bmatrix} N_{11}(s) & N_{12}(s) \\ N_{21}(s) & N_{22}(s) \end{bmatrix} = P_{11} + P_{12}K(I - P_{22}K)^{-1}P_{21} \\
&= \begin{bmatrix} \Delta_1 & 0 & \dots & 0 \\ 0 & \dots & 0 & 0 \\ 0 & \dots & \Delta_{14} & 0 \\ 0 & \dots & W_uKS & -W_uKSG_sB_d \\ 0 & \dots & W_pS & W_pSG_sB_d \end{bmatrix} \quad (3.16)
\end{aligned}$$

The conception of H_∞ optimization is to search for a stabilizing function K to limit the largest gain in case of any input directed from w to z that is the maximum individual value of the closed-loop transfer function $N(s)$, which can be represented by the H_∞ standard as expressed in (3.17).

$$\|N\|_\infty = \max_\omega \bar{\delta}(N(j\omega)) = \gamma_{min} < \gamma \quad (3.17)$$

The optimal solution of (3.17) is noted as γ_{min} , which can be deduced using the standard form of two-Riccati equations (Doyle, Glover, Khargonekar, & Francis, 1989). The γ -iteration algorithm, which describe an appropriate value $\gamma_{min} < \gamma$ to reach the optimal value of γ_{min} , as an H_∞ optimization compromise issue. In case of nominal scheme, γ can be taken as 1.

3.2 Proposed Control and Protection Techniques for the Induction Motor

Sensorless control is a straightforward control scheme. Vector control can be implemented without the need for sophisticated digital processing circuitry (dos Santos, Goedtel, da Silva, & Suetake, 2014). This special feature makes it a reliable standby control setup in an anticipation of fault. Although it is commonly realized in an open loop, a closed-loop technique is also employed in higher precision applications, such as speed response estimation. To maintain the motor speed at its predetermined value, a PI controller is utilized to regulate the speed of the motor slip.

The three phases of currents and voltages are converted to two-phase dq axes. Such conversion can be expressed mathematically as a set of three-phase currents as (S. Saleh & Ozkop, 2016a). The rotor flux space vector rotates owing to the synchronous rotation of the dq frame. The mathematical formulation of torque in an induction motor is shown in equation 3.18 (Odhano, Bojoi, Boglietti, Roşu, & Griva, 2015):

$$T_e = \frac{3}{2} p \frac{L_m}{L_r} (\Phi_{rd} i_{sq} - \Phi_{rd} i_{sd}) \quad (3.18)$$

Considering the sense of direction of the vectors in Figure. 3.5, it implies that Φ_{rd} becomes zero, thus the resulting equation reduces as in equation 3.19:

$$T_e = \frac{3}{2} p \frac{L_m}{L_r} (\Phi_{rd} i_{sq}) \quad (3.19)$$

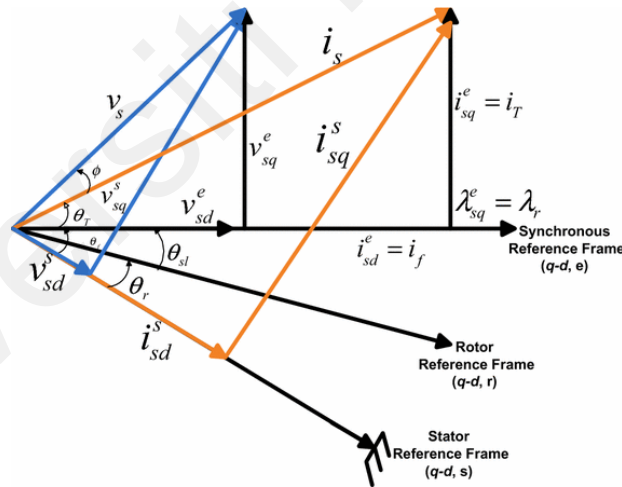


Figure 3.5: The reference frame for vector control

It can be deduced from equation (3.19), that the motor torque can be managed by regulating i_{sq} . Due to its ease of implementation, vector control equipped with a sensor is adopted as the main controller in this study.

When the voltage to frequency ratio is equal and kept constant, the stator flux in the motor is in proportion with the supply frequency and the applied voltage. Therefore, any variations in the frequency cause the speed to change. But when the voltage to frequency ratio is retained at an equal ratio, the torque and flux are being kept constant for the entire range of speed. The speed is fine-tuned by searching for the best f , while retaining $\frac{V}{f}$ at constant to prevent saturation of the flux, as expressed in equations (3.20) and (3.21):

$$E_{airgap} = kf\varphi_{airgap} \quad (3.20)$$

Considering an unvarying airgap flux:

Considering the scheme depicted in (Ammar, Bourek, Benakcha, & Ameid, 2017), the reference model can be represented by equations (3.21) through (3.25):

$$p\lambda_{dr} = \frac{L_r}{L_m \left(v_{ds} - \left(R_s i_{ds} + \frac{\sigma L_s di_{ds}}{dt} \right) \right)} \quad (3.21)$$

$$p\lambda_{qr} = \frac{L_r}{L_m \left(v_{qs} - \left(R_s i_{qs} + \frac{\sigma L_s di_{qs}}{dt} \right) \right)} \quad (3.22)$$

The following equations represent the adaptive model:

$$p\lambda'_{qr} = \frac{R_r L_m}{L_r \left(i_{qs} - \left(\frac{R_r}{L_r} \right) \lambda'_{qr} - \omega_0 \lambda'_{dr} \right)} \quad (3.23)$$

$$p\lambda'_{dr} = R_r L_m / L_r \left(i_{ds} - \left(\frac{R_r}{L_r} \right) \lambda'_{dr} - \omega_0 \lambda'_{qr} \right) \quad (3.24)$$

$$\varepsilon = \lambda_{qr} \lambda'_{dr} - \lambda_{dr} \lambda'_{qr} \quad (3.25)$$

The error between the adaptive outputs and reference, together with the speed reference, acts as input to the booster/enhancer block depicted in Figure.3.6.

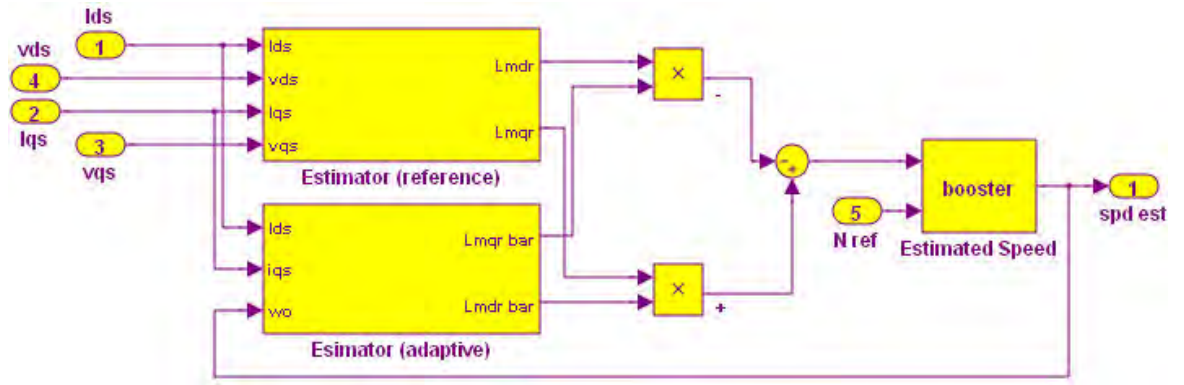


Figure 3.6: The EMRAS implementation in Simulink

The signals are kept at 0, as its initial value. The rate limiter regulates the variation of the signal through it by decreasing the gradient. The lower limit is referred to as falling slew parameter (γ), while the upper limit is termed the rising slew parameter (δ). The rate limiter output is computed as in expressions (3.26) through (3.28):

$$O_{\frac{o}{p}}(i) = \nabla t \delta + N(t - 1) \quad (3.26)$$

$$O_{\frac{o}{p}}(i) = \nabla t \gamma + N(t - 1) \quad (3.27)$$

$$O_{\frac{o}{p}}(i) = N(i) \quad (3.28)$$

The rate limiter input is denoted N. The output is channeled to a Zero Order Hold (ZOH) to form continuous time input by keeping each sample value stable over one sample period. The ZOH is analogous to a hypothetical filter that produces a piece-wise signal as expressed in equations (3.29) and (3.30):

$$o_{ZOH \frac{o}{p}}(t) = \sum_n^{\infty} = -\infty N_{in}[n] \text{rect}\left(\frac{t - nT}{T} - \frac{1}{2}\right) \quad (3.29)$$

Lastly, the measured speed is computed as in equation (3.30):

$$\omega_{\frac{o}{pBMRAS}}(i) = \omega_{reference}(i) - \omega_{Booster}(i) \quad (3.30)$$

3.2.1 Wavelet Index Algorithm for the Induction Motor

Wavelets are basic functions in continuous time, with localized function and zero mean. Wavelet analysis of a signal extracts essential information hidden in a signal. Wavelets possess compact support and are of orthonormal function. Thus, their coefficients can be computed from the inner product (Burrus et al., 1998). Fourier transformation produces global information (i.e. approximations) about signal, but not local information (or details). The wavelets can precisely identify the details or the important information on a small scale, due to its localization property. Hence, wavelets are more effective in extracting signature information present in a signal or function.

The stator currents of the IM drive are taken and applied to the wavelet index unit for the decomposition of the frequencies. The decomposition is achieved by the application of high pass filter (HPF) an inbuilt function of the wavelet index. This HPF is utilized to capture the frequencies that are associated with fault occurrence, and are within the limits of high-frequency band classified as $x_h: \frac{\pi}{2} \leq \omega < \pi$, whereas the frequencies that are only associated with momentary transients i.e. resulting speed and load changes are relocated to the low-frequency band classified as $x_l: 0 \leq \omega < \frac{\pi}{2}$.

Shannon entropy in Equation (3.31), is used in estimating the entropy of the respective paradigm (parent) s of the DWT subspace and viewing it in correlation to its current (children) subspace (Gilbert Strang & Truong Nguyen, 1996).

$$E_{(S)} = - \sum_n^{N-4} S_n^2 \log(S_n^2) \quad (3.31)$$

To be used as depicted in Figure 3.7, the entropy should have the following property: $(E(0) = 0)$.

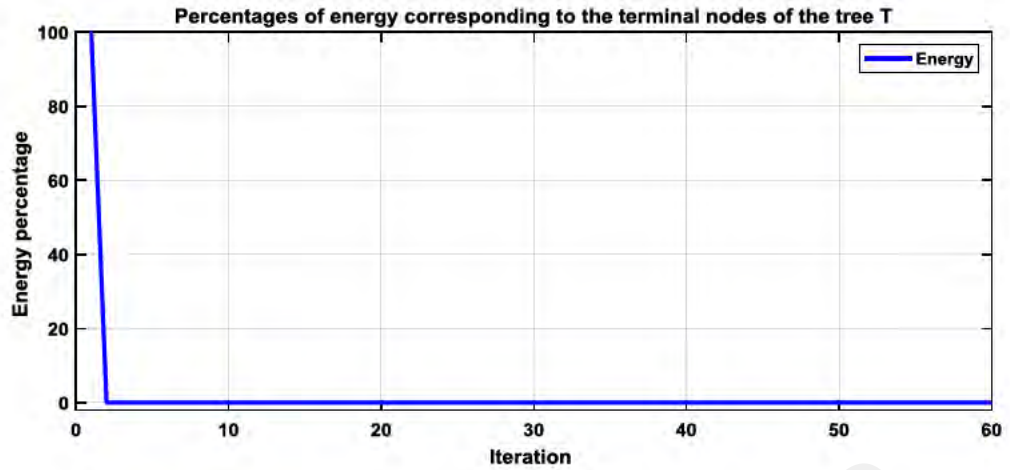


Figure 3.7: Entropy proportion in percentage

The development of the wavelet index has been performed using the db10 of the Daubechies wavelet and the protection unit for the analysis of stator currents. This function is illustrated in Figure 3.8.

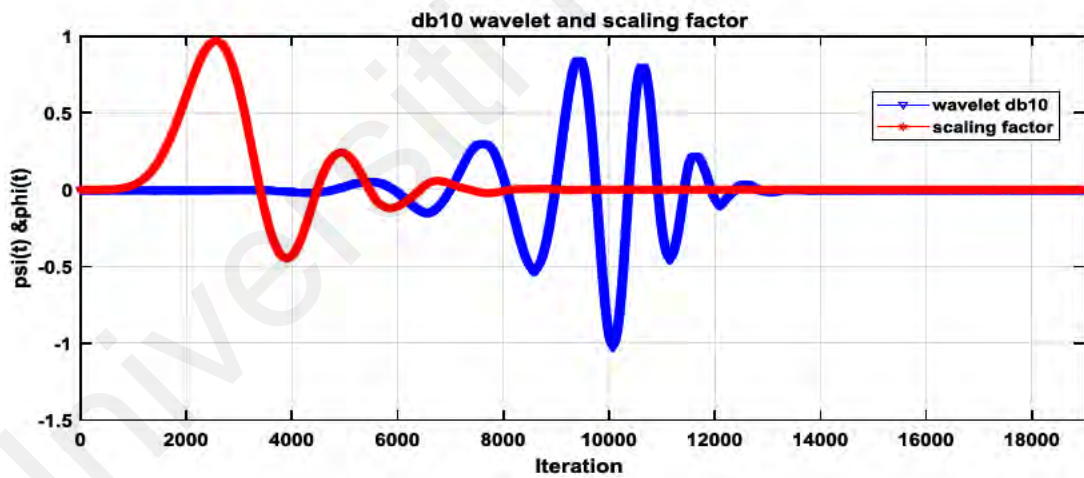


Figure 3.8: The scaling factor (red) and the Daubechies Wavelet function (db10)

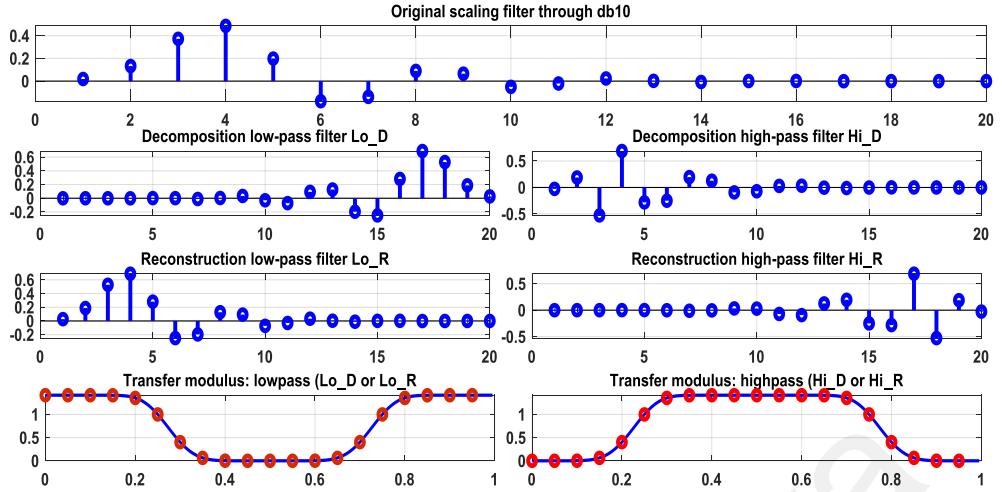


Figure 3.9: Wavelet decomposition and reconstruction

A criterion for the square property is required from the wavelet function so that equation (3.32) holds:

$$|\Psi(\omega)|^2 = 1 \quad (3.32)$$

Let $\{\Psi_{a,b}(x)\}$, with $a, b \in R$ and $a \neq 0$, be a family of functions deduced from a single function $\Psi(x) \in L_2(R)$ by dilation and translation. Then, the original function Ψ expressed in equation (3.33) is typically smooth and well concentrated:

$$\Psi_{a,b}(x) = \frac{1}{\sqrt{|a|}} \Psi\left(\frac{x-b}{a}\right) \quad (3.33)$$

If the original wavelet Ψ is centered on 0 with width w , then $\Psi_{a,b}$ is centered on b with a width aw . Parameter b represents the time location (if x stands for time), and the scale is obtained from a . The parameter scaling is related to frequency.

In this work, the differences in the waveform of stator currents are exploited as the criterion for the fault classification. The current signal is channeled to the wavelet transform unit circuit. The valuable information is captured from the details of the sub-

band signals during the processing, which are coded according to their energies. The concentration of large amount of energy in the high-frequency sub-band of stator current can also serve as an indicator of the wavelet index. Usually, the index is determined using equation (3.34):

$$W_{\text{indx}} = \frac{\text{abs}(\text{energy}(d8))}{\text{average}(\text{energy } I_s)} \quad (3.34)$$

In which d8 represents the decomposition at the 8th level detail by the HPF upsampling and downsampling action. The Simulink implementation is shown in Figure 3.10.

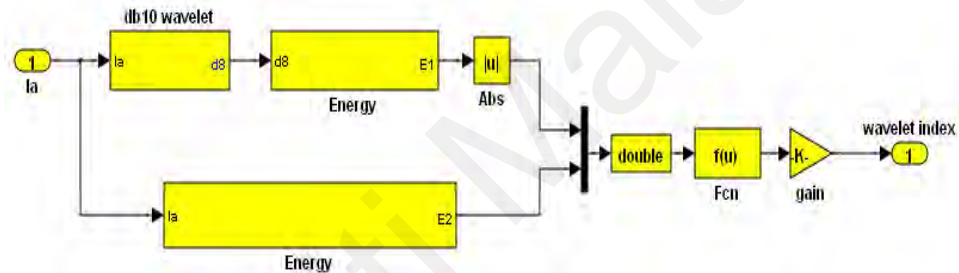


Figure 3.10: Simulink wavelet index implementation

3.2.2 The Platform of the Fault-Tolerant Control

One of the essential applications of fault-tolerant control is in the industries operating with IM drives, especially considering the formidable costs of unintended stops of its operations. This study describes the approach of quadric-control co-working to achieve the robustification of the IM. In healthy operation, the drive is run by sensor vector control. When a fault occurs in the encoder, it switches to sensorless mode of vector control. In the event of a short or open circuit in the stator, the scheme reverts to closed-loop of V/f control mode, while open-loop V/f control mode is activated when a minimum voltage fault occurs as shown in Figure 3.11.

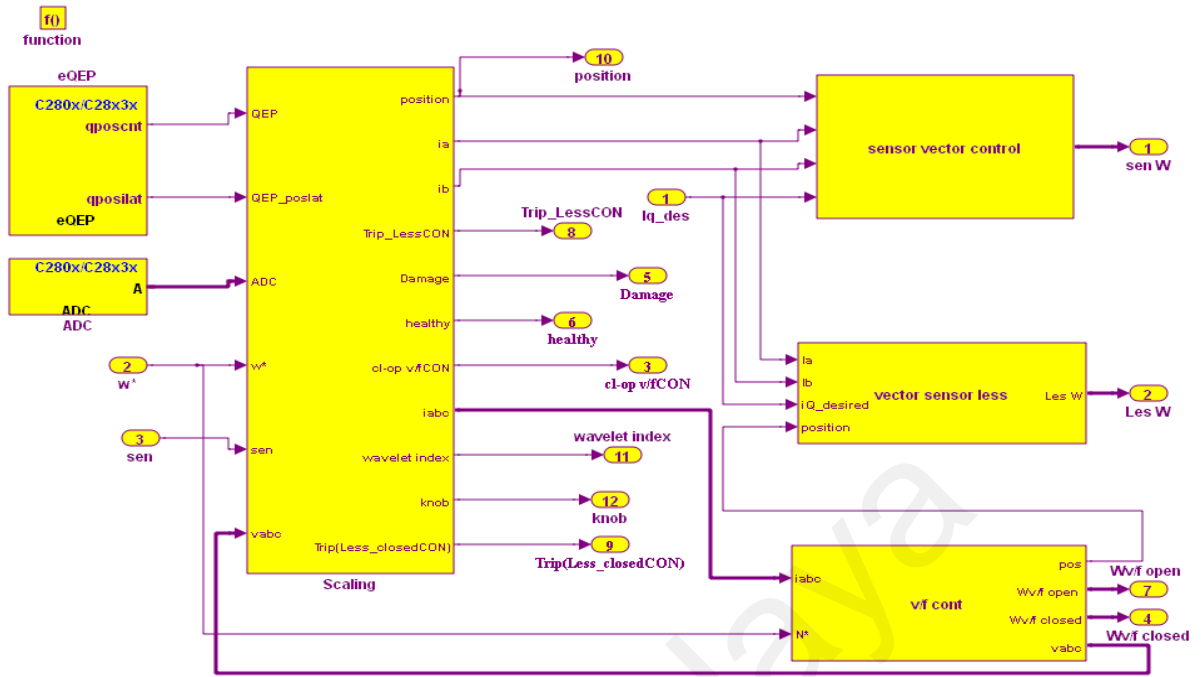


Figure 3.11: Fault-tolerant control algorithm

The Simulink execution of one section of the fault identification and confinement unit is illustrated in Figure 3.12.

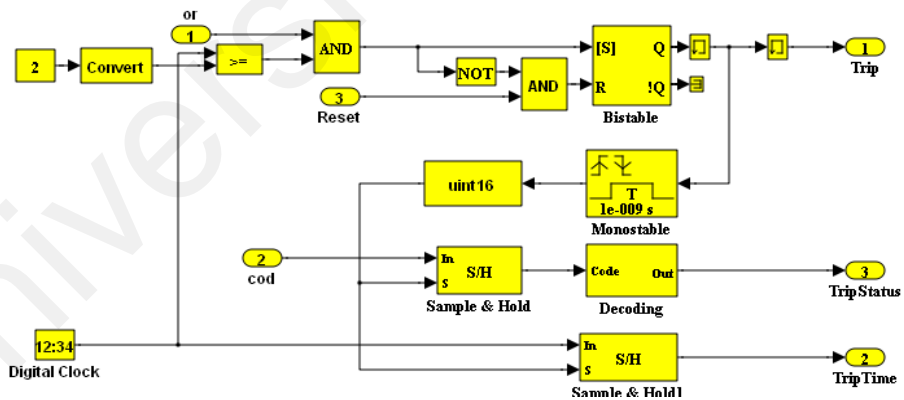


Figure 3.12: Fault detection and isolation unit implementation in Simulink

The overall unit that observes the location and time of the fault occurrence in the general data recorded is depicted in Figure 3.13.

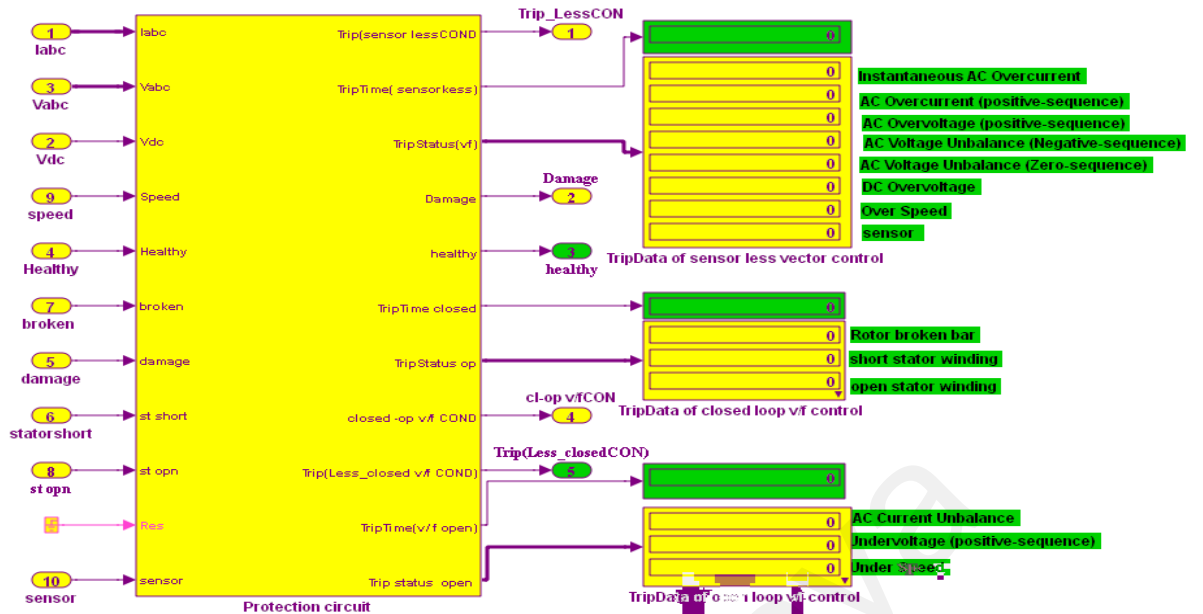


Figure 3.13: Trip data for the individual controllers executed in Simulink

When an insignificant level of noise is erroneously diagnosed or classified as a fault, the scheme changes back swiftly to sensor mode of vector control. Lastly, the occurrence of two or more faults at once activates the protection circuit. The recommended algorithm is simulated using the Digital Motor Control (DMC) blocks, owing to its ease of compilation from C through the Texas Instruments F28335 DSP. Figure 3.14 depicts its Simulink representation.

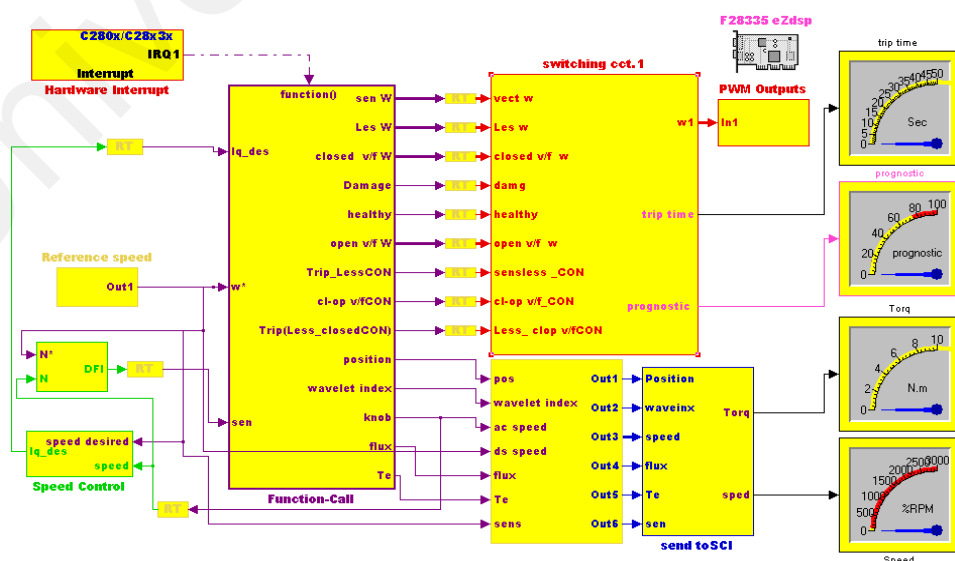


Figure 3.14: Simulink model of FTC scheme

The switching mechanism of the FTC depends upon any of the controller capability to accurately tackle the fault that is occurring at that instant. The vector control in the normal operation than in the closed-loop or open-loop in the low level of operation. The protection step would be the final step if all controllers cannot handle the operation in the satisfactory operation of the induction motor itself. The control scheme block diagram is shown in Figure 3.15.

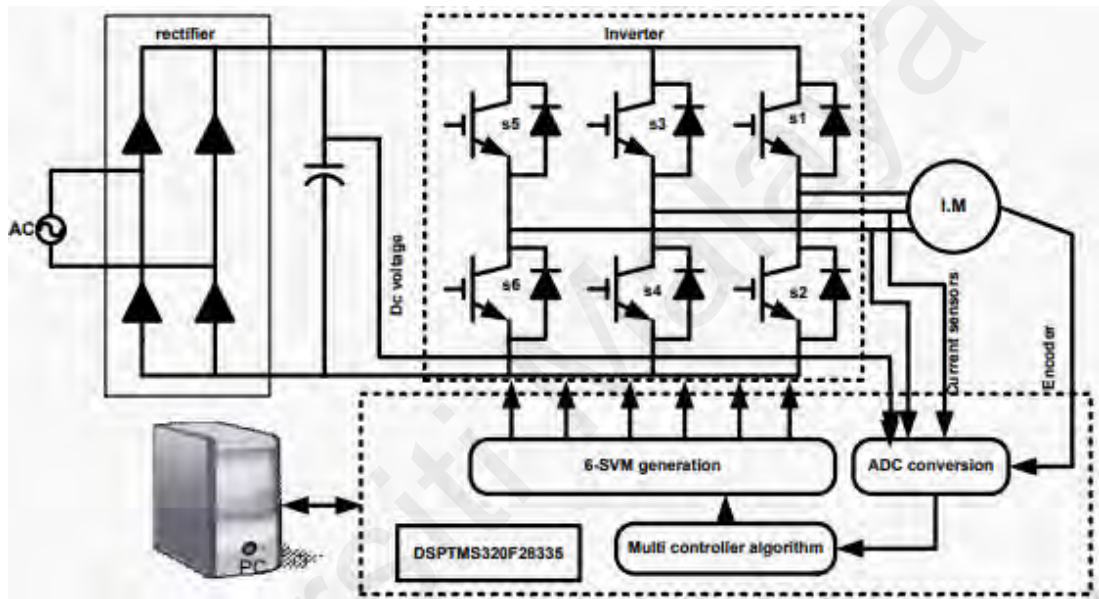


Figure 3.15: Multisensory control scheme block diagram

The formation of synchronization is achieved due to the interswitching action between the exact controller that initiates the action of the wavelet index and SVM vector controller generation. Thus, the deployment of space vector PWM can be accomplished through the following equations. The derivation of voltage and angle can be achieved from expression (3.35) through (3.42):

$$\begin{bmatrix} v_d \\ v_q \end{bmatrix} = \begin{bmatrix} 1 & -0.5 & -0.5 \\ 0 & \frac{\sqrt{3}}{2} & -\frac{\sqrt{3}}{2} \end{bmatrix} \begin{bmatrix} v_{an} \\ v_{bn} \\ v_{cn} \end{bmatrix} \quad (3.35)$$

The reference of the voltage equation is represented in equation (3.36):

$$v_{refer} = \sqrt{v_q^2 + v_d^2} \quad (3.36)$$

The calculation of the angle is carried out using equation (3.37)

$$\alpha = \tan^{-1} \left(\frac{v_q}{v_d} \right) \quad (3.37)$$

The time span can be computed in accordance with the expressions (3.38) to (3.42).

$$T_1 = T_2 a \frac{\sin\left(\frac{\pi}{3} - \alpha\right)}{\sin\left(\frac{\pi}{3}\right)} \quad (3.38)$$

$$a = \frac{|v_{refer}|}{\frac{2}{3} v_{dc}} \quad (3.39)$$

$$T_z = \frac{1}{f_z} \quad (3.40)$$

$$T_2 = T_z a \frac{\sin(\alpha)}{\sin\left(\frac{\pi}{3}\right)} \quad (3.41)$$

$$T_0 = T_z - (T_1 + T_2) \quad (3.42)$$

The switching time for the six portions can be measured, as depicted in Figure 3.16.

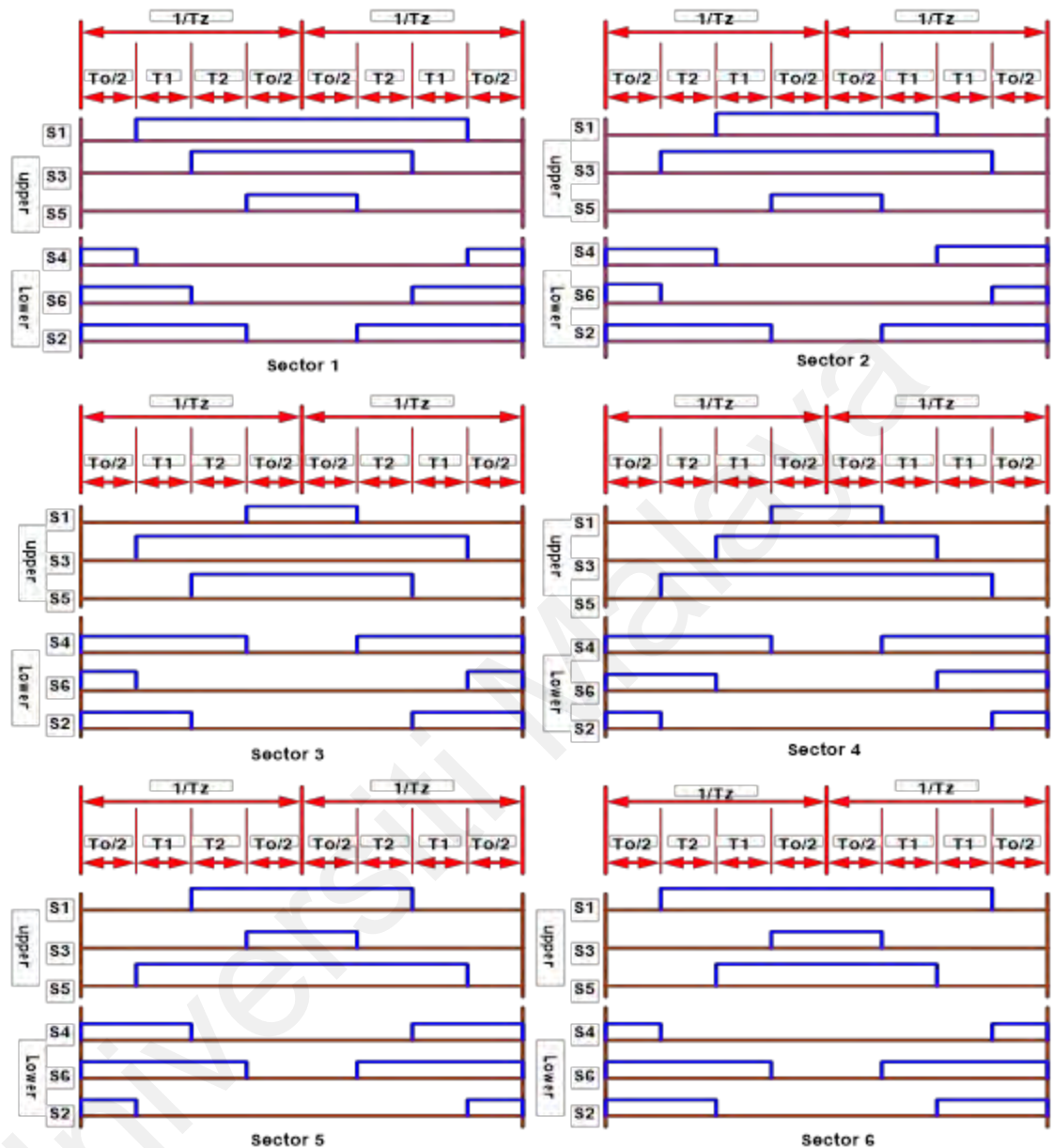


Figure 3.16: Switching fashion for the space vector PWM

The combination of phase magnitude responses, with an impulse response of 20kHz at each level, generates the sampling frequency. Figure 3.17 shows the magnitude of the first low pass filter implementation, while Figure 3.18 shows the last magnitude and phase of high pass filter.

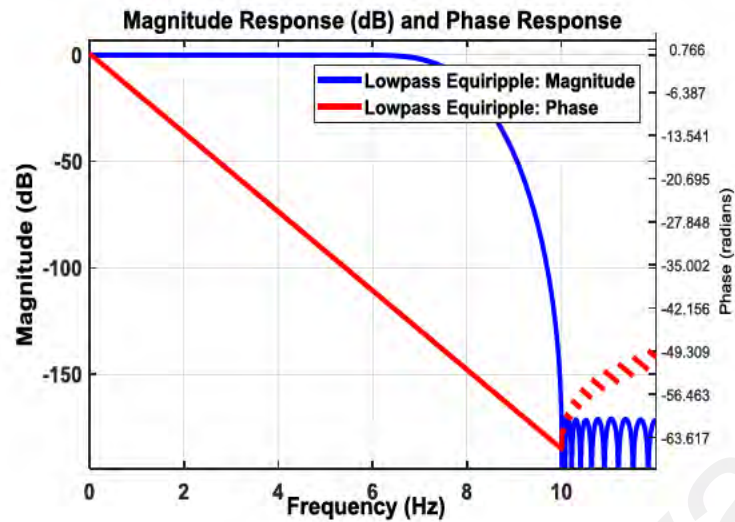


Figure 3.17: Low pass filter (0-10) kHz magnitude and phase response

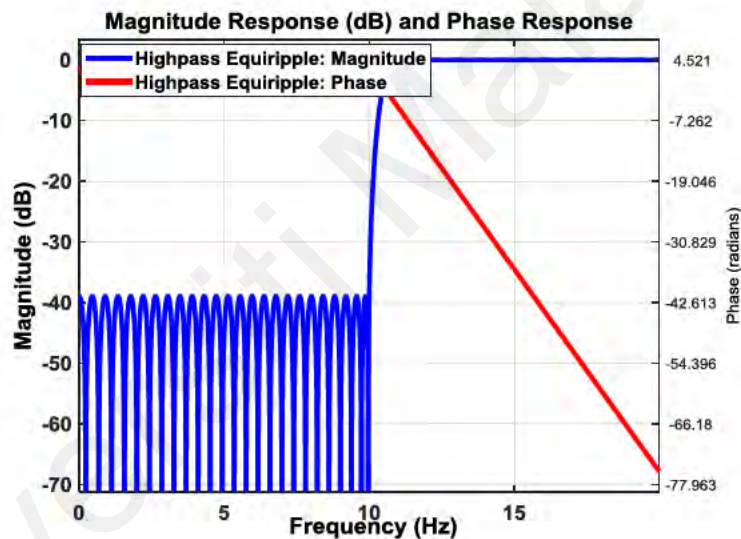


Figure 3.18: High pass filter (9.76-19.5313) Hz magnitude and phase response

The condition for detecting a fault in an IM is among the critical stages in diagnosing the fault. The processing of the faults requires satisfying certain condition, specified by the designed wavelet index. In this case, the condition is attached directly between the wavelet index with maximum detail (d8) and the original stator current (I_s). The detail step by step of the multisensory control technique, that renders its construction almost indestructible, is shown in Figure 3.19.

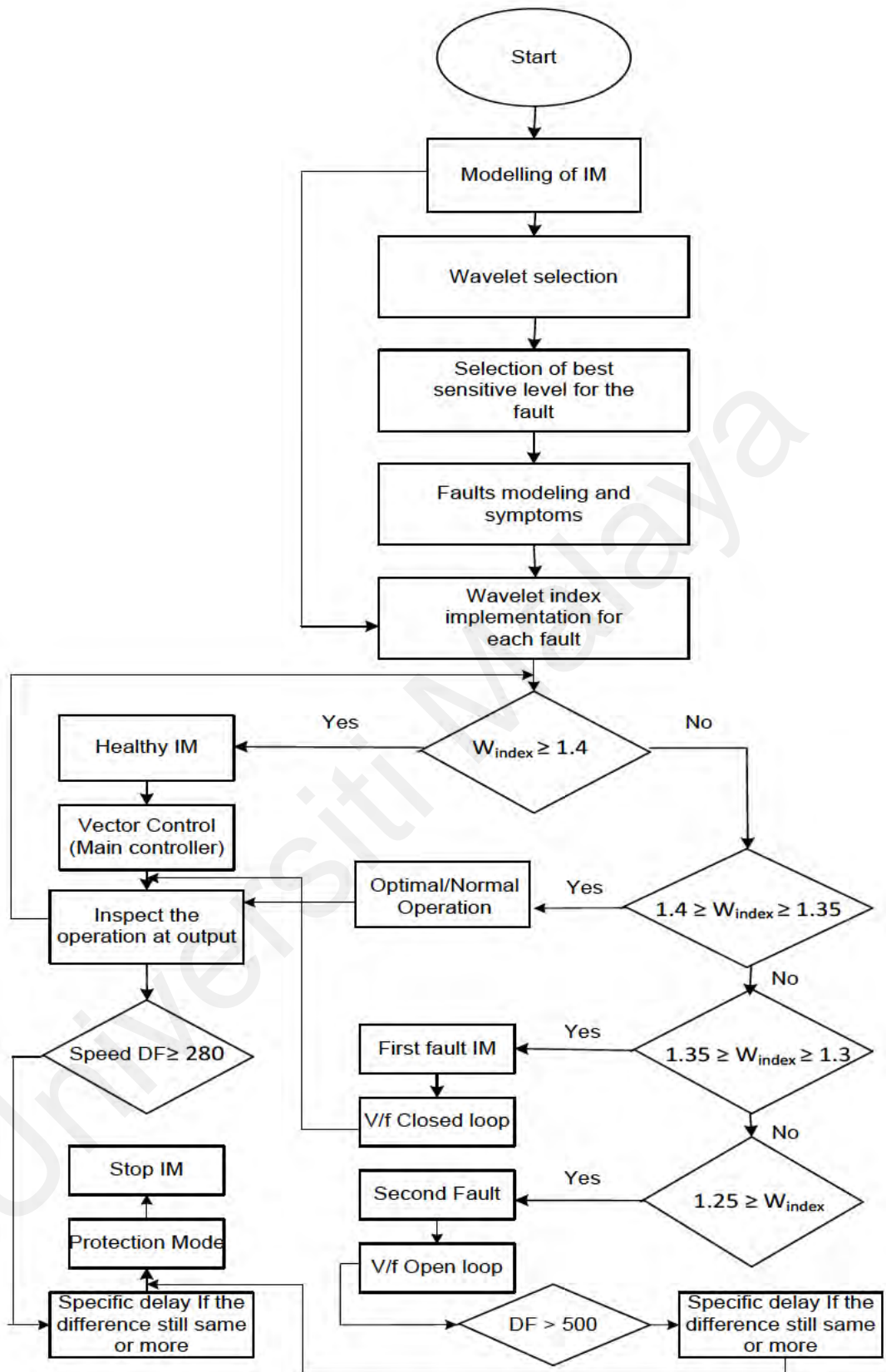


Figure 3.19: FTC Strategy flowchart using the multisensory control technique

3.3 Summary

This chapter has presented two distinct frameworks of protection techniques for DFIG and the IM drive. Protecting the power converters was focused and emphasized in the former, whereas the general protection against damages during fault events is offered to the later. In the DFIG, the underlying philosophy was to replace the traditional crowbar with the digital one. A novel digital protection for RSC and GSC has been elaborated by processing the d-q-axis current factors with the WPT. The d-q WPT-based digital protection algorithm is embedded within the main PI-VC controller, which offered simple implementation with minimal computational burden. Similarly, in the induction motor, wavelet approach has been developed for the fault diagnosis. To ensure a safe and uninterrupted operation of the motor, an enhanced model adaptive reference control is employed to improve the operational efficiency of the motor, which is based on multisensory scheme.

CHAPTER 4: : RESULTS AND DISCUSSION

4.1 Introduction

This chapter presents the simulation results of the DFIG, operating under various fault scenarios in the stator and the rotor of the machine. The absorption of reactive power from the grid during the crowbar action will be examined under the traditional Proportional Resonant (PR) control and the robust H-infinity (H_∞) control optimization technique, to compare their performance, basically the grid distortion rejection capacity. Computer simulations in MATLAB/Simulink have been carried out for evaluating the effectiveness of the wavelet-based protective scheme features. In a similar study, a complete simulation and experimental result of the induction motor drive are presented. The combination of multisensory and enhanced model reference adaptive system fortified the drive and makes it more fault tolerant. Also, wavelet approach has been developed for the fault diagnosis of the induction motor.

4.2 Platform of Simulation Studies and Results for the DFIG

A system of 1.5 MW, 690V, 50Hz DFIG wind conversion system (Hamon, Elkington, & Ghandhari, 2010) (Abad & Iwanski, 2014; Camille, 2010), is simulated in MATLAB Simulink. To show the efficacy of the proposed wavelet diagnosis technique employed as a RSC and GSC protection scheme, which is implemented under both Proportional Integral (PI) and H_∞ control systems. The RSC and GSC are modelled mathematically as ideal switches, hence no losses or harmonics are anticipated. Regarding the objective of examining the effectiveness of the digital protection based on d-q WPT, in the detection and accurate clarification of faults, 3 – Φ currents were taken from the simulated DFIG, at the rotor and the stator under various fault scenarios and non-fault events. The MATLAB codes was developed and executed to read 3 – Φ current data to compute I_d

and I_q , which are then applied to the half-band digital HPF $h[n]$ to extract the salient features in Y_{dq} .

The I_d and I_q obtained from the proportional integral vector controller (PI-VC) are taken and employed as inputs to the d-q WPT-based digital protection. The output of the d-q WPT-based digital protection was a trip signal. The trip signal was then sent to a digital-to-analog (DAC). The port of the DAC is then linked with a three-channel opto-coupler driver circuit prior to its application on the TRIAC switches (S. A. Saleh et al., 2014). These TRIAC switches were employed to emulate a circuit breaker (CB) that connects between the rotor and the inverter. MATLAB simulink's predicted model block (PED) is employed to validate the wavelet detection units.

4.2.1 Simulation Results During an Open Circuit Fault in the Rotor Windings

The objective of this test was to study the feedback capability of the multiframe wavelet protection to the open circuit fault in the rotor windings. The d-q axis of the rotor currents is processed using the WPT, by extracting the high-frequency sub-band content of the detailed coefficients and convoluted, which will then decide to trip or not based on the value of $Y_{dq} \geq 0$.

An open circuit fault is applied at the rotor windings for about 3.5 seconds by creating an infinite voltage and 0 supply current at one of the rotor phases. The rotor winding faults is among the frequent occurring faults in wound rotor machine. Supposing a fault in the rotor winding, it is usually observed that the faulty position is also rotating with the rotor, thereby affecting other parameters in the generator. Figure 4.1 depicts the open circuit rotor fault and the fault is reflecting in either the direct rotor current I_{dr} or quadrature rotor current I_{qr} .

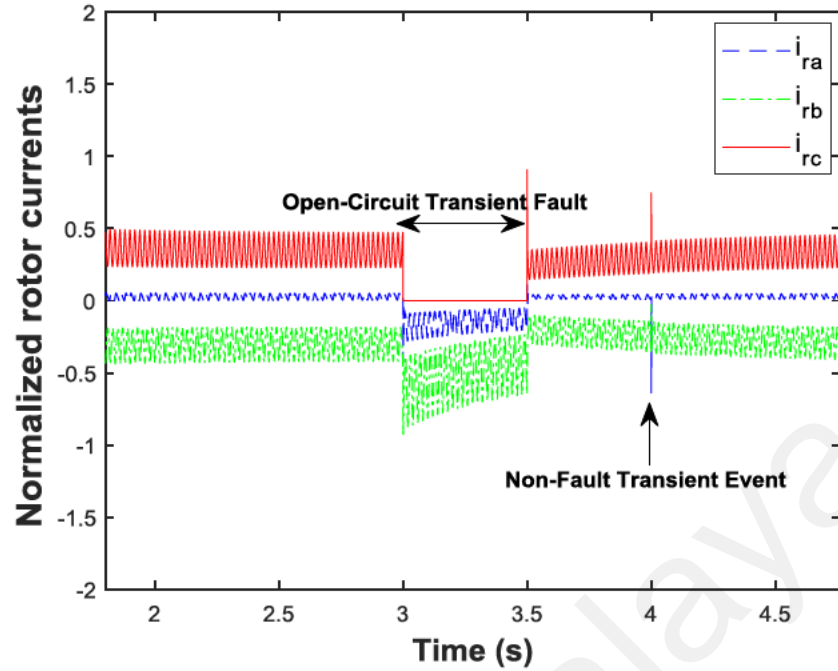


Figure 4.1: Simulation Response of 3-phase rotor current during the open circuit fault in phase A

It can be observed from Figure 4.1, that an interruption or discontinuity in one of the phases, the green phase, which occurred because of an open circuit fault in the phase due to control malfunctioning or from other sources in real-time machine operation. Additionally, voltage sags are introduced in the remaining two phases owing to the fault occurrence in one phase, which are related to the fault conditions as it lasted for more than half period. There are also impulsive transients that occurred on the remaining two phases, which can be because of load changes or switching of an inductive load.

Large current sag can be noticed in Figure 4.2(a) the direct-axis rotor current I_{dr} in addition to its sag also the sag along I_{qr} as in Figure 4.2(b) combined, using the unbiased method $X_{dq} = I_{dr}^2 + I_{qr}^2$ will lead to a nonzero value of Y_{dq} triggered by the fault.

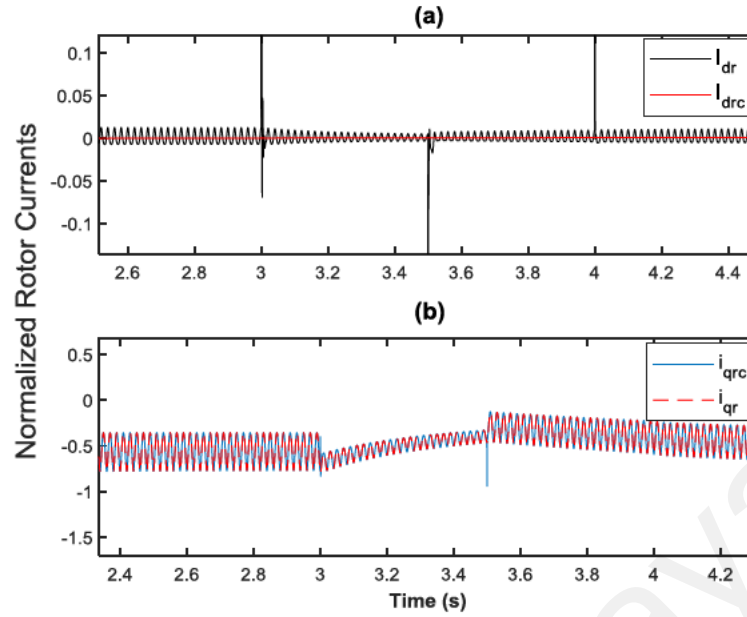


Figure 4.2: Simulation Response of the direct and quadrature axis rotor current during the rotor open circuit fault

A significant voltage sag is observed in the quadrature rotor current i_{rq} shown in Figure 4.2, which is a low voltage for more than half period, and as such would be classified by the WPT as a fault scenario.

A sag can be seen in the quadrature rotor currents, which is a brief decrease in currents for more than half period and can then be classified as a fault caused by the open circuit or outage in one of the phases this can lead to the value of $Y_{dq} > 0$.

4.2.2 Simulation Results During a Short Circuit Fault in the Rotor Windings

Applying a short-circuit fault in the rotor is to cause a 0-supply voltage and infinite flow of current in any one of the rotor phases, this type of fault is more severe and therefore protective measures are mostly implemented against this type of fault to prevent damages, to the fragile components in the system, such as power electronic devices particularly the (RSC). Figure 4.3 shows the simulation results of short-circuit fault in the rotor of the DFIG. It is seen that a high inrush and uncontrollable current, will flow at the rotor circuits, towards the RSC, hence of the TRIAC crowbar switch will be activated to

prevent damages to the converter. In this case the $Y_{dq} > 0$ and therefore classified as a fault event.

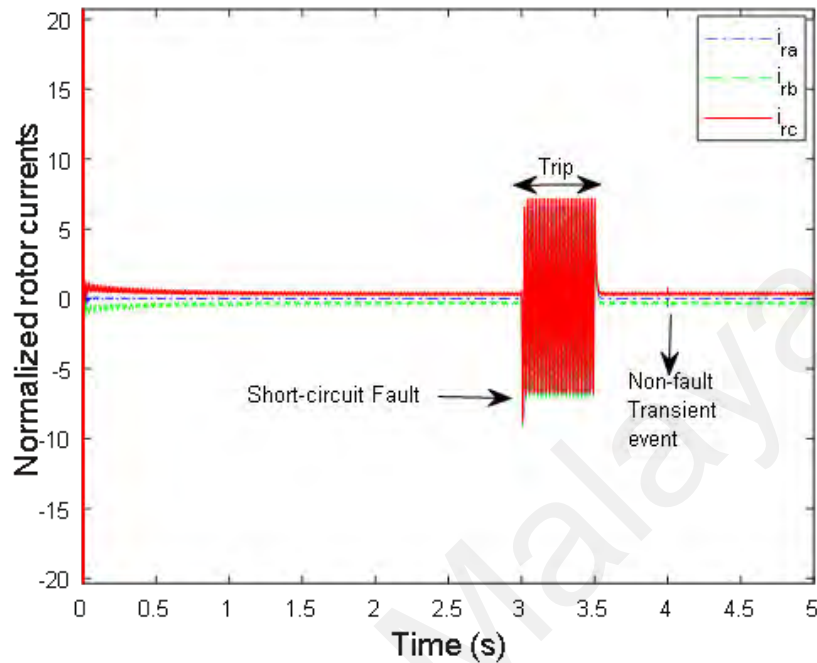


Figure 4.3: Simulation Response of the Three-phase Rotor Current during Short-Circuit Fault

Considering a wound rotor machines, the faulty position is as well moving with the rotor, thus affecting the other two phases by introducing voltage swells and slight fluctuation Figure 4.4a in I_{dr} and Figure 4.4b shows I_{qr} to be relatively stable. As mentioned earlier such type of fault scenario is realized by making the resistance value of the short-circuited phase/path approximately zero. The anomaly in the phase will then be determined by the windowing capability of the wavelet to classify it as a real fault or just a momentary impulsive transient. As seen from Figure 4.4a, an impulsive transient occurred at two periods of the rotor operation, which has nothing to do with fault but rather due to load changes or speed changes. thus, leading to the value of the convolution equation of Y_{dq} to be approximately zero.

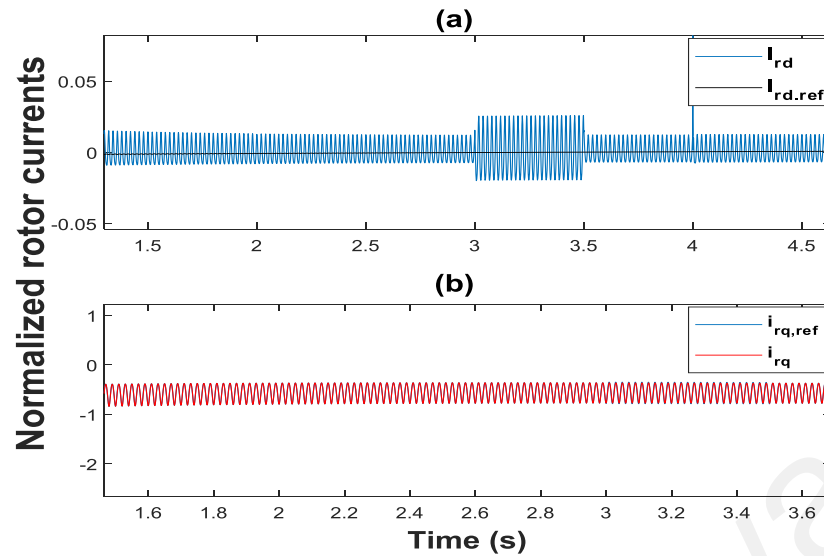


Figure 4.4: Simulation Response of the direct-quadrature Rotor Current during Short-Circuit Fault

The swells appearing at the direct-current level is due to the occurrence of the short circuit fault in one or more phases or windings of the rotor. This type of fault can easily lead to the current surge, at the rotor side, that can be hazardous and cause damage to the RSC. The swells appeared at the current level owing to the increase in the rms line-voltage for about 110 to 180 percent of the nominal line-voltage for the duration of 0.5 cycle to 1 minute.

4.3 Non-Fault Transient Events in the Rotor Circuits

In this section the transients that occurred, which are not connected to any of the faults common in DFIG-based WECS are discussed. Thus, the events such as rotor speed changes, wind speed changes that causes flickers are introduced. These events are associated with a momentarily or short-lived transient, that causes no damage or significantly affect the machine's normal operation.

4.3.1 Transients due to the rotor speed changes.

The changes in the speed rotor is often characterized with a transient phenomenon, although, is not related to fault but some signal processing techniques based on Fourier

transform cannot be able to classify it as non-fault events, rather it will also be classified as a fault event. The rotor speed changes were emulated by implementing a step changes to the speed of the rotor in rev/sec. Figure 4.5, shows the simulated result of the rotor speed changes.

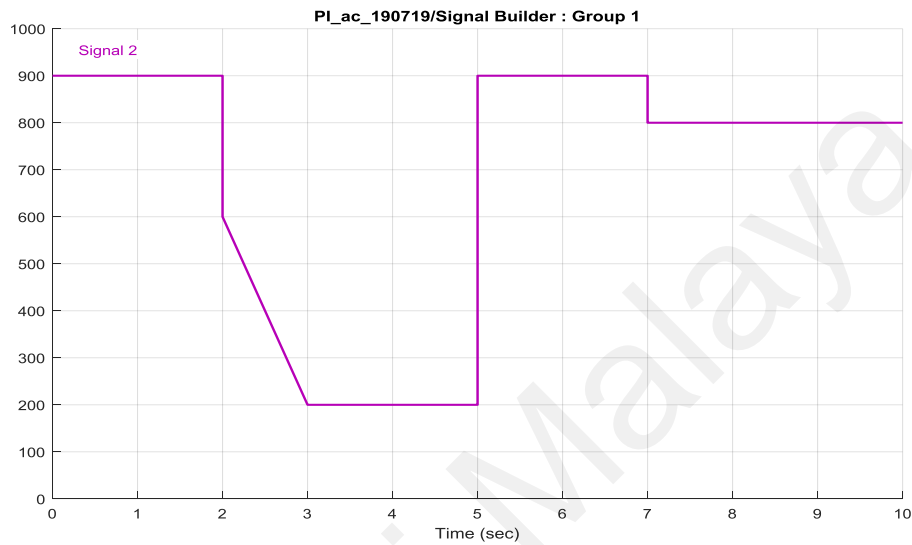


Figure 4.5: Simulation of the Wind Speed Changes

4.3.2 Flickers in the Rotor Owing to the Wind Speed Changes.

Variations in wind speed was simulated by applying step changes to the load torque T_L of the DFIG system, during which a transient phenomenon was observed, and the d-q wavelet protection classify this as non-fault events, unlike the DFT which will deemed it as a real fault occurrence.

It is seen from Figure 4.6, that because of variable wind speed affected the operation of the wind turbine, which in turn translated as a voltage fluctuation by the electromagnetic torque and appeared as a short duration and repetitive fluctuation on the voltage level. This non-fault event was simulated in the MATLAB using the signal builder function and often refers to as flickers.

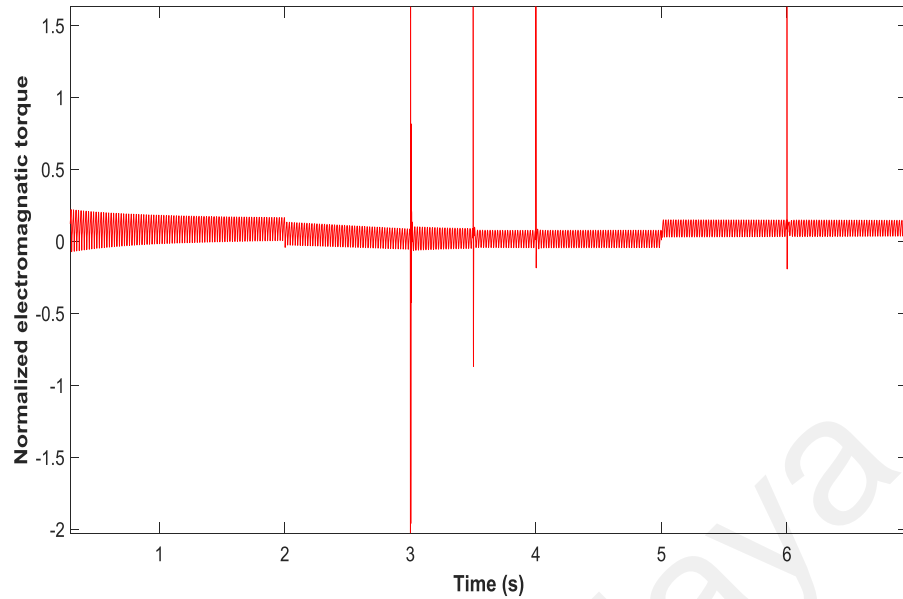


Figure 4.6: Simulation Response of wind Variation in DFIG with Flickers

4.4 Transient Fault Events in the Stator Circuit

The stator of a grid connected DFIG is subjected to a number of fault scenarios, ranging from phase-ground, phase-phase or short and the open circuit faults. As the stator is directly connected to the grid in the common topology, any of such fault in the grid phases will have direct impact on the stator of the generator. Therefore, this section presents the common types of transients' fault that may as directly in the stator circuit or indirectly at the utility grid.

4.4.1 Simulation Results During an Open Circuit in the Stator Winding/Grid

The case of an open-circuit event in the stator was emulated in one of the grid phase using maximum voltage and zero supply current principle, and was studied by collecting the three-phase currents taken by the simulated DFIG to the wavelet circuit, which will then be converted to direct-quadrature current in the form of I_{ds} and I_{qs} and applied to the wavelet circuit for onward processing.

One of the most frequent faults considering electrical machines are stator related fault. Simulation of such faults is achieved by connecting any of the stator phases, in such a way that its resistances path becomes infinite. In the first step one phase was open circuited. The response of the WPT is expected to discriminate between the outage in the phase for the substantial period, and the very narrow pulse for less than $0.5\mu s$, occurred perhaps because of load changes or utility switching both shown in Figure 4.7. This interruption is mainly caused due to the ground fault, which is mostly associated with open circuit fault.

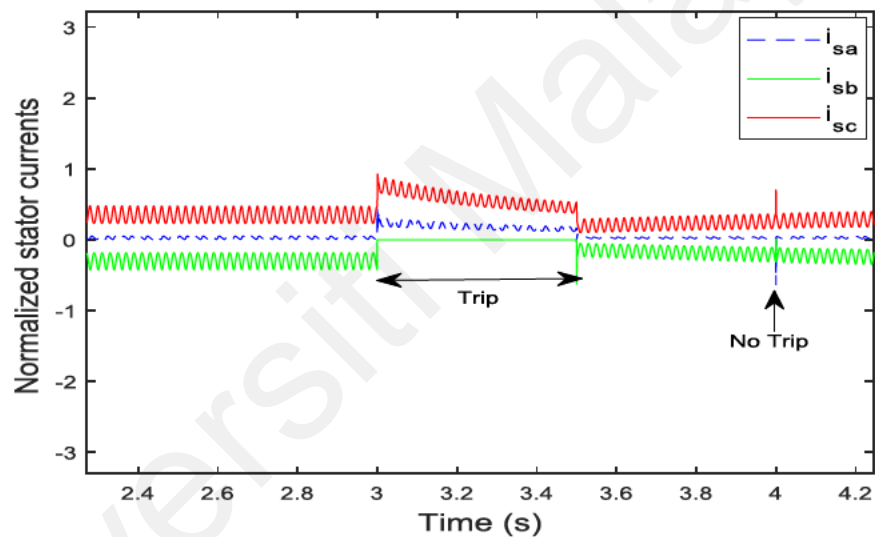


Figure 4.7: Simulation Response of the Three-Phase Stator Currents During an Open Circuit Test

The significant sag or low voltage is seen in the current level of the I_{qs} and I_{ds} shown in Figure 4.8(a) and 4.8(b) respectively, would certainly lead to a non-zero value of Y_{dq} and thus be classified as a fault scenario, which would then transmit a trip signal to the TRIAC switch of the affected phase.

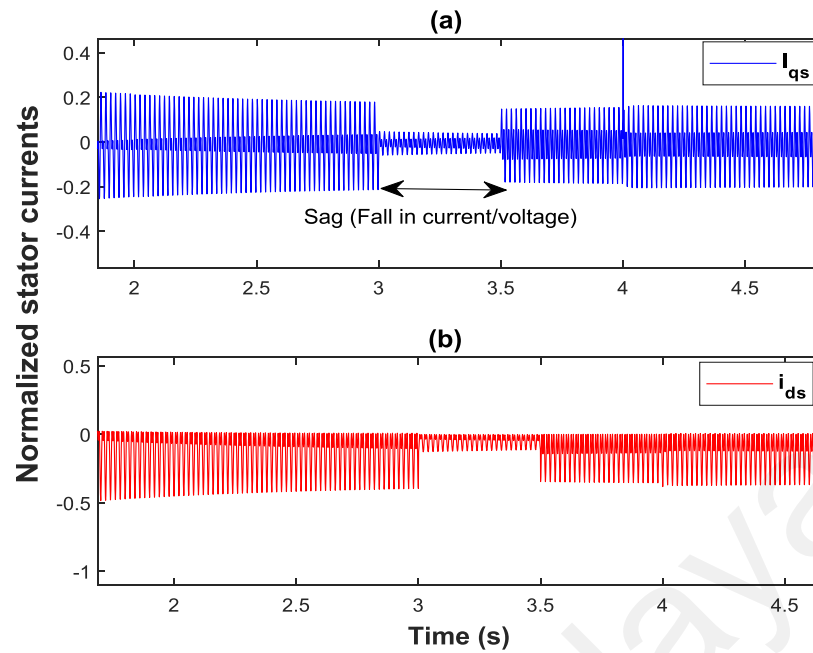


Figure 4.8: Simulation Response of the direct-quadrature Stator current during an Open Circuit Fault

Meanwhile, the result of the three-phase stator current. I_{sa} , I_{sb} and I_{sc} , during the open circuit fault is shown in Figure 4.9. It can be seen from the figure in addition to the open circuit fault, it also depicts speed and load changes, in which after the transformation to the $d - q$ components and applied to the algorithm is expected to discern between the open circuit fault and the changes due to speed and load.

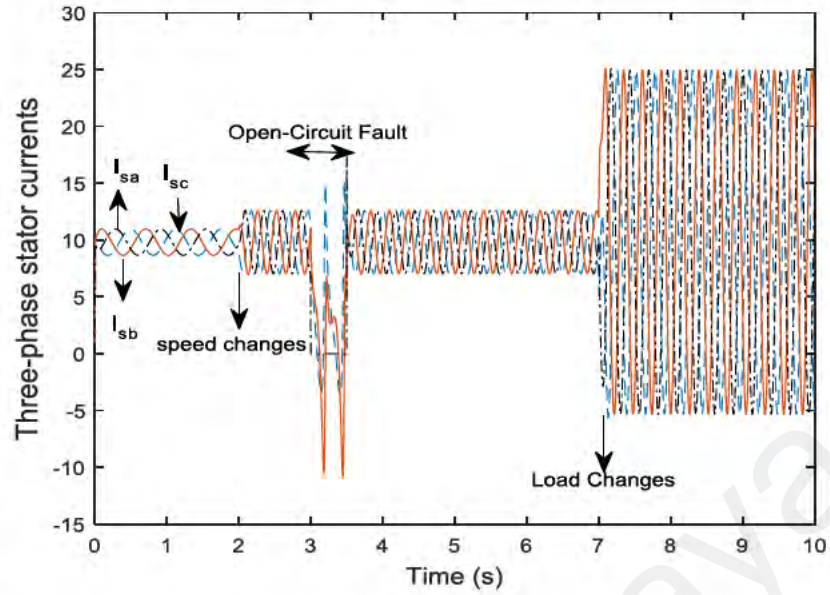


Figure 4.9: Simulation Response of the Three-phase stator current during an open circuit fault

4.4.2 Simulation Results During a Short Circuit in the Stator Windings or in the Grid.

For the short circuit winding faults, the stator resistance of the DFIG is connected, in such a way to gradually reduced its value to zero, the formula in equation (4.1), is usually applied, in order to achieve the zero-resistance value in the stator winding. The severity of the short circuit fault is observed to have high index and can cause serious damages to the power electronic devices incorporated in the topology, thus the value of $Y_{dq} > 0$.

$$R_{sh} = 0.1R_{org} \quad (4.1)$$

In addition to the fault occurrence shown in Figure 4.10, there are three non-faults events that occurred in the grid owing to the load changes and the starting of large inductive loads. The first two are the spikes and the last one is representing a dip. The phaselet can distinguish between the actual faults and the three non-fault events due to its feature extraction capacity and based on the classification of the convolution technique $Y_{dq} = 0$.

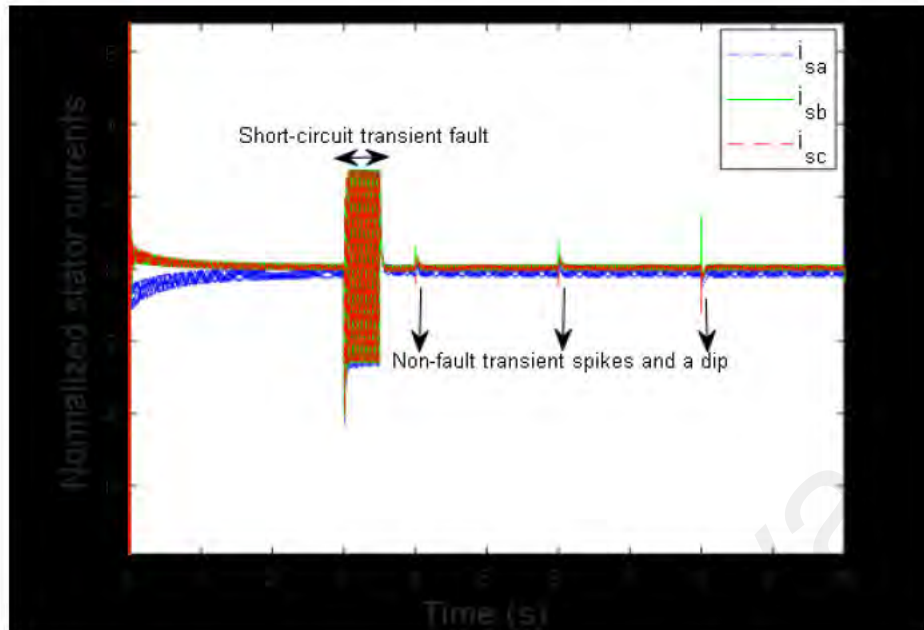


Figure 4.10: Simulated Response to the short circuit fault in the Stator of the generator with Spikes and Dips

Similarly, the result of the short circuit fault test, performed on the offline simulated DFIG, is illustrated in Figure 4.11. The Y_{dq} convolution function demonstrated insensitivity to the various speed and loading levels. On the other hand, it readily detects the transient distortion owing to the fault occurrence. This is because of the extraction of high frequency subband by the Y_{dq} algorithm, which possess a nonzero value.

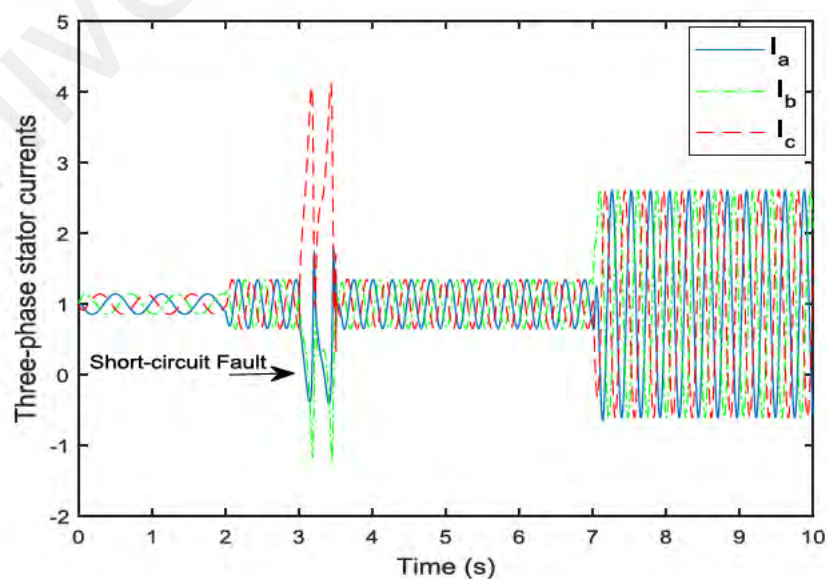


Figure 4.11: Simulation Response of the Direct-axis Stator Current during the Short Circuit Fault

The I_{qs} and I_{ds} in Figure 4.12 (a) and (b) respectively, obtained from the proportional integral vector-control PI-VC were employed as the inputs to the d-q WPT-based digital protection, the output of the d-q WPT-based digital protection was a trip signal when the fault severity becomes high and cannot be controlled. The spike in the result is related to the non-fault event, therefore the digital protection using the WPT can successfully distinguish and trip only when its fault.

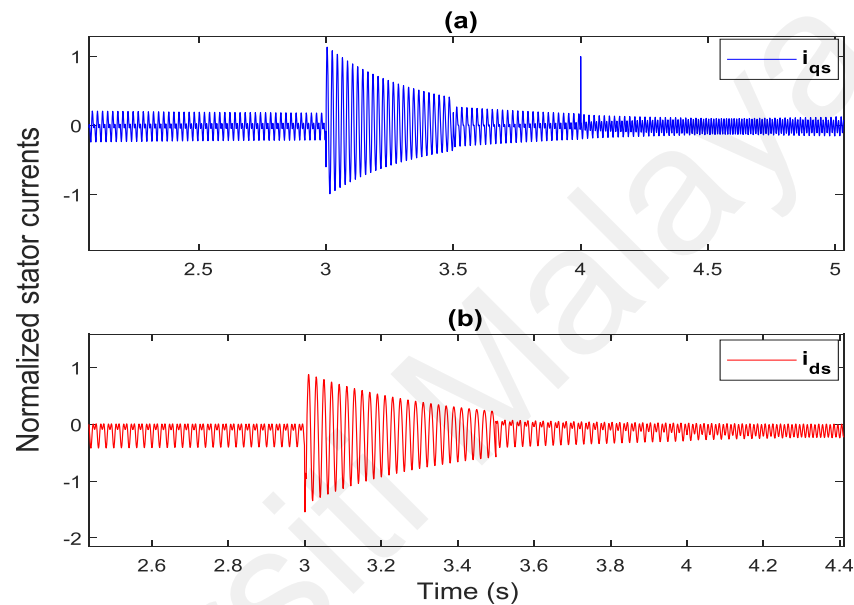


Figure 4.12: Simulation Response of the direct-quadrature Axis Stator Current during the Short Circuit Fault

The objective of this test is to demonstrate the ability of the wavelets to distinguish between short circuit fault of different magnitude and the step changes such as load and speed changes. It can be seen from Figure 4.13 and 4.14, that the detail coefficients have significant value, well above the zero-mark depending on the short-circuit loop. On the other hand, for the case of load changes and speed changes the details have a zero value, which will lead to the value of $Y_{dq} = 0$ after the convolution. The trip signal is generated owing to the high value of Y_{dq} , resulted by the energy concentrated in the high-frequency sub-bands of I_d and I_q , which experienced transient components due to the short-circuit fault.

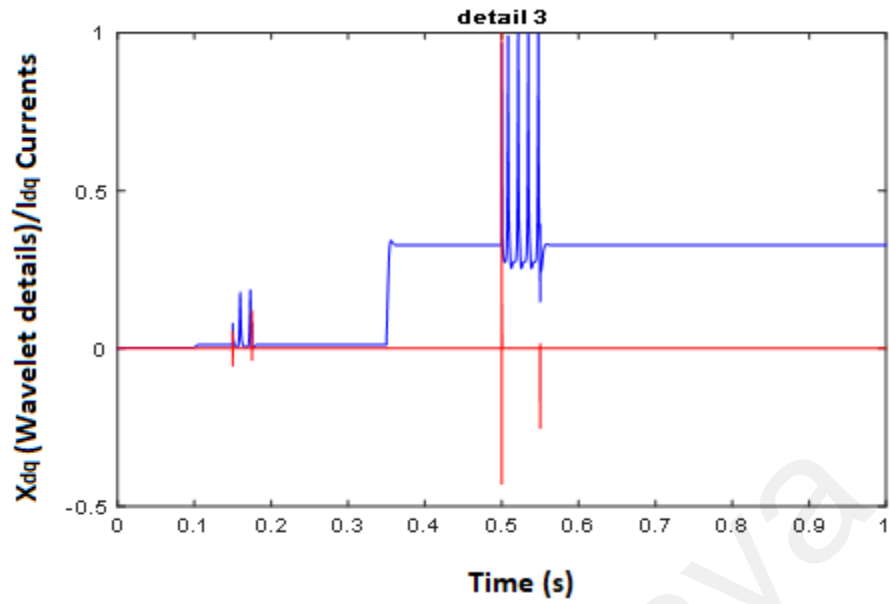


Figure 4.13: Simulation Response of the d-q WPT Digital Protection and its Localization Ability

The value of the details for the short circuit faults is very significant in magnitude as the red vertical line indicates, this will certainly lead to the $Y_{dq} > 0$, and therefore classified as a fault scenario, this is depicted in Figure 4.14.

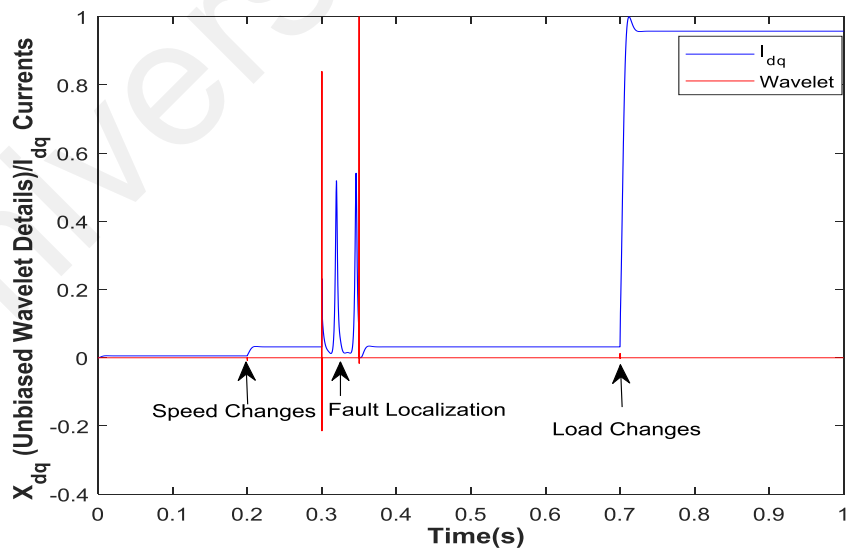


Figure 4.14: Simulation Response of the d-q WPT and its Localization Effects on the Fault

4.5 Non-Fault Transient Events in the Stator Circuits

The stator of the DFIG is also prone to external disturbances that are taking place at the utility grid, in addition to the actual transient faults. These external disturbances include white Gaussian noise, inductive load changes that are usually associated with momentary transients that cannot be classified as faults. This section describes this non-fault transient phenomena occurring at the grid coupled with DFIG.

4.5.1 White Gaussian noise in the grid

The design of standard power grids and the addition of decoupling capacitance has become of paramount importance, to control power-grid-induced noise. The connection of DFIG-WECS may introduce some undesirable noise as in Figure 4.15, that may not be due to the fault occurrence and need to be eliminated using the wavelet filters. Thresholding is a process in which certain wavelet coefficients are modified to attain denoising of the contaminated signal, while still preserving the essential features of the signal.

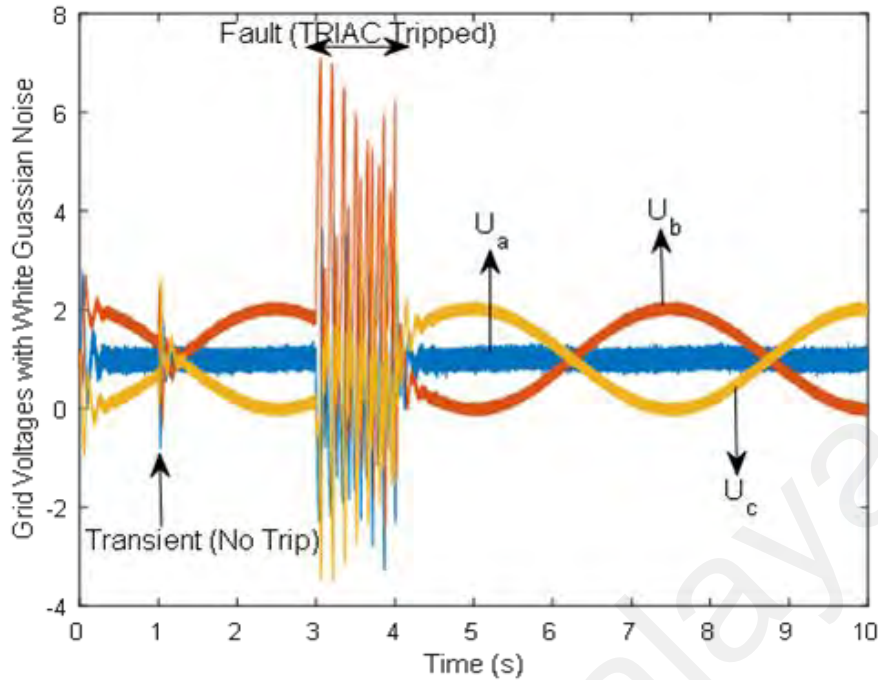


Figure 4.15: Simulation Response to the Injected Noise to a Grid connected to the Stator of a generator

In this process, the assumption is that the data collected from the grid voltage signal is of the form $v = u + noise$, where v is the received signal that is contaminated with noise and u is the actual grid signal. The noise was assumed to be random and that $|noise| < k$ for some constant k . In other words, the noise is uniformly bounded on both sides of the actual signal. As an example, the noise is induced to the grid, from the MATLAB white Gaussian noise function, and the objective here is to mitigate the effect and recover the original grid signal u .

Since the actual signal u is mostly constant, it is expected that the majority of detail coefficient to be 0. However, the added noise makes many of the data entry values small, but nonzero. If thresholding is applied to eliminate what appeared to be the added noise as in Figure 4.15, it is desired that the signal u be retrieved, after applying hard

thresholding with a tolerance $\lambda = 0.0075$ and reversing the processing it is possible to obtain the denoised data.

Since the actual signal u is generally constant, most of the detail coefficients are expected to be zero. Nevertheless, the induced noise makes many of these signal entries small, but nonzero. If thresholding is applied to eliminate what appeared to be the induced noise, the original signal u should be recovered.

4.5.2 Voltage Spikes and Dips

Different components and elements in distributed energy sources may be exposed to several transient disturbances, which can be initiated by fault and non-fault conditions. A short (momentarily) outage or spikes would not noticeably affect large generator and motors but could cause major damages to digital clocks and general electronic devices. The objective of this test is to examine the response of the WPT based digital protection to step changes i.e. transients occurring in the rotor and stator that are not related to fault scenarios.

The spikes and a dip as shown in Figure 4.16, occurred mostly as a result of switching surge or impulse produced by load changes or speed changes in the system. Following these changes, there is an immediate readjustment of the potential differences and currents in most part of the system. Such readjustments take place very quickly, and the corresponding momentary fluctuations of the current are the transients.

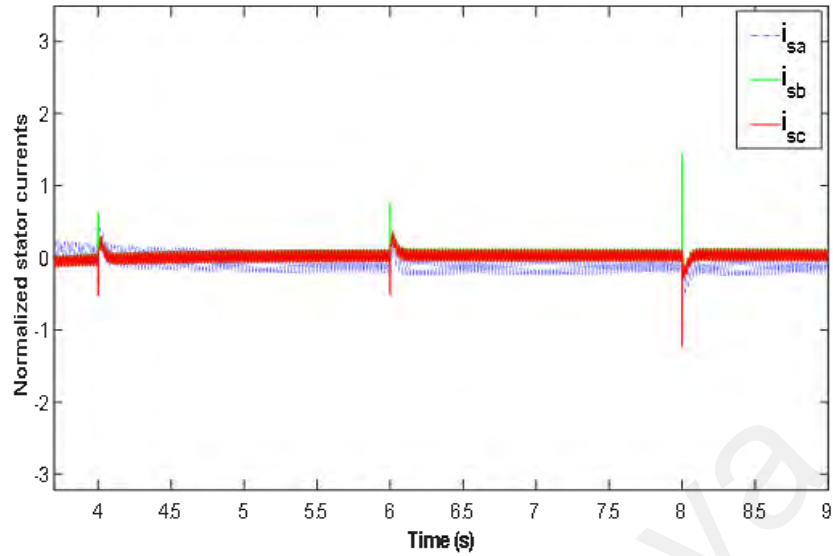


Figure 4.16: Simulation Response of the Non-fault events, such as the Spikes and Dips at the grid during the DFIG Operation

The modelling of voltage spikes and dips that will subsequently be reflected at the current level was performed mathematically by applying the impulse response expression for the spikes as in equation (4.2);

$$s(t) = f(t) \cdot e^{-(\lambda t + \delta)} \quad (4.2)$$

Where λ : decay rate

δ : time shift

$f(t)$: step function

$$f(t) = \begin{cases} 0 & \text{if } t < \delta \\ \sigma & \text{if } t > \delta \end{cases}$$

Whereas the dip can simply be modelled by negating equation (4.2) as in expression (4.3);

$$s(t) = -f(t) \cdot e^{-(\lambda t + \delta)} \quad (4.3)$$

Table 4.1 summarizes the hypothetical digital crowbar comparison with the traditional crowbar and algorithm based on discrete Fourier transform (DFT) algorithm.

Table 4.1: Comparison of the proposed techniques and existing ones

Subject	Conventional Crowbar	DFT	$d - q$ Wavelet
Restoration time	μ minute	45.8ms and above (S. Saleh et al., 2012)	7.1ms
(VAR) Absorption	High	minimal	least
Inputs	I_{ar}, I_{br}, I_{cr} (by measurement)	I_{ar}, I_{br}, I_{cr} (by measurement)	I_{dr} and I_{qr} from the rotor side controller
Sensitivity to generator's parameter variations	Susceptible	Susceptible	Immune
Effect of harmonics distortions	Susceptible	Susceptible	Immune
Magnitude of transient fault current	Susceptible	Susceptible	Immune
Implementation	Hardware	Digital	Digital

4.6 Mitigation of Grid Reactive Power with H_{∞} Optimization

As mentioned earlier during the grid fault, the crowbar is activated to protect the RSC, by inhibiting its operation and thus isolates the RSC from the DFIG rotor (W. H. Huang, Huo, Hu, & Xu, 2013). This action causes the machine to draw reactive power from the grid, because it is transformed into a regular induction machine. This condition prevails at the instant when the grid is in desperate for the reactive power. During these faulty conditions and as a result of the reactive power compensation equipment, the grid experiences severe perturbations and voltage/current distortion, especially when working under proportional resonant-vector (PR-V) control. In order to minimize these perturbations as well as the absorption of the reactive power from the grid, H_{∞} robust

control has been remarkably implemented in many electrical control areas such as voltage source inverters (VSI) (Gryning, Wu, Blanke, Niemann, & Andersen, 2015). As an advanced control technique, the controlled system of the H_∞ robust control is uncertain and can be multi input multi output (MIMO) framework.

This section introduces the H_∞ robust rotor controller, developed for the DFIG based WTs to achieve the suppression of perturbations and distortions, minimizes absorption of the grid reactive power and the interruptions at the rotor of the machine, during crowbar traditional protective action.

Based on the common DFIG model in the time domain (Muller et al., 2002), a 4th order generator model at the synchronously rotating dq frame can be represented by the state space equation in (4.4).

$$\begin{cases} \dot{x} = Ax + [B_1, B_2][u, d]^T \\ y = Cx + Du \end{cases} \quad (4.4)$$

Where $x = [i_{ds} \ i_{qs} \ i_{dr} \ i_{qr}]$, $y = [i_{dr} \ i_{qr}]$, $u = [u_{dr} \ u_{qr}]$ and $d = [u_{ds}, u_{qs}]$. All parameters and variables are converted into the nominal system and the parameters are in form of matrixes (Y. Wang et al., 2016).

It can be seen from Figure 4.17, that the performance of the H_∞ controller is not much affected by the parameter perturbations or current distortions owing to fault occurrence. Under the H_∞ control a good tracking performance is indicated in Figure 4.17, and robust stability when there is parameter perturbation and voltage/current distortion.

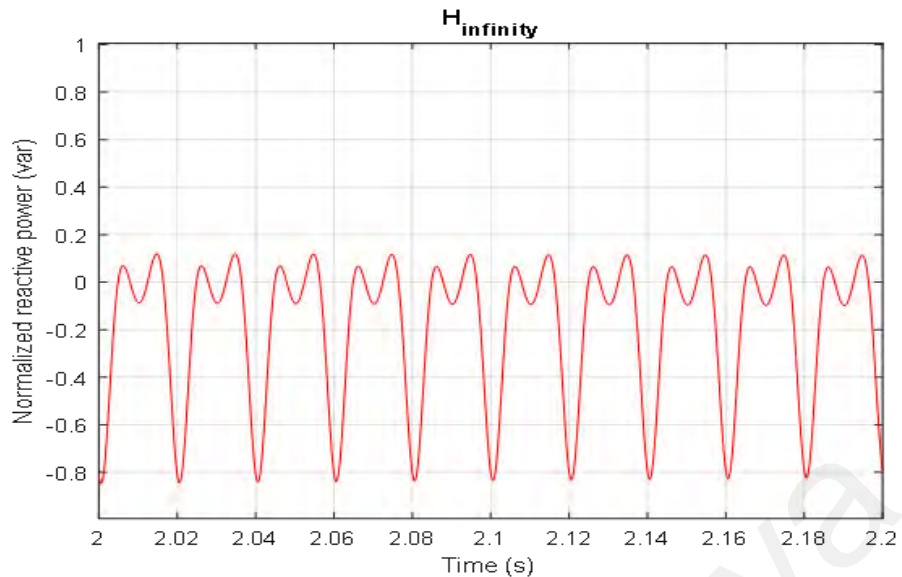


Figure 4.17: Simulation Response of Reactive Power under H_{∞} Control Optimization

While in Figure 4.18 the proportional integral plus resonant (PIR) controller, the reactive power control performance is certainly influenced by the voltage distortions. Under the fault conditions, the stability and robust performance of the H_{∞} controller is observed to be superior to that of (PIR) controller, because the weighing functions are formed to accurately track the unbalance current components.

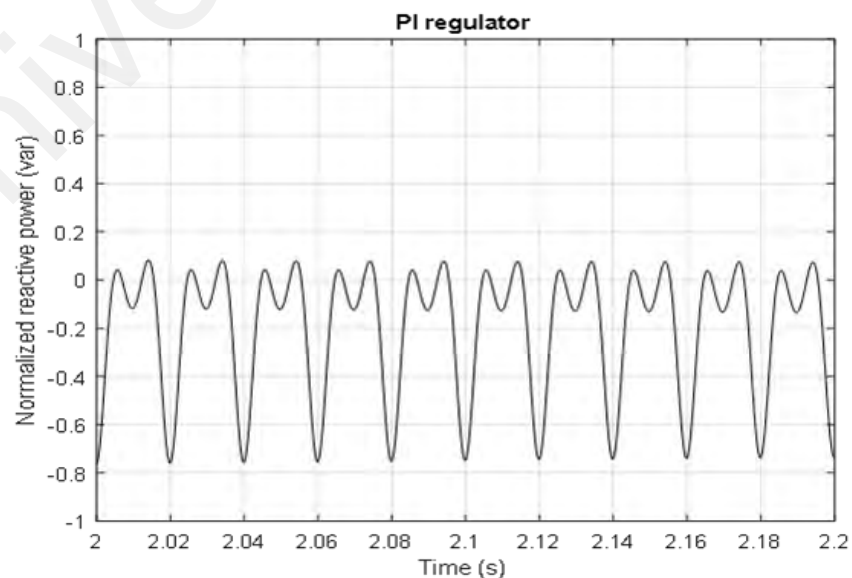


Figure 4.18: Simulation Response of Reactive Power under Classical PI-Vector Control

The DFIG is more vulnerable to grid voltage and the impact is more severe. The system robust stability (RS) and robust performance (RP) can be made reliable by adding the H_∞ standard to restrict all the tendencies of the uncertain system into a bound (Djukanovic, Khammash, & Vittal, 1998; Doyle et al., 1989).

The grid voltage disturbances during fault and non-fault events can be described by the H_∞ norm. The H_∞ norm means the maximum amplitude or energy from any input variable to the output variable of MIMO system (Y. Wang et al., 2016). The wind speed is set as a constant of 15ms^{-1} , and the reactive power reference was set as 0.

4.7 Results and Discussion for the Induction Motor

The backbone of the experimental outline of the IM drive is supported by DSP TMS320F28335. The processing of the stator current signal is achieved by the filter bank due to its upsampling and down sampling actions. The results of the healthy stator current of IM drive are presented in Figure 4.19. The short momentarily spikes are not related to fault occurrence. They occur only because of the sensitive nature of the wavelets, hence the high accuracy in classifying a fault.

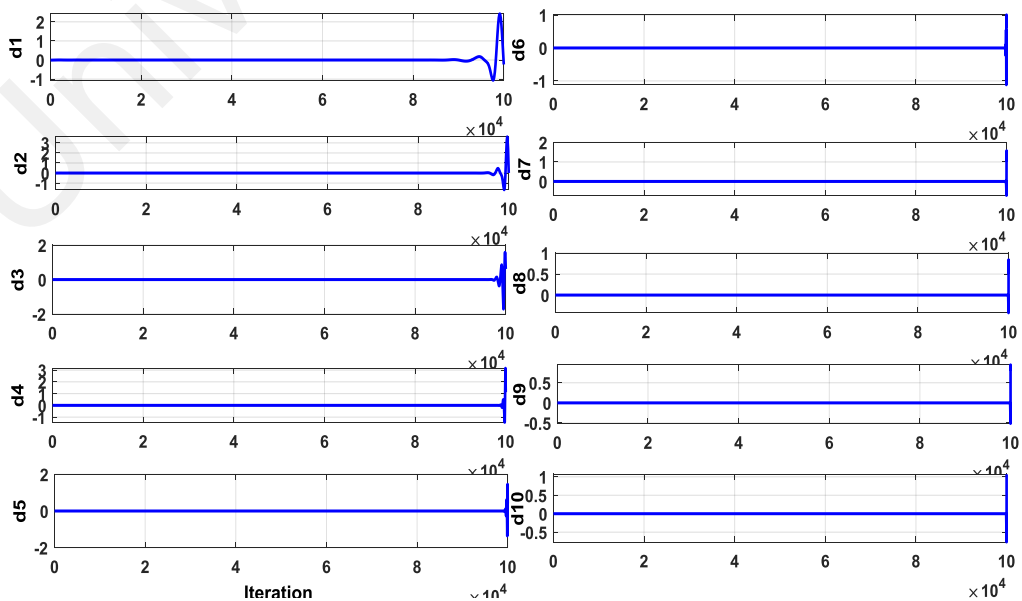


Figure 4.19: Wavelet analysis in faultless motor

The normal operation of the IM and inverter are indicated by the DC link, as can be seen from Figure 4.20 and Figure 4.21 for healthy and faulty inverter respectively. In this thesis, the inverter will be considered as healthy and without faults after the replacement of the burn IGBT transistor. For the healthy inverter case, the DC voltage was 362 V and it reduced until 150V in the faulty inverter which is good observation of inverter fault.

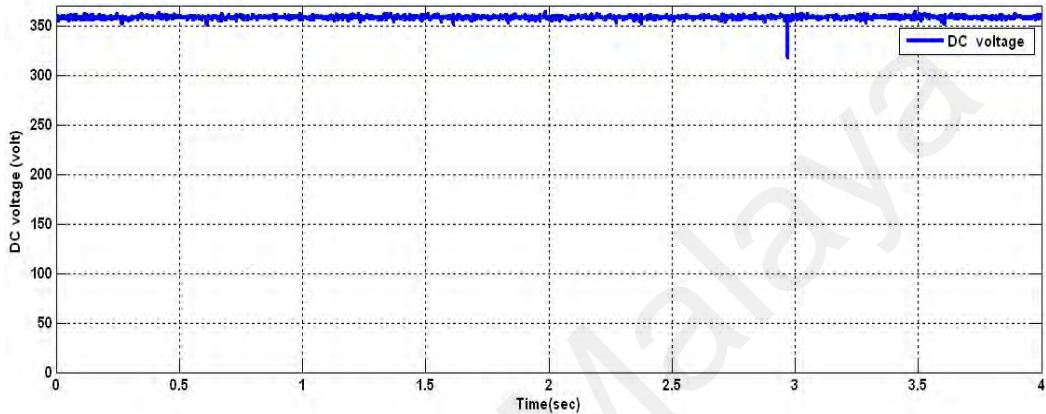


Figure 4.20 Experimental DC level in the healthy inverter

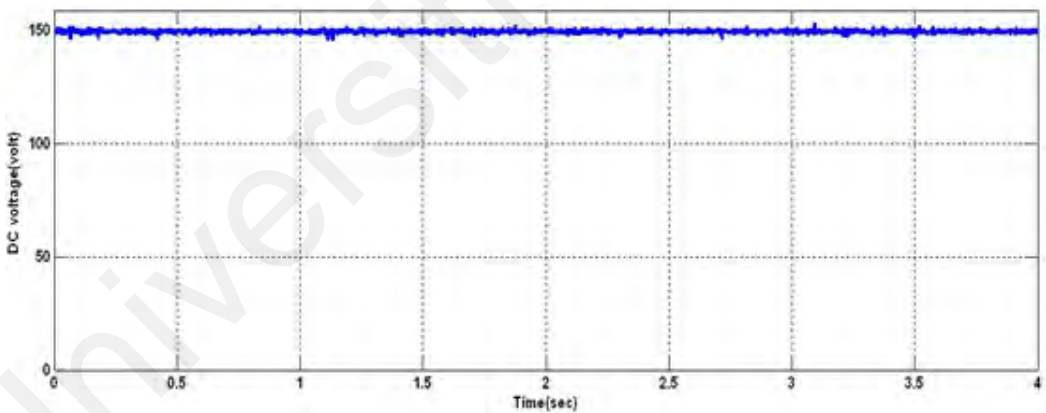


Figure 4.21 Experimental DC level in the faulty inverter

The laboratory equipment required for the experiment to apply the wavelet index in order to detect and evaluate the short-circuit fault in the stator of the motor is demonstrated in Figure 4.22.

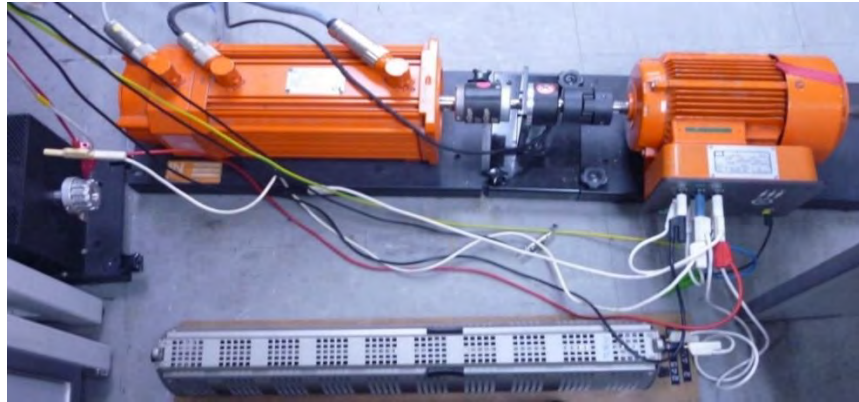


Figure 4.22: Laboratory scheme to analyze the short-circuit fault in the stator with wavelet index

Laboratory layout for analyzing open-circuit fault in the IM stator winding with wavelet index is illustrated in Figure 4.23.



Figure 4.23: Laboratory procedure for assessing the open-circuit fault in the stator, with wavelet index

The laboratory deployment for the experiment is depicted in Figure 4.24.

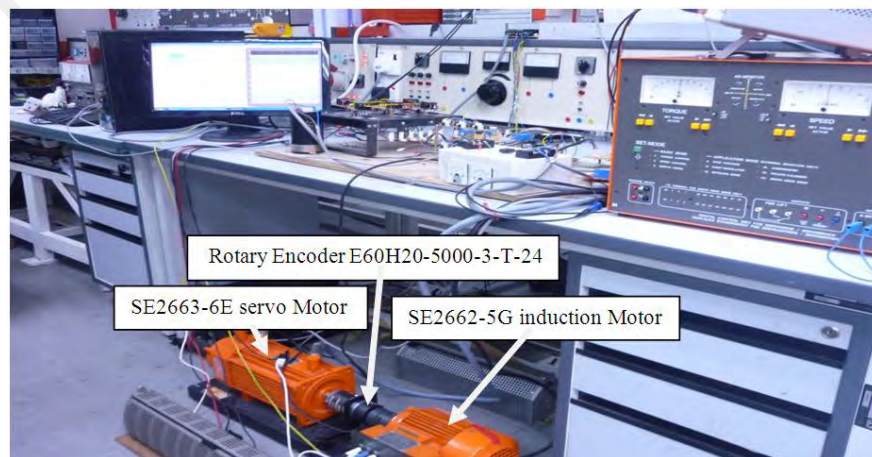


Figure 4.24: Induction motor setup

Examining the faulty and the normal operations of the IM drives are the two basic scenarios on which this experimental study is based. The open-circuit in the stator winding, sensor fault, short-circuit in the stator winding and minimum voltage were all analyzed. The compilation of fault-tolerant control after its implementation with MATLAB Simulink was achieved by the DSP F28335 controller. This is all visible from the experimental procedure illustrated in Figure 4.25. IEEE standards (Table 4.2) were adopted as the criteria for monitoring the parameters.

Table 4.2: The IEEE standard for observing the parameters of induction motor

Report of Fault Monitoring of an Induction Motor		
Faults	Acceptable Values	Values Limits
AC over current	Twice rated	1.5 rated
AC under voltage	5-25% PNDA & PNDI	Up to 40%
AC overvoltage	$\pm 10\%$	$\pm 10\%$
Unbalance ac voltage	IEEE stand of 1 – 5%	1 – 3%
Overvoltage due to DC	V_{dc}	V_{dc}
High speed	+25%	+10%
Low Speed	-25%	-10%
Broken rotor bar	For 2 poles is 20% < 2m	For 2 poles is 20% < 2m
Stator short-winding	For 2 poles is 10% < 2m	For 2 poles is 10% < 2m
Destruction	Denied	Denied

Meanwhile Table 4.3 enlist the induction motor parameters.

Table 4.3: The induction motor parameters

Motor Parameter	Rating
Current	2.5A
Voltage	400v
Power	1kW
Speed	2780rpm
No of poles	2
R_s	20.9 Ω
R_r	19.5 Ω
L_s	0.05H
L_r	0.05H

The variation of the real speed with regard to the reference speed would indicate the fault in the speed sensor as in Figure 4.25.

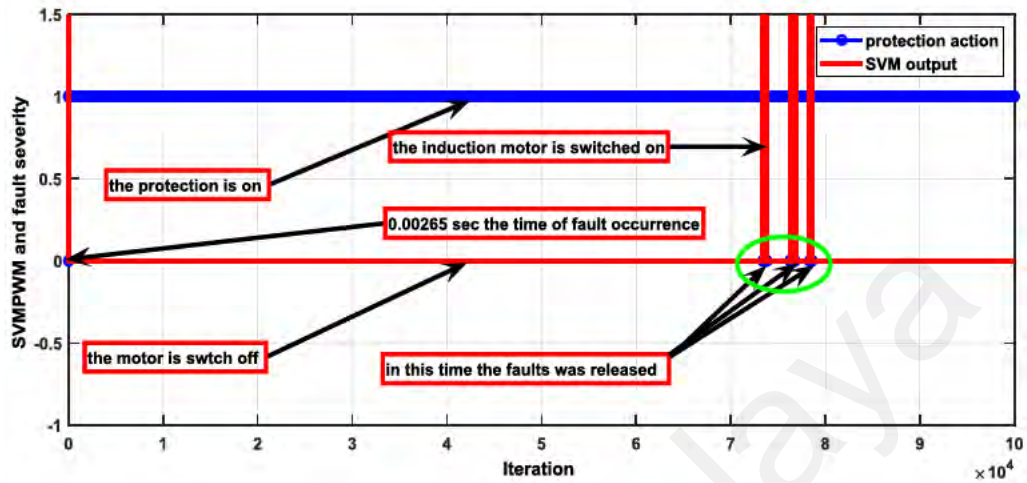


Figure 4.25: Speed difference with the binary indication

In the event that the distinction between the reference and actual speed exceeds 10%, a logic 1 appears to choose the sensorless vector control. When there is variation of less than 10 %, always the normal operation or logic 0 as in Figure 4.26.

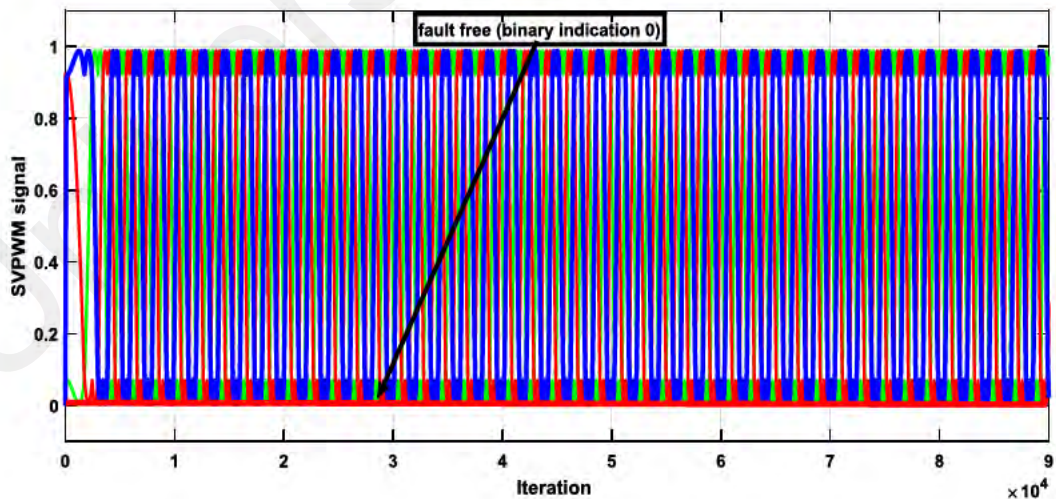


Figure 4.26: SVM control signal with 0 binary indication in healthy induction motor

The waveform of the current that represent the short-circuit fault occurrence at the period of $t = 2$ sec, is presented in Figure 4.27.

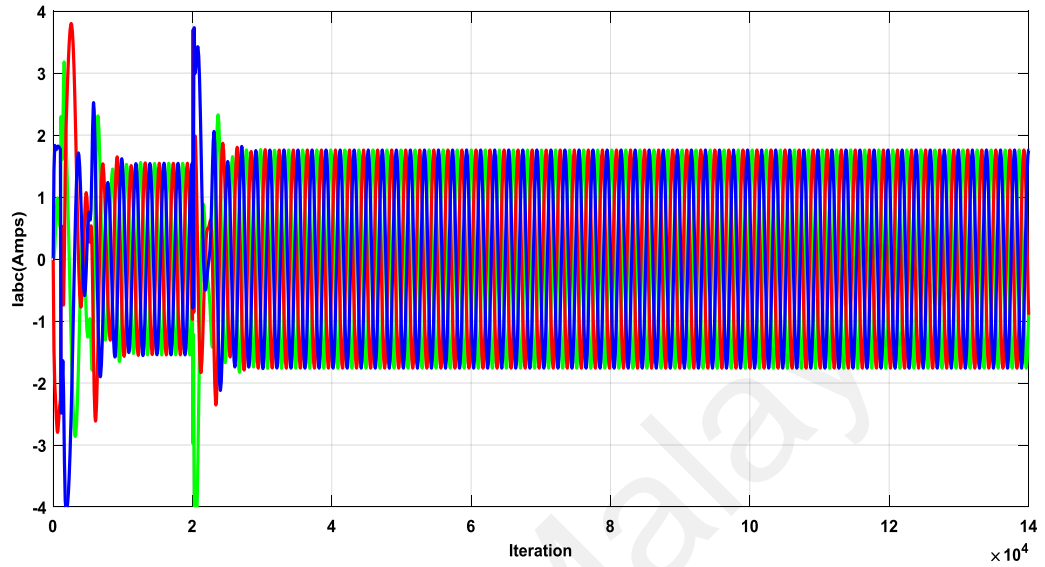


Figure 4.27: Stator current with fault injection

The corresponding wavelet waveform and the speed recovery is depicted in Figure 4.28 and Figure 4.29, respectively.

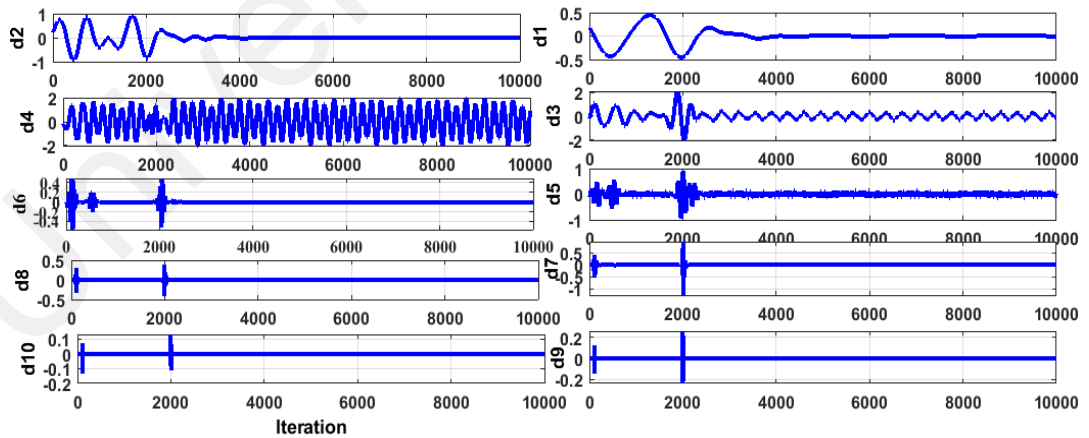


Figure 4.28: Wavelet decomposition

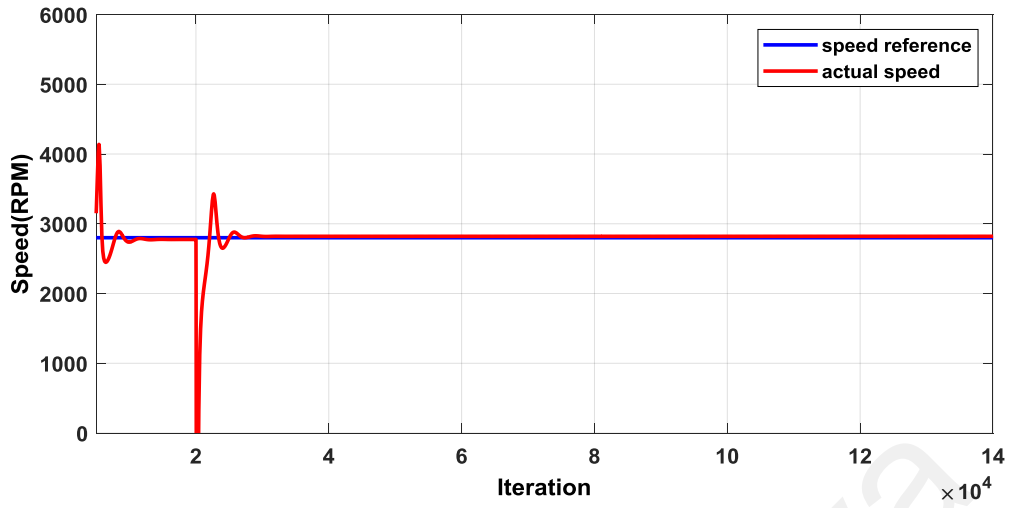


Figure 4.29: Speed reaction and recovery time

The monitoring unit response is shown in Figure 4.30.

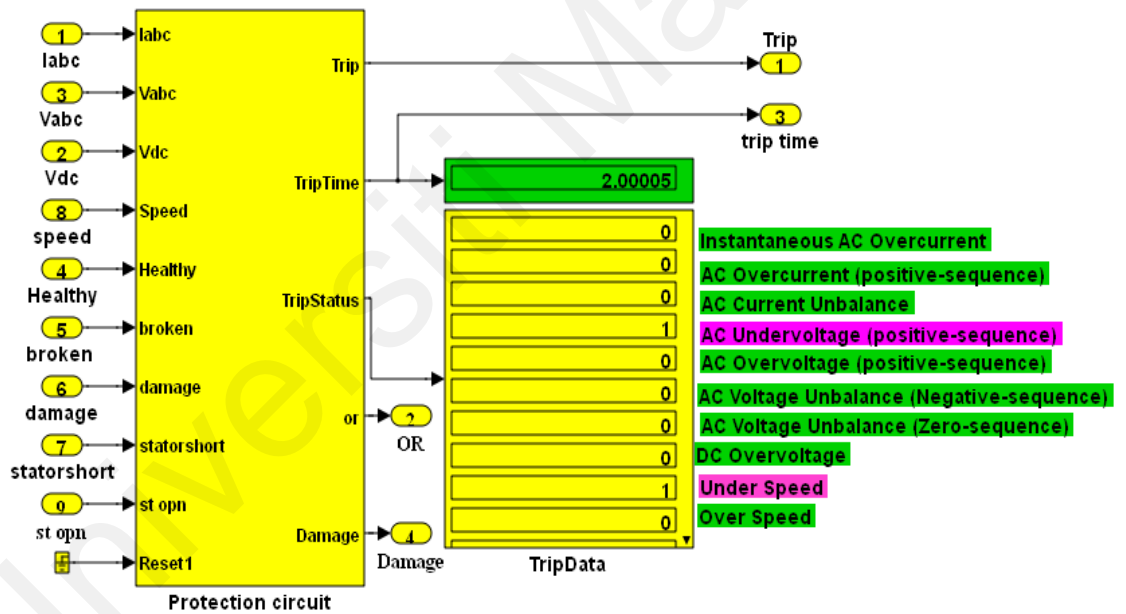


Figure 4.30: Monitoring outputs for faults at 2 sec

Current waveform of the faulty system at $t = 6$ sec with its corresponding wavelet is presented in Figure 4.31 and Figure 4.32, respectively.

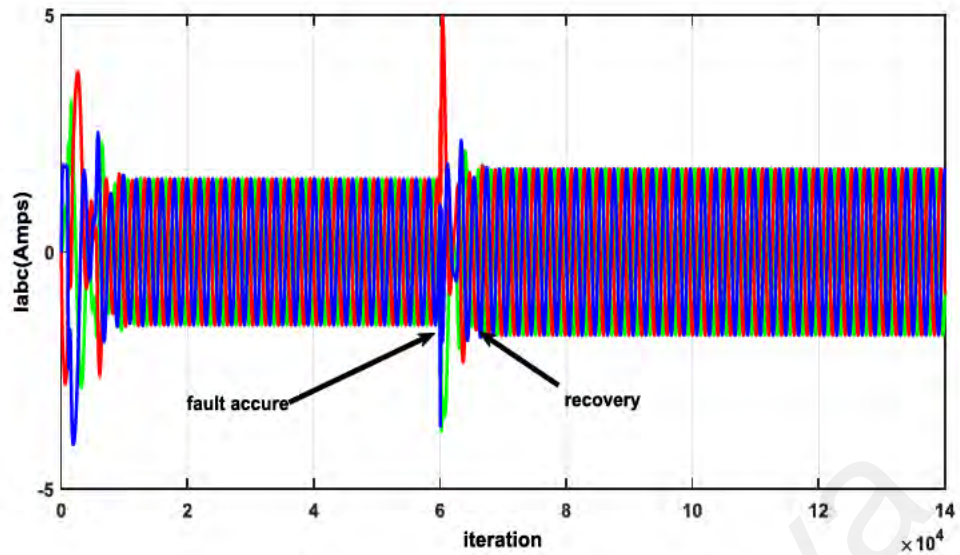


Figure 4.31: Stator current with fault injection

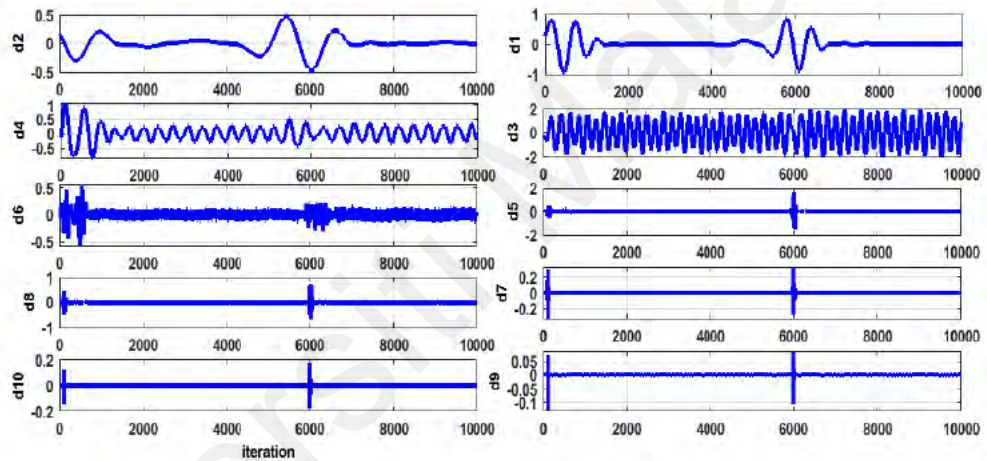


Figure 4.32: Wavelet decomposition

The transient response and injection of stator open winding fault at 6sec are so clear in the decomposition of stator current wavelet. The speed recovery is quite clear after applying the FTC algorithm. An open-circuit fault and short-circuit fault was generated for the period of 1.4sec and 1.12sec, respectively, in the stator winding in order to assess the mobility and compatibility of the algorithm compiled by the fault-tolerant controller. It was observed that the restoration time for the open-circuit fault is less than the restoration time for the short-circuit fault in the IM drive (Figure 4.33).

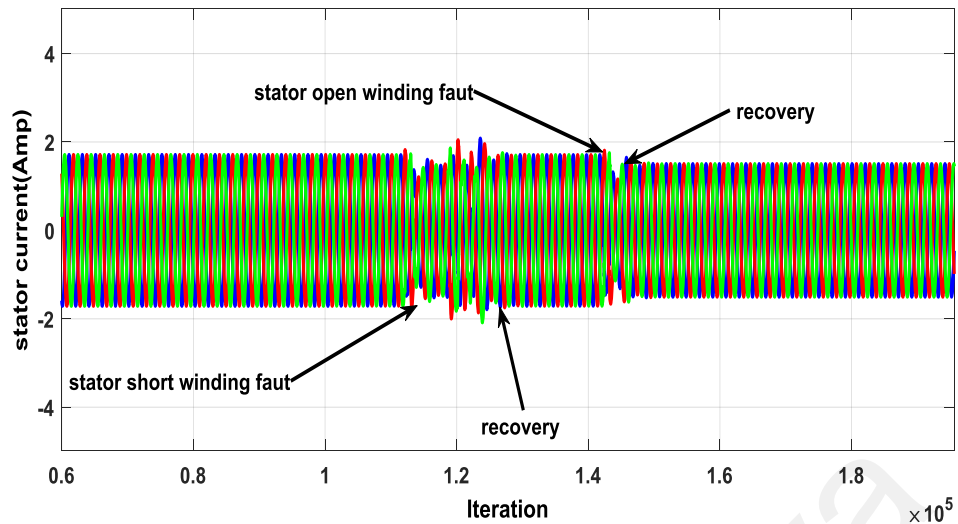


Figure 4.33: Multiple faults at different times

The objective of this test is to study the degree-of-freedom of the algorithm supporting the fault-tolerant control and its mobility to retreat to the sensor vector mode control. The open and short circuit faults were initiated concurrently in the stator winding by disconnecting one of the windings in the stator's phase and activating a solid-state switch across any of the desired phases of the stator, respectively. The faults were injected in the scheme at 1.16 sec to observe the operation of the induction motor drive, which was found to be stopping when the protection unit takes over from the fault-tolerant algorithm. On the other hand, the controller exits from the protective control mode and shifts to the sensor mode vector control and vice versa, as the injected fault is mitigated in a period of 1.48sec. Figure 4.34 shows the simulated result.

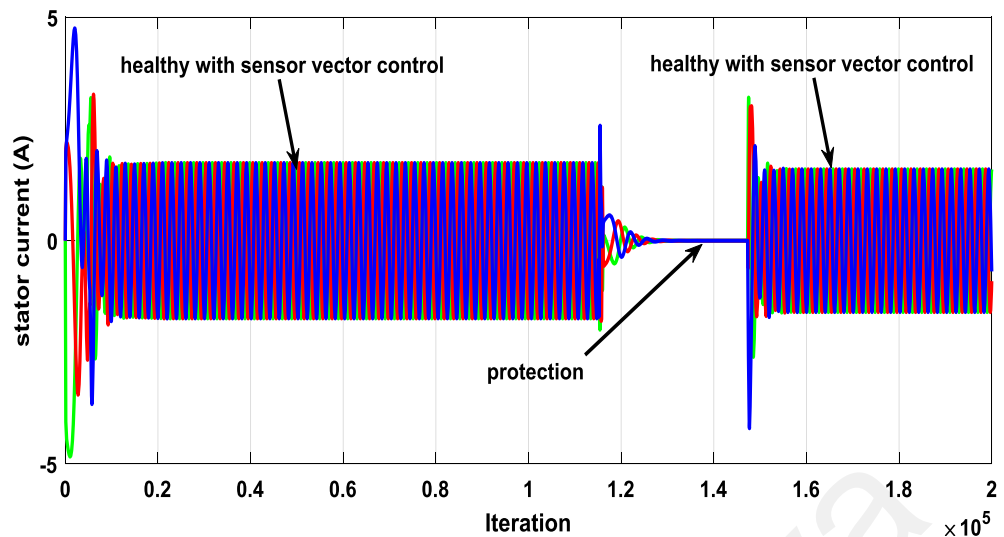


Figure 4.34: Stator current

Lastly, the three individual fault events are simulated, namely, the minimal voltage, open and short stator winding faults. The minimum possible voltage is attained by decreasing the source voltage below the 200V requirement. During the starting period of the motor, its operation was found to be normal. Subsequently, open and short winding faults occurred at two distinct time durations i.e. at 4sec. The voltage is then decreased to a value lower than 200V for the purpose of simulating the third fault for the duration of 5sec. Then both the open winding and reduced voltage were applied at 7sec. Consequently, at the time the vector control was commanding, the V/F control mode takes charge after 4sec in order to remedy the short or open winding faults in the stator. This multisensory control technique changed over to open mode of V/F control to offset the last fault and regulate the IM drive operation with negligible distortion. In case of a severe fault, the protection circuit is energized to interrupt the running motor, illustrated in Figure 4.35.

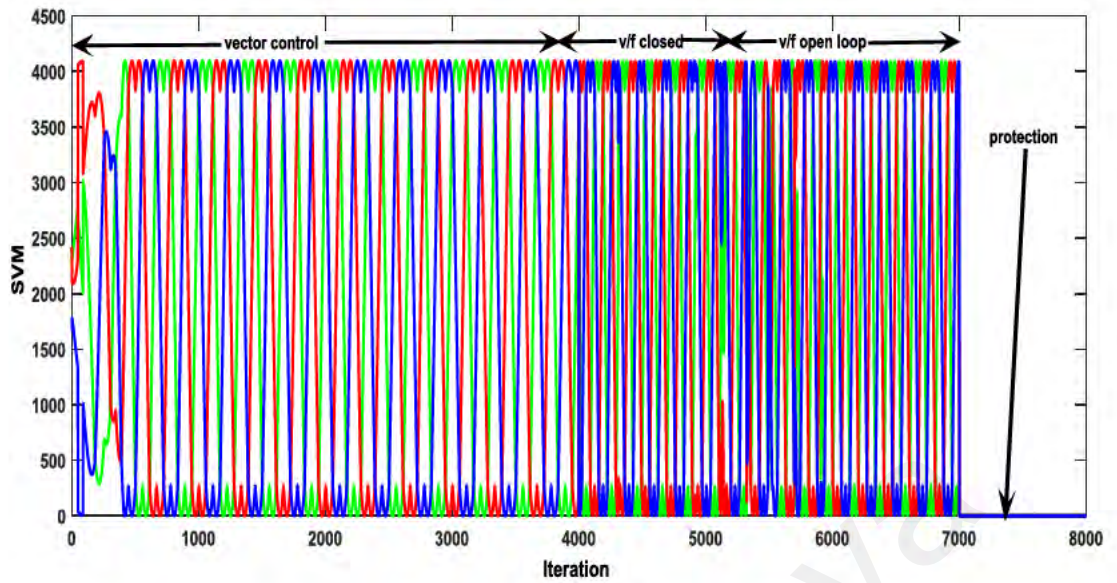


Figure 4.35: Signal from the SVM to control the inverter under various control technique

The derivation of the mathematical relationship between the designed wavelet index and the overall effect of stator resistance is instrumental for the intervals in the wavelet index. The expression for the wavelet index at 1600 rpm with a curve fitting is linearly represented as in equation (4.5):

$$W_{ind} = 0.0217 \times R_{shunt\ effect} + 1.796 \quad (4.5)$$

The linear curve fitting with a 900 rpm wavelet index can be expressed in equation (4.6):

$$W_{ind} = 0.0843 \times R_{shunt\ effect} + 1.7822 \quad (4.6)$$

The linear curve fitting equation (4.7), having 400 rpm wavelet indicator is:

$$W_{ind} = 0.0986 \times R_{shunt\ effect} + 1.146 \quad (4.7)$$

The linear curve that fits the open winding of the stator and a wavelet ratio of 1600RPM is expressed in (4.8):

$$W_{ind} = 0.00919 \times R_{series\ effect} + 1.369 \quad (4.8)$$

The linear equation which fits a curve in the stator open winding, with 900 *rpm* wavelet indicator is expressed as in (4.9):

$$W_{ind} = 0.0084 \times R_{series\ effect} + 1.257 \quad (4.9)$$

The linear curve befitting equation (4.10) of the stator open winding having a 450 *rpm* wavelet index ratio is:

$$W_{ind} = 0.0024 \times R_{series\ effect} + 0.943 \quad (4.10)$$

The combination of various digital signal processing techniques with other control strategies have been suggested and implemented to attain a robust IM topology, in its industrial applications by many authors. Table 4.4. enlist some relevant fault diagnosis methods and compared with the one presented herein. It is observed that the multisensory control and the wavelet analysis offers more rugged configuration of the induction motor. This is because of the ability of the control technique to interswitch from one form to another in about four ways, allowed by the multi-control scheme thereby significantly minimizing the chances of fault occurrence. The wavelet prognostic property of the developed wavelet algorithm helps in accurately detecting, any anticipated fault occurrence.

Table 4.4: Comparison of recent fault diagnostic techniques of the Induction motor, using advance signal processing techniques

Concept	Applications	Drawbacks	Reference
Enhanced cyclic modulation spectral analysis, based on the CWT	Best for diagnosis of broken rotor bar, for induction motor.	Difficulty in selecting the optimal filter banks.	(Zhen et al., 2019)
Empirical wavelet thresholding	Bearing fault detection	Adaptability issues, regarding the Fourier transform segment	(Zepeng Liu et al., 2020)
WPT+FFT+MLPNN	Identification of rotor breakage in induction motor with 98.80% accuracy.		(Zolfaghari, Noor, Rezazadeh Mehrjou, Marhaban, & Mariun, 2018b)
Empirical wavelet and Fuzzy entropy	Motor bearing fault detection	Highly enhanced protective	(Deng et al., 2018)
A combination of matching pursuit (MP) and DWT for feature identification	Fault prognostic method using stator currents and vibration signals of induction machines	Various loadings during testing and training, usually causes some setbacks	(Ali, Shabbir, Liang, Zhang, & Hu, 2019)
Multi-label Convolutional Neural Network and Wavelet transform.	Complicated gearbox diagnostic procedure, with high classification accuracy.	Online implementation demands trained data	(P. Liang et al., 2019)
Continuous wavelet and enhanced model reference adaptive system	Stator and rotor faults detection of the motor.	Multisensory techniques eliminate almost all the disadvantages and made the motor highly resistance to faults.	(Abubakar, Mekhilef, Gaeid, Mokhlis, & Al Mashhadany, 2020)

The db10 is selected as the appropriate mother wavelet candidate, for analyzing the stator current, because of its optimal performance in the analysis of dynamic signal with discontinuities or abrupt jumps. Also, due to its significant vanishing moments, db10 can accurately detect and localized the abrupt changes and the discontinuity, which occurred during the open and short stator winding fault. The wavelet index of health case and different values of stator resistance can be shown as in Figure 4.36.

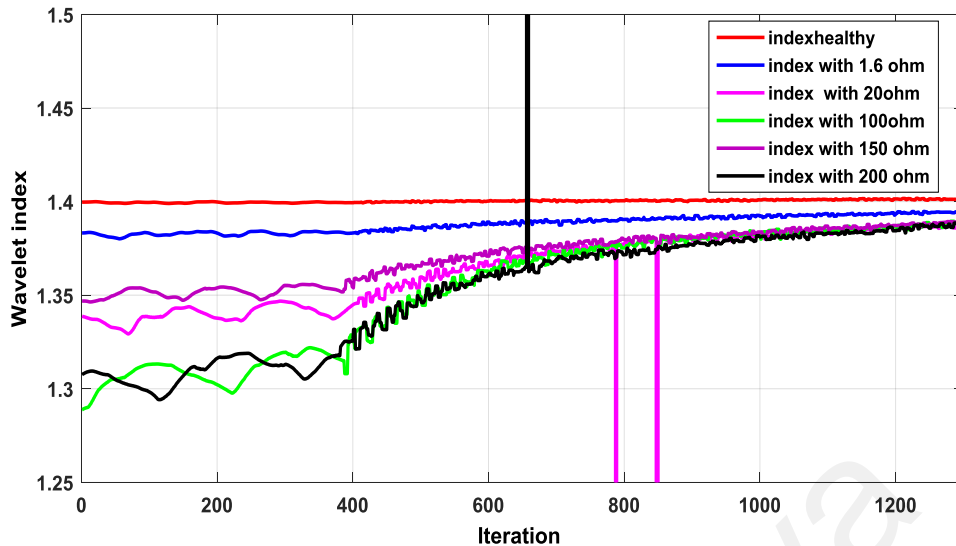


Figure 4.36: Different values of wavelet index correspond to stator resistance

4.8 Summary

This chapter presented the results of the development, and the working of a new digital crowbar and GSC protection scheme of a grid connected DFIG. Additionally, for the DFIG the d-q current for the rotor and stator were utilized, for the extraction of special feature during the fault occurrence. The d-q currents were studied with WPT, to diagnose the actual fault and to trip given a specified condition. The responses to the WPT protection scheme have been found to be accurate reliable, fast and insensitive to the type and location of faults. In addition to that, the evaluation of Y_{dq} demonstrated insensitivity to the loading levels of the protected generator, as well as the type of the fault (open circuit or short circuit). With regard to the induction motor, a fault tolerant drive based on the enhanced multisensory and model reference. Detailed simulation and experimental results have been presented, and the control scheme was shown to be flexible. This is because it is capable of reconfiguring itself from one form of control algorithm to the other in four possible ways. Similarly, wavelet analysis based on the db10 was used to diagnose the faulty current.

CHAPTER 5: CONCLUSION AND FUTURE WORK

5.1 Conclusion

The power converters in DFIG must be protected from overcurrent and overvoltage. The junction temperature of power semiconductor devices must be maintained within their maximum permissible values. A fast-acting fuse is normally connected in series with each device for overcurrent protection under fault conditions. However, fuses and other protection means are inadequate to offer protection to the power converters employed in DFIG-based WECS. A crowbar may be required to provide protection against damages, which the high inrush current may cause during open or short circuit fault at the rotor.

This type of analysis is employed in designing digital protection scheme in renewable systems, electric generators and power electronic converters. The integration of wind energy into an existing grid has presented a technical challenge to the traditional crowbar or to the general protection scheme utilized in power system. The proposed digital protection for RSC and GSC is described, which operates by processing the d-q-axis current components using the WPT. The d-q WPT-based digital protection has exhibited simple implementation with minimal computational complexities. Several transient disturbances initiated by fault and non-fault events have been studied.

Similarly, the robustification procedure of induction motor drive using the FTC technique, and its positive impact in prolonging the lifespan of the power converter, employed in the motor has also been presented. This is achieved by the introduction and deployment of a multisensory control strategy that interoperates between the individual controller to remedy or circumvent the anticipated fault. When the functionality of the active controller is adversely affected, it switches to its quadruplet sister as a backup. The idea of this interoperability is analogous to the 'handshaking' protocol, a term used in computer science. Furthermore, a protection unit is retrofitted that utilizes the wavelet

index in classifying and detecting the faults. This has the advantage of minimal sensitivity to the loading level, location and type of the faults.

This distinct feature of wavelet makes it an accurate tool for diagnosing a fault in motor drives, including the induction motor because it can distinguish between the transient response from the speed or load changes and the actual occurrence of the real fault. In addition to that, FTC and protection technique was developed based on the motor electrical parameters, such as rotor/stator voltage or current, to minimize the complexity of the monitoring scheme. This approach improves further the ruggedness of the motor and hence its reliability.

5.2 Future Works

The digitization of protection and control systems for wind energy technology during the integration to an existing utility will enable plug-and-play operations in renewable energy harnessing and applications. Plug-and-play is a terminology used in computer science, in which the software and hardware operate together automatically to allocate resources. This permits hardware adaption and incorporation of new ones, with insignificant or noticeable adjustments. The objective is to have the means of plugging in an external device and using it instantly, with no substantial alteration in the original configuration of the system. The above-mentioned feature is essential in the future of wind micro turbines, which are expected to play an assisting role and participate in the assigning of resources. The hardware is analogous to the wind turbines, power electronics interface, generators and the loads, whereas the software is analogous to the digital signal processors (DSP) or field-programmable gate array (FPGA).

The implementation of digital motor control (DMC) can be put forward as future work, which can be attained in accordance with the equations of the vector control and v/f control technique. Furthermore, plug in controllers such as the direct torque control can

be inserted in this scheme during the transition period. Another predictive validity for the case of the induction motor, can be focused from the power converter view point. This can be carried out by examining the impact by switching on the stability of the inverter. In addition to that, the diagnosis of the inverter fault can be taken into consideration in greater depth.

Universiti Malaya

REFERENCES

- Abad, G., & Iwanski, G. (2014). Properties and control of a doubly fed induction machine. *Power Electronics for Renewable Energy Systems, Transportation and Industrial Applications*, 270-318.
- Abd-el-Malek, M., Abdelsalam, A. K., Hassan, O. E. J. M. S., & Processing, S. (2017). Induction motor broken rotor bar fault location detection through envelope analysis of start-up current using Hilbert transform. *93*, 332-350.
- Abdelemam, A. M., El-Rifaie, A. M., & Moussa, S. M. (2017). Discrete wavelet transform based protection for a wind farm double fed induction generator. Paper presented at the 2017 IEEE International Conference on Environment and Electrical Engineering and 2017 IEEE Industrial and Commercial Power Systems Europe (EEEIC/I&CPS Europe).
- Abdelgayed, T. S., Morsi, W. G., & Sidhu, T. S. J. I. T. o. S. G. (2017). A new approach for fault classification in microgrids using optimal wavelet functions matching pursuit. *9(5)*, 4838-4846.
- Abdelsalam, I., Adam, G. P., & Williams, B. W. (2016). Current source back-to-back converter for wind energy conversion systems. *IET Renewable Power Generation*, *10(10)*, 1552-1561.
- Abubakar, U., Mekhilef, S., Gaeid, K. S., Mokhlis, H., & Al Mashhadany, Y. I. J. I. E. P. A. (2020). Induction motor fault detection based on multi-sensory control and wavelet analysis.
- Adapa, A., Bhowmick, S., & John, V. J. I. T. o. I. E. (2020). Low-Frequency DC-Link Capacitor Current Mitigation in Reduced Switch Count Single-Phase to Three-Phase Converter.
- Afrandideh, S., Haghjoo, F., Cruz, S. M., & Milasi, M. E. J. I. T. o. I. E. (2020). Detection of Turn-to-Turn Faults in the Stator and Rotor of Synchronous Machines during Startup.
- Akhtar, M. J., Behera, R. K. J. I. J. o. E., & Electronics, S. T. i. P. (2020). Space Vector Modulation for Distributed Inverter Fed Induction Motor Drive for Electric Vehicle Application.
- Alam, M. S., & Abido, M. A. Y. (2018). Fault ride through capability enhancement of a large-scale PMSG wind system with bridge type fault current limiters. *Advances in Electrical and Computer Engineering*, *18(1)*, 43-50.
- Ali, M. Z., Shabbir, M. N. S. K., Liang, X., Zhang, Y., & Hu, T. J. I. T. o. I. A. (2019). Machine learning-based fault diagnosis for single-and multi-faults in induction motors using measured stator currents and vibration signals. *55(3)*, 2378-2391.
- Ali, M. Z., Shabbir, M. N. S. K., Zaman, S. M. K., & Liang, X. J. I. T. o. I. A. (2020). Single-and Multi-Fault Diagnosis Using Machine Learning for Variable Frequency Drive-Fed Induction Motors. *56(3)*, 2324-2337.

- Alsmadi, Y. M., Xu, L., Blaabjerg, F., Ortega, A. P., Abdelaziz, A. Y., Wang, A., & Albataineh, Z. (2018). Detailed Investigation and Performance Improvement of the Dynamic Behavior of Grid-Connected DFIG-Based Wind Turbines under LVRT Conditions. *IEEE Transactions on Industry Applications*.
- Ameid, T., Menacer, A., Talhaoui, H., & Azzoug, Y. J. I. t. (2018). Discrete wavelet transform and energy eigen value for rotor bars fault detection in variable speed field-oriented control of induction motor drive. *79*, 217-231.
- Amini, J., & Moallem, M. J. I. T. o. I. E. (2016). A fault-diagnosis and fault-tolerant control scheme for flying capacitor multilevel inverters. *64*(3), 1818-1826.
- Amirat, Y., Benbouzid, M., Wang, T., Bacha, K., & Feld, G. J. A. A. (2018). EEMD-based notch filter for induction machine bearing faults detection. *133*, 202-209.
- Amirat, Y., Benbouzid, M. E. H., Al-Ahmar, E., Bensaker, B., & Turri, S. (2009). A brief status on condition monitoring and fault diagnosis in wind energy conversion systems. *Renewable and sustainable energy reviews*, *13*(9), 2629-2636.
- Ammar, A., Bourek, A., Benakcha, A., & Ameid, T. (2017). Sensorless stator field oriented-direct torque control with SVM for induction motor based on MRAS and fuzzy logic regulation. Paper presented at the 2017 6th International Conference on Systems and Control (ICSC).
- Arabaci, H., & Mohamed, M. A. J. I. J. o. I. E. I. (2020). A knowledge-based diagnosis algorithm for broken rotor bar fault classification using FFT, principal component analysis and support vector machines. *8*(1), 19-37.
- Attoui, I., Fergani, N., Boutasseta, N., Oudjani, B., Deliou, A. J. J. o. S., & Vibration. (2017). A new time–frequency method for identification and classification of ball bearing faults. *397*, 241-265.
- Badrzadeh, B., Gupta, M., Singh, N., Petersson, A., & Max, L. (2012). Power system harmonic analysis in wind power plants—Part I: Study methodology and techniques. Paper presented at the Industry Applications Society Annual Meeting (IAS), 2012 IEEE.
- Badrzadeh, B., Zamastil, M. H., Singh, N. K., Breder, H., Srivastava, K., & Reza, M. J. I. T. o. I. A. (2012). Transients in wind power plants—Part II: Case studies. *48*(5), 1628-1638.
- Bana, P. R., Panda, K. P., Naayagi, R., Siano, P., & Panda, G. J. I. a. (2019). Recently developed reduced switch multilevel inverter for renewable energy integration and drives application: topologies, comprehensive analysis and comparative evaluation. *7*, 54888-54909.
- Baroudi, J. A., Dinavahi, V., & Knight, A. M. (2007). A review of power converter topologies for wind generators. *Renewable energy*, *32*(14), 2369-2385.
- Barrero, F., & Duran, M. J. J. I. T. o. I. E. (2015). Recent advances in the design, modeling, and control of multiphase machines—Part I. *63*(1), 449-458.

- Bayhan, S., Kakosimos, P., & Rivera, M. (2018). Predictive torque control of brushless doubly fed induction generator fed by a matrix converter. Paper presented at the Compatibility, Power Electronics and Power Engineering (CPE-POWERENG), 2018 IEEE 12th International Conference on.
- Bazan, G. H., Scalassara, P. R., Endo, W., Goedel, A., Godoy, W. F., & Palácios, R. H. C. J. E. P. S. R. (2017). Stator fault analysis of three-phase induction motors using information measures and artificial neural networks. 143, 347-356.
- Bessous, N., Zouzou, S., Bentrach, W., Sbaa, S., Sahraoui, M. J. I. J. o. S. A. E., & Management. (2018). Diagnosis of bearing defects in induction motors using discrete wavelet transform. 9(2), 335-343.
- Bisht, N., Das, A. J. I. J. o. E., & Electronics, S. T. i. P. (2020). A Multiple Fault Tolerant Topology of Cascaded H-Bridge Converter for Motor Drives Using Existing Pre-charge Windings.
- Bizjak, G., Zunko, P., & Povh, D. (1995). Circuit breaker model for digital simulation based on Mayr's and Cassie's differential arc equations. IEEE Transactions on Power Delivery, 10(3), 1310-1315.
- Breder, M. R. a. H. (2009). V-110 cable system transient study. Retrieved from Vindforsk, Stockholm, Sweden:
- Burriel-Valencia, J., Puche-Panadero, R., Martinez-Roman, J., Sapena-Bano, A., & Pineda-Sanchez, M. J. S. (2018). Fault diagnosis of induction machines in a transient regime using current sensors with an optimized slepian window. 18(1), 146.
- Burrus, C. S., Gopinath, R. A., Guo, H., Odegard, J. E., & Selesnick, I. W. (1998). Introduction to wavelets and wavelet transforms: a primer (Vol. 1): Prentice hall New Jersey.
- Cabal-Yepeze, E., Fernandez-Jaramillo, A. A., Garcia-Perez, A., Romero-Troncoso, R. J., & Lozano-Garcia, J. M. J. I. T. o. E. E. S. (2015). Real-time condition monitoring on VSD-fed induction motors through statistical analysis and synchronous speed observation. 25(8), 1657-1672.
- Camille, H. (2010). Doubly-fed Induction Generator Modeling and Control in DigSilent Power Factory. MA thesis, KTH School of Electrical Engineering,
- Chang, E.-C. (2018). Improving Performance for Full-Bridge Inverter of Wind Energy Conversion System Using a Fast and Efficient Control Technique. Energies, 11(2), 262.
- Chang, Y., Hu, J., Tang, W., & Song, G. (2018). Fault Current Analysis of Type-3 WTs Considering Sequential Switching of Internal Control and Protection Circuits in Multi Time Scales during LVRT. IEEE Transactions on Power Systems.
- Chattopadhyay, R., De, A., & Bhattacharya, S. (2014). Comparison of PR controller and damped PR controller for grid current control of LCL filter based grid-tied inverter under frequency variation and grid distortion. Paper presented at the 2014 IEEE Energy Conversion Congress and Exposition (ECCE).

- Chen, B., Shen, B., Chen, F., Tian, H., Xiao, W., Zhang, F., & Zhao, C. J. M. (2019). Fault diagnosis method based on integration of RSSD and wavelet transform to rolling bearing. 131, 400-411.
- Chen, J., Chen, J., & Gong, C. (2014). On optimizing the transient load of variable-speed wind energy conversion system during the MPP tracking process. *IEEE Transactions on Industrial Electronics*, 61(9), 4698-4706.
- Chen, Z., Guerrero, J. M., & Blaabjerg, F. (2009). A review of the state of the art of power electronics for wind turbines. *IEEE Transactions on Power electronics*, 24(8), 1859-1875.
- Chicco, G., & Mazza, A. J. E. (2019). 100 years of symmetrical components. 12(3), 450.
- Chowdhury, S., Wheeler, P., Huang, Z., Rivera, M., & Gerada, C. J. I. P. E. (2018). Fixed switching frequency predictive control of an asymmetric source dual inverter system with a floating bridge for multilevel operation. 12(3), 450-457.
- Guidelines for representation of network elements when calculating transients, (1990).
- Climente-Alarcon, V., Riera-Guasp, M., Antonino-Daviu, J., Roger-Folch, J., & Vedreno-Santos, F. (2012). Diagnosis of rotor asymmetries in wound rotor induction generators operating under varying load conditions via the Wigner-Ville Distribution. Paper presented at the International Symposium on Power Electronics Power Electronics, Electrical Drives, Automation and Motion.
- da Costa, C., Kashiwagi, M., Mathias, M. H. J. C. S. i. M. S., & Processing, S. (2015). Rotor failure detection of induction motors by wavelet transform and Fourier transform in non-stationary condition. 1, 15-26.
- Daneshi-Far, Z., Capolino, G.-A., & Henao, H. (2010). Review of failures and condition monitoring in wind turbine generators. Paper presented at the The XIX International Conference on Electrical Machines-ICEM 2010.
- Datta, U., Kalam, A., & Shi, J. (2018). Power system transient stability with aggregated and dispersed penetration of hybrid distributed generation. Paper presented at the 2018 Chinese Control And Decision Conference (CCDC).
- Daubechies, I. (1996). Where do wavelets come from? A personal point of view. *Proceedings of the IEEE*, 84(4), 510-513.
- De Santiago-Perez, J. J., Rivera-Guillen, J. R., Amezcua-Sanchez, J. P., Valtierra-Rodriguez, M., Romero-Troncoso, R. J., Dominguez-Gonzalez, A. J. M. S., & Technology. (2018). Fourier transform and image processing for automatic detection of broken rotor bars in induction motors. 29(9), 095008.
- De Souza, J. S., Meza, E. M., Schilling, M. T., & Do Coutto Filho, M. B. (2004). Alarm processing in electrical power systems through a neuro-fuzzy approach. *IEEE Transactions on Power Delivery*, 19(2), 537-544.
- Dekate, S., & Bhargava, A. (2018). Voltage and Frequency Control of Three Phase PWM Induction Motor.

- Delgado-Arredondo, P. A., Garcia-Perez, A., Morinigo-Sotelo, D., Osornio-Rios, R. A., Avina-Cervantes, J. G., Rostro-Gonzalez, H., . . . Vibration. (2015). Comparative study of time-frequency decomposition techniques for fault detection in induction motors using vibration analysis during startup transient. 2015.
- Deng, W., Zhang, S., Zhao, H., & Yang, X. J. I. A. (2018). A novel fault diagnosis method based on integrating empirical wavelet transform and fuzzy entropy for motor bearing. 6, 35042-35056.
- Djukanovic, M., Khammash, M., & Vittal, V. (1998). Application of the structured singular value theory for robust stability and control analysis in multimachine power systems. I. Framework development. *IEEE Transactions on Power Systems*, 13(4), 1311-1316.
- dos Santos, T. H., Goedel, A., da Silva, S. A. O., & Suetake, M. J. E. p. s. r. (2014). Scalar control of an induction motor using a neural sensorless technique. 108, 322-330.
- Doyle, J. C., Glover, K., Khargonekar, P. P., & Francis, B. A. (1989). State-space solutions to standard H_2 and H_∞ control problems. *IEEE Transactions on Automatic control*, 34(8), 831-847.
- Duong, M. Q., Grimaccia, F., Leva, S., Mussetta, M., & Le, K. H. (2015). Improving transient stability in a grid-connected squirrel-cage induction generator wind turbine system using a fuzzy logic controller. *Energies*, 8(7), 6328-6349.
- Duong, M. Q., Grimaccia, F., Leva, S., Mussetta, M., & Le, K. H. (2016). A hybrid Fuzzy-PI cascade controller for transient stability improvement in DFIG wind generators. Paper presented at the 2016 IEEE International Conference on Fuzzy Systems (FUZZ-IEEE).
- Duong, M. Q., Leva, S., Mussetta, M., & Le, K. H. (2018). A Comparative Study on Controllers for Improving Transient Stability of DFIG Wind Turbines During Large Disturbances. *Energies*, 11(3), 480.
- Duran, M. J., & Barrero, F. J. I. T. o. I. E. (2015). Recent advances in the design, modeling, and control of multiphase machines—Part II. 63(1), 459-468.
- Dybkowski, M., & Bednarz, S. A. J. E. (2019). Modified Rotor Flux Estimators for Stator-Fault-Tolerant Vector Controlled Induction Motor Drives. 12(17), 3232.
- El-Moursi, M. S., Bak-Jensen, B., & Abdel-Rahman, M. H. (2010). Novel STATCOM controller for mitigating SSR and damping power system oscillations in a series compensated wind park. *IEEE Transactions on Power electronics*, 25(2), 429-441.
- El Menzhi, L., & Saad, A. (2013). Induction Motor Fault Diagnosis Using Voltage Spectrum of Auxiliary Winding and Lissajous Curve of its Park Components. Paper presented at the Advanced Materials Research.
- Farah, N., Talib, M. H. N., Shah, N. S. M., Abdullah, Q., Ibrahim, Z., Lazi, J. B. M., & Jidin, A. J. I. A. (2019). A Novel Self-Tuning Fuzzy Logic Controller Based Induction Motor Drive System: An Experimental Approach. 7, 68172-68184.

- Farhadi, M., Fard, M. T., Abapour, M., & Hagh, M. T. J. I. T. o. P. E. (2017). DC–AC converter-fed induction motor drive with fault-tolerant capability under open-and short-circuit switch failures. 33(2), 1609-1621.
- Farzan Moghaddam, A., & Van den Bossche, A. J. E. (2020). Direct Usage of Photovoltaic Solar Panels to Supply a Freezer Motor with Variable DC Input Voltage. 9(1), 167.
- Fei, Q., Deng, Y., Li, H., Liu, J., & Shao, M. J. I. A. (2019). Speed Ripple Minimization of Permanent Magnet Synchronous Motor Based on Model Predictive and Iterative Learning Controls. 7, 31791-31800.
- Feijóo, A., Cidrás, J., & Carrillo, C. (2000). A third order model for the doubly-fed induction machine. *Electric Power Systems Research*, 56(2), 121.
- Fernandez, L. M., Saenz, J. R., & Jurado, F. (2006). Dynamic models of wind farms with fixed speed wind turbines. *Renewable energy*, 31(8), 1203-1230.
- Firouzi, M., & Gharehpetian, G. B. J. I. T. o. S. E. (2017). LVRT performance enhancement of DFIG-based wind farms by capacitive bridge-type fault current limiter. 9(3), 1118-1125.
- Flannery, P., & Venkataramanan, G. (2008). Unbalanced voltage sag ride-through of a doubly fed induction generator wind turbine with series grid side converter. Paper presented at the Industry Applications Society Annual Meeting, 2008. IAS'08. IEEE.
- Gao, H., Zhang, W., Wang, Y., & Chen, Z. J. E. (2019). Fault-Tolerant Control Strategy for 12-Phase Permanent Magnet Synchronous Motor. 12(18), 3462.
- Garapati, D. P., Jegathesan, V., & Veerasamy, M. J. A. S. E. J. (2018). Minimization of power loss in newfangled cascaded H-bridge multilevel inverter using in-phase disposition PWM and wavelet transform based fault diagnosis. 9(4), 1381-1396.
- García, H., Segundo, J., Rodríguez-Hernández, O., Campos-Amezcuca, R., & Jaramillo, O. J. E. (2018). Harmonic Modelling of the Wind Turbine Induction Generator for Dynamic Analysis of Power Quality. 11(1), 104.
- Gautam, D., Vittal, V., & Harbour, T. (2009). Impact of increased penetration of DFIG-based wind turbine generators on transient and small signal stability of power systems. *IEEE Transactions on Power Systems*, 24(3), 1426-1434.
- Geebelen, B., Leterme, W., & Van Hertem, D. (2015). Analysis of DC breaker requirements for different HVDC grid protection schemes.
- Geng, H., Liu, L., & Li, R. (2018). Synchronization and Reactive Current Support of PMSG based Wind Farm during Severe Grid Fault. *IEEE Transactions on Sustainable Energy*.
- Ghods, A., & Lee, H.-H. J. N. (2016). Probabilistic frequency-domain discrete wavelet transform for better detection of bearing faults in induction motors. 188, 206-216.

- Glowacz, A., Glowacz, W., Glowacz, Z., & Kozik, J. J. M. (2018). Early fault diagnosis of bearing and stator faults of the single-phase induction motor using acoustic signals. 113, 1-9.
- Glowacz, A., & Glowacz, Z. J. M. (2016). Diagnostics of stator faults of the single-phase induction motor using thermal images, MoASoS and selected classifiers. 93, 86-93.
- Godoy, W. F., da Silva, I. N., Goedtel, A., & Palácios, R. H. C. J. A. S. C. (2015). Evaluation of stator winding faults severity in inverter-fed induction motors. 32, 420-431.
- Gontijo, G. F., Tricarico, T. C., Franca, B. W., da Silva, L. F., van Emmerik, E. L., & Aredes, M. J. I. T. o. S. E. (2018). Robust Model Predictive Rotor Current Control of a DFIG Connected to a Distorted and Unbalanced Grid Driven by a Direct Matrix Converter.
- Gonzalez-Prieto, I., Duran, M., Bermúdez, M., Barrero, F., Martin, C. J. I. J. o. E., & Electronics, S. T. i. P. (2019). Assessment of virtual-voltage-based model predictive controllers in six-phase drives under open-phase faults.
- González-Prieto, I., Duran, M. J., & Barrero, F. J. J. I. T. o. P. E. (2016). Fault-tolerant control of six-phase induction motor drives with variable current injection. 32(10), 7894-7903.
- Gopinath, R. A. (2005). Phaselets of framelets. IEEE transactions on signal processing, 53(5), 1794-1806.
- Gou, B., Xu, Y., Xia, Y., Deng, Q., & Ge, X. J. I. T. o. P. E. (2020). An Online Data-driven Method for Simultaneous Diagnosis of IGBT and Current Sensor Fault of 3-Phase PWM Inverter in Induction Motor Drives.
- Gouichiche, A., Safa, A., Chibani, A., & Tadjine, M. J. I. T. o. E. E. S. (2020). Global fault-tolerant control approach for vector control of an induction motor. e12440.
- Gowthami, K., & Kalaivani, L. (2019). Fault Classification of Induction Motor Bearing Using Adaptive Neuro Fuzzy Inference System. Paper presented at the 2019 Fifth International Conference on Electrical Energy Systems (ICEES).
- Gryning, M. P., Wu, Q., Blanke, M., Niemann, H. H., & Andersen, K. P. (2015). Wind turbine inverter robust loop-shaping control subject to grid interaction effects. IEEE Transactions on Sustainable Energy, 7(1), 41-50.
- Guezmil, A., Berriri, H., Pusca, R., Sakly, A., Romary, R., & Mimouni, M. F. J. A. J. o. C. (2019). High order sliding mode observer-based backstepping fault-tolerant control for induction motor. 21(1), 33-42.
- Guo, H., & Liu, M.-K. (2018). Induction motor faults diagnosis using support vector machine to the motor current signature. Paper presented at the 2018 IEEE Industrial Cyber-Physical Systems (ICPS).
- Gururaj, M., & Padhy, N. P. (2018). PHIL experimentation on fault ride through behavior of doubly fed induction generator based wind system in the presence of fault

current limiter. Paper presented at the 2018 IEEMA Engineer Infinite Conference (eTechNxT).

- Guzman, H., Barrero, F., & Duran, M. J. J. I. t. o. i. e. (2014). IGBT-gating failure effect on a fault-tolerant predictive current-controlled five-phase induction motor drive. 62(1), 15-20.
- Guzman, H., Duran, M. J., Barrero, F., Zarri, L., Bogado, B., Prieto, I. G., & Arahall, M. R. J. I. T. o. I. E. (2015). Comparative study of predictive and resonant controllers in fault-tolerant five-phase induction motor drives. 63(1), 606-617.
- Gyftakis, K. N., Antonino-Daviu, J. A., Garcia-Hernandez, R., McCulloch, M., Howey, D. A., & Cardoso, A. J. (2015a). Comparative experimental investigation of broken bar fault detectability in induction motors. Paper presented at the 2015 IEEE 10th International Symposium on Diagnostics for Electrical Machines, Power Electronics and Drives (SDEMPED).
- Gyftakis, K. N., Antonino-Daviu, J. A., Garcia-Hernandez, R., McCulloch, M. D., Howey, D. A., & Cardoso, A. J. M. J. I. T. o. I. A. (2015b). Comparative experimental investigation of broken bar fault detectability in induction motors. 52(2), 1452-1459.
- Haidar, A. M., Muttaqi, K. M., & Hagh, M. T. J. I. T. o. I. A. (2017). A coordinated control approach for dc link and rotor crowbars to improve fault ride-through of dfig-based wind turbine. 53(4), 4073-4086.
- Hamon, C., Elkington, K., & Ghandhari, M. (2010). Doubly-fed induction generator modeling and control in DigSilent PowerFactory. Paper presented at the 2010 International Conference on Power System Technology.
- Han, Q., Ding, Z., Xu, X., Wang, T., Chu, F. J. M. S., & Processing, S. (2019). Stator current model for detecting rolling bearing faults in induction motors using magnetic equivalent circuits. 131, 554-575.
- Hansen, A. D., Jauch, C., Sørensen, P. E., Iov, F., & Blaabjerg, F. (2004). Dynamic wind turbine models in power system simulation tool DIgSILENT (8755031986). Retrieved from
- Hansen, A. D., & Michalke, G. J. R. e. (2007). Fault ride-through capability of DFIG wind turbines. 32(9), 1594-1610.
- Hasani, A., Haghjoo, F., Bak, C. L., & da Silva, F. F. (2019). Performance Evaluation of Some Industrial Loss of Field Protection Schemes Using a Realistic Model in The RTDS. Paper presented at the 2019 IEEE International Conference on Environment and Electrical Engineering and 2019 IEEE Industrial and Commercial Power Systems Europe (EEEIC/I&CPS Europe).
- Hashemi, S., & Sanaye-Pasand, M. (2018). Study of out-of-step phenomena in grid-connected inverter-interfaced synchronous generators. Paper presented at the Compatibility, Power Electronics and Power Engineering (CPE-POWERENG), 2018 IEEE 12th International Conference on.

- Hassan, O. E., Amer, M., Abdelsalam, A. K., & Williams, B. W. J. I. E. P. A. (2018). Induction motor broken rotor bar fault detection techniques based on fault signature analysis—a review. 12(7), 895-907.
- Henao, H., Capolino, G.-A., Fernandez-Cabanas, M., Filippetti, F., Bruzzese, C., Strangas, E., . . . Hedayati-Kia, S. J. I. i. e. m. (2014). Trends in fault diagnosis for electrical machines: A review of diagnostic techniques. 8(2), 31-42.
- Hmidet, A., & Boubaker, O. J. M. P. i. E. (2020). Real-Time Low-Cost Speed Monitoring and Control of Three-Phase Induction Motor via a Voltage/Frequency Control Approach. 2020.
- Hosseinzadeh, M., & Rajaei Salmasi, F. (2016). Analysis and detection of a wind system failure in a micro-grid. *Journal of Renewable and Sustainable Energy*, 8(4), 043302.
- Hosseinzadeh, M., & Salmasi, F. R. (2016). Fault-tolerant supervisory controller for a hybrid AC/DC micro-grid. *IEEE Trans. Smart Grid*, 99.
- Hu, J., Yuan, H., & Yuan, X. (2017). Modeling of DFIG-based WTs for small-signal stability analysis in DVC timescale in power electronic power systems. *IEEE Transactions on Energy Conversion*, 32(3), 1151-1165.
- Hu, K., Liu, Z., Tasiu, I. A., & Chen, T. J. I. T. o. T. E. (2020). Fault Diagnosis and Tolerance with Low Torque Ripple for Open-Switch Fault of IM Drives.
- Huang, S.-J., & Hsieh, C.-T. (1999). High-impedance fault detection utilizing a Morlet wavelet transform approach. *IEEE Transactions on Power Delivery*, 14(4), 1401-1410.
- Huang, W., Hua, W., Chen, F., & Zhu, J. J. I. T. o. I. E. (2019). Enhanced Model Predictive Torque Control of Fault-Tolerant Five-Phase Permanent Magnet Synchronous Motor With Harmonic Restraint and Voltage Preselection. 67(8), 6259-6269.
- Huang, W., Sun, H., Luo, J., Wang, W. J. M. S., & Processing, S. (2019). Periodic feature oriented adapted dictionary free OMP for rolling element bearing incipient fault diagnosis. 126, 137-160.
- Huang, W. H., Huo, X. X., Hu, S. J., & Xu, H. H. (2013). Phase lead correction for VSI single-loop control. Paper presented at the 2013 IEEE International Conference on Applied Superconductivity and Electromagnetic Devices.
- Hughes, F. M., Anaya-Lara, O., Jenkins, N., & Strbac, G. (2005). Control of DFIG-based wind generation for power network support. *IEEE Transactions on Power Systems*, 20(4), 1958-1966.
- Iglesias-Martínez, M. E., de Córdoba, P. F., Antonino-Daviu, J. A., & Conejero, J. A. J. I. T. o. I. A. (2019). Detection of nonadjacent rotor faults in induction motors via spectral subtraction and autocorrelation of stray flux signals. 55(5), 4585-4594.

- Jabr, H. M., & Kar, N. C. (2007). Effects of main and leakage flux saturation on the transient performances of doubly-fed wind driven induction generator. *Electric Power Systems Research*, 77(8), 1019-1027.
- Jauch, C., Sørensen, P., Norheim, I., & Rasmussen, C. (2007). Simulation of the impact of wind power on the transient fault behavior of the Nordic power system. *Electric Power Systems Research*, 77(2), 135-144.
- Jayaraman, K., & Kumar, M. J. I. T. o. P. E. (2019). Design of Passive Common-Mode Attenuation Methods for Inverter-Fed Induction Motor Drive With Reduced Common-Mode Voltage PWM Technique. 35(3), 2861-2870.
- Jia, G., Chen, M., Tang, S., Zhang, C., & Zhao, B. J. I. T. o. P. E. (2020). A Modular Multilevel Converter With Active Power Filter for Submodule Capacitor Voltage Ripples and Power Losses Reduction. 35(11), 11401-11417.
- Jia, K., Li, Y., Fang, Y., Zheng, L., Bi, T., & Yang, Q. (2018). Transient current similarity based protection for wind farm transmission lines. *Applied Energy*, 225, 42-51.
- Jiang, D., Yu, W., Wang, J., Zhao, Y., Li, Y., & Lu, Y. J. I. A. (2019). A Speed Disturbance Control Method Based on Sliding Mode Control of Permanent Magnet Synchronous Linear Motor. 7, 82424-82433.
- Jiang, X., Huang, W., Cao, R., Hao, Z., & Jiang, W. (2016). Fault tolerant control of dual-winding fault-tolerant permanent magnet motor drive with three-phase four-leg inverter. Paper presented at the 2016 19th International Conference on Electrical Machines and Systems (ICEMS).
- Jie, W. (2009). Control technologies in distributed generation system based on renewable energy. Paper presented at the 2009 3rd International Conference on Power Electronics Systems and Applications (PESA).
- Jin, M., & Weiming, M. (2006). Power converter EMI analysis including IGBT nonlinear switching transient model. *IEEE Transactions on Industrial Electronics*, 53(5), 1577-1583.
- Jin, W., Lu, Y., & Huang, T. J. I. A. (2019). Improved Blocking Scheme for CPL Current Protection in Wind Farms Using the Amplitude Ratio and Phase Difference.
- John, V. J. I. T. o. I. A. (2019). Microwave Tube Fault-Current Model for Design of Crowbar Protection. 55(5), 4934-4943.
- Junyent-Ferré, A., Gomis-Bellmunt, O., Sumper, A., Sala, M., & Mata, M. (2010). Modeling and control of the doubly fed induction generator wind turbine. *Simulation Modelling Practice and Theory*, 18(9), 1365-1381.
- Kayikci, M., & Milanovic, J. (2008). Assessing transient response of DFIG-based wind plants—The influence of model simplifications and parameters. *IEEE Transactions on Power Systems*, 23(2), 545-554.
- Kazmierkowski, M. P., & Malesani, L. (1998). Current control techniques for three-phase voltage-source PWM converters: A survey. *IEEE Transactions on Industrial Electronics*, 45(5), 691-703.

- Keskes, H., Braham, A., & Lachiri, Z. J. E. P. S. R. (2013). Broken rotor bar diagnosis in induction machines through stationary wavelet packet transform and multiclass wavelet SVM. 97, 151-157.
- Khadar, S., Kouzou, A., Rezzaoui, M. M., Hafaifa, A. J. P. P. E. E., & Science, C. (2020). Sensorless control technique of open-end winding five phase induction motor under partial stator winding short-circuit. 64(1), 2-19.
- Khan, M., Radwan, T. S., & Rahman, M. A. (2007). Real-time implementation of wavelet packet transform-based diagnosis and protection of three-phase induction motors. IEEE Transactions on Energy Conversion, 22(3), 647-655.
- Khlaief, A., Saadaoui, O., Abassi, M., Chaari, A., & Boussak, M. J. I. J. o. E. (2020). Open Circuit Fault Detection and FTC for Sensorless PMS Motor Control Based on the Back-EMF SMO.
- Kompella, K. D., Mannam, V. G. R., Rayapudi, S. R. J. J. o. E. S., & Technology, I. (2016). DWT based bearing fault detection in induction motor using noise cancellation. 3(3), 411-427.
- Kompella, K. D., Rao, M. V. G., & Rao, R. S. J. A. S. E. J. (2018). Bearing fault detection in a 3 phase induction motor using stator current frequency spectral subtraction with various wavelet decomposition techniques. 9(4), 2427-2439.
- Konar, P., & Chattopadhyay, P. J. A. S. C. (2015). Multi-class fault diagnosis of induction motor using Hilbert and Wavelet Transform. 30, 341-352.
- Kramer, W., Chakraborty, S., Kroposki, B., & Thomas, H. (2008). Advanced power electronic interfaces for distributed energy systems. National Renewable Energy Laboratory, Cambridge, MA Rep. NREL/Tp-581-42672, 1.
- Kumar, G. K., & Elangovan, D. J. I. P. E. (2019). Review on fault-diagnosis and fault-tolerance for DC-DC converters. 13(1), 1-13.
- Kumar, S., Mukherjee, D., Guchhait, P. K., Banerjee, R., Srivastava, A. K., Vishwakarma, D., & Saket, R. J. I. A. (2019). A comprehensive review of condition based prognostic maintenance (CBPM) for induction motor. 7, 90690-90704.
- Kundur, P., Balu, N. J., & Lauby, M. G. (1994). Power system stability and control (Vol. 7): McGraw-hill New York.
- Lamabadu, D., & Rajakaruna, S. (2017). Dynamic Analysis of a Novel Single-Phase Induction Generator Using an Improved Machine Model. IEEE Transactions on Energy Conversion, 32(1), 1-11.
- Lamim Filho, P. C., Santos, D. C., Batista, F. B., & Baccarini, L. M. J. I. S. J. (2020). Axial Stray Flux Sensor proposal for Three-Phase Induction Motor Fault Monitoring by means of orbital analysis.
- Layadi, N., Djerioui, A., Zeghlache, S., Mekki, H., Houari, A., Gong, J., . . . Engineering. (2020). Fault-Tolerant Control Based on Sliding Mode Controller for Double-Star Induction Machine. 45(3), 1615-1627.

- Ledesma, P., & Usaola, J. J. I. t. o. e. c. (2005). Doubly fed induction generator model for transient stability analysis. 20(2), 388-397.
- Lee, J.-H., Pack, J.-H., & Lee, I.-S. J. A. S. (2019). Fault Diagnosis of Induction Motor Using Convolutional Neural Network. 9(15), 2950.
- Lee, S. B., Hyun, D., Kang, T.-j., Yang, C., Shin, S., Kim, H., . . . Kim, H.-D. J. I. T. o. I. A. (2015). Identification of false rotor fault indications produced by online MCSA for medium-voltage induction machines. 52(1), 729-739.
- Lei, Y., Mullane, A., Lightbody, G., & Yacamini, R. (2006). Modeling of the wind turbine with a doubly fed induction generator for grid integration studies. IEEE Transactions on Energy Conversion, 21(1), 257-264.
- Li, D.-Y., Li, P., Cai, W.-C., Song, Y.-D., & Chen, H.-J. (2018). Adaptive fault-tolerant control of wind turbines with guaranteed transient performance considering active power control of wind farms. IEEE Transactions on Industrial Electronics, 65(4), 3275-3285.
- Li, G., Deng, C., Wu, J., Chen, Z., & Xu, X. J. A. S. (2020). Rolling Bearing Fault Diagnosis Based on Wavelet Packet Transform and Convolutional Neural Network. 10(3), 770.
- Li, M., Yu, D., Chen, Z., Xiahou, K., Ji, T., & Wu, Q. (2018). A Data-Driven Residual-Based Method for Fault Diagnosis and Isolation in Wind Turbines. IEEE Transactions on Sustainable Energy.
- Li, W., Chao, P., Liang, X., Sun, Y., Qi, J., & Chang, X. (2018). Modeling of complete fault ride-through processes for DFIG-Based wind turbines. Renewable energy, 118, 1001-1014.
- Liang, H., Chen, Y., Liang, S., & Wang, C. J. A. S. (2018). Fault detection of stator inter-turn short-circuit in PMSM on stator current and vibration signal. 8(9), 1677.
- Liang, J., Howard, D. F., Restrepo, J. A., & Harley, R. G. (2013). Feedforward transient compensation control for DFIG wind turbines during both balanced and unbalanced grid disturbances. IEEE Transactions on Industry Applications, 49(3), 1452-1463.
- Liang, J., Qiao, W., & Harley, R. (2011). Feed-forward transient current control for low-voltage ride-through enhancement of DFIG wind turbines. Paper presented at the 2011 IEEE/PES Power Systems Conference and Exposition.
- Liang, P., Deng, C., Wu, J., Yang, Z., Zhu, J., & Zhang, Z. J. C. i. I. (2019). Compound fault diagnosis of gearboxes via multi-label convolutional neural network and wavelet transform. 113, 103132.
- Liao, J., Zhu, X., & Wang, Q. J. I. A. (2019). Transient Current Similarity-Based Protection for Interconnecting Transformers in Wind Farms. 7, 45744-45757.
- Liu, J., Yao, W., Fang, J., Wen, J., Cheng, S. J. I. J. o. E. P., & Systems, E. (2018). Stability analysis and energy storage-based solution of wind farm during low voltage ride through. 101, 75-84.

- Liu, W., Zhang, W., Han, J., & Wang, G. (2012). A new wind turbine fault diagnosis method based on the local mean decomposition. *Renewable energy*, 48, 411-415.
- Liu, Y., & Bazzi, A. M. J. I. t. (2017). A review and comparison of fault detection and diagnosis methods for squirrel-cage induction motors: State of the art. 70, 400-409.
- Liu, Z., Liu, C., Li, G., Liu, Y., & Liu, Y. (2015). Impact study of PMSG-based wind power penetration on power system transient stability using EEAC theory. *Energies*, 8(12), 13419-13441.
- Liu, Z., Sun, X., Zheng, Z., Jiang, D., & Li, Y. J. I. T. o. P. E. (2019). Optimized Current Trajectory Tracking Control of a Five-Phase Induction Machine Under Asymmetrical Current Limits. 35(5), 5290-5303.
- Liu, Z., Zhang, L., & Carrasco, J. J. R. E. (2020). Vibration analysis for large-scale wind turbine blade bearing fault detection with an empirical wavelet thresholding method. 146, 99-110.
- Lopes, J. P., Hatziargyriou, N., Mutale, J., Djapic, P., & Jenkins, N. (2007). Integrating distributed generation into electric power systems: A review of drivers, challenges and opportunities. *Electric Power Systems Research*, 77(9), 1189-1203.
- Lorenzo-Bonache, A., Honrubia-Escribano, A., Jiménez-Buendía, F., Molina-García, Á., & Gómez-Lázaro, E. J. E. (2017). Generic type 3 wind turbine model based on IEC 61400-27-1: Parameter analysis and transient response under voltage dips. 10(9), 1441.
- Lu, B., & Sharma, S. K. (2009). A literature review of IGBT fault diagnostic and protection methods for power inverters. *IEEE Transactions on Industry Applications*, 45(5), 1770-1777.
- Luong, P., & Wang, W. J. I. A. T. o. M. (2020). Smart Sensor-Based Synergistic Analysis for Rotor Bar Fault Detection of Induction Motors. 25(2), 1067-1075.
- Maamouri, R., Trabelsi, M., Boussak, M., M'Sahli, F. J. E. P. C., & Systems. (2018). Fault diagnosis and fault tolerant control of a three-phase VSI supplying sensorless speed controlled induction motor drive. 46(19-20), 2159-2173.
- Mao, H., Li, W., Feng, X., & Zhang, H. J. C. (2020). Active Fault Tolerance Control Based on Consistent Matrix for Multimotor Synchronous System. 2020.
- Martucci, S. A. (1994). Symmetric convolution and the discrete sine and cosine transforms. *IEEE transactions on signal processing*, 42(5), 1038-1051.
- May, S., Sergey, E., & Ilya, I. Universal and Energy Efficient Transistor Autonomous Inverter on Semiconductor Switches.
- Meng, W., Yang, Q., Ying, Y., Sun, Y., Yang, Z., & Sun, Y. (2013). Adaptive power capture control of variable-speed wind energy conversion systems with guaranteed transient and steady-state performance. *IEEE Transactions on Energy Conversion*, 28(3), 716-725.

- Minaz, M. R. J. I. t. (2020). An effective method for detection of stator fault in PMSM with 1D-LBP.
- Mohan, N., Undeland, T. M., & Robbins, W. P. (2003). Power Electronics, Hoboken. In: NJ, USA: Wiley.
- Mohseni, M., & Islam, S. M. (2012). Transient control of DFIG-based wind power plants in compliance with the Australian grid code. *IEEE Transactions on Power electronics*, 27(6), 2813-2824.
- Mohseni, M., Islam, S. M., & Masoum, M. A. (2011). Enhanced hysteresis-based current regulators in vector control of DFIG wind turbines. *IEEE Transactions on Power electronics*, 26(1), 223-234.
- Monfared, O. A., Doroudi, A., Darvishi, A. J. C.-T. i. j. f. c., electrical, m. i., & engineering, e. (2019). Diagnosis of rotor broken bars faults in squirrel cage induction motor using continuous wavelet transform.
- Mosaad, M. I. (2018). Model reference adaptive control of STATCOM for grid integration of wind energy systems. *IET Electric Power Applications*, 12(5), 605-613.
- Mossa, M. A., Echeikh, H., Iqbal, A., Duc Do, T., & Al-Sumaiti, A. S. J. A. S. (2020). A Novel Sensorless Control for Multiphase Induction Motor Drives Based on Singularly Perturbed Sliding Mode Observer-Experimental Validation. 10(8), 2776.
- Mróz, J., & Poprawski, W. J. E. (2019). Improvement of the Thermal and Mechanical Strength of the Starting Cage of Double-Cage Induction Motors. 12(23), 4551.
- Muller, S., Deicke, M., & De Doncker, R. W. (2002). Doubly fed induction generator systems for wind turbines. *IEEE Industry applications magazine*, 8(3), 26-33.
- Munim, W. N. W. A., Duran, M. J., Che, H. S., Bermúdez, M., González-Prieto, I., & Abd Rahim, N. J. I. T. o. P. E. (2016). A unified analysis of the fault tolerance capability in six-phase induction motor drives. 32(10), 7824-7836.
- Muyeen, S., Ali, M. H., Takahashi, R., Murata, T., Tamura, J., Tomaki, Y., . . . Sasano, E. (2006). Transient stability analysis of grid connected wind turbine generator system considering multi-mass shaft modeling. *Electric power components and systems*, 34(10), 1121-1138.
- Muyeen, S., Ali, M. H., Takahashi, R., Murata, T., Tamura, J., Tomaki, Y., . . . Sasano, E. (2007). Comparative study on transient stability analysis of wind turbine generator system using different drive train models. *IET Renewable Power Generation*, 1(2), 131-141.
- Nian, H., Zhou, Y., & Zeng, H. J. I. T. o. P. E. (2015). Zero-sequence current suppression strategy for open winding PMSG fed by semiconverter. 31(1), 711-720.
- Nunes, M. V., Lopes, J. P., Zurn, H. H., Bezerra, U. H., & Almeida, R. G. (2004). Influence of the variable-speed wind generators in transient stability margin of the

- conventional generators integrated in electrical grids. *IEEE Transactions on Energy Conversion*, 19(4), 692-701.
- Odhano, S. A., Bojoi, R., Boglietti, A., Roşu, Ş. G., & Griva, G. J. I. t. o. I. A. (2015). Maximum efficiency per torque direct flux vector control of induction motor drives. *51(6)*, 4415-4424.
- Ojaghi, M., Sabouri, M., & Faiz, J. J. I. t. o. e. e. s. (2014). Diagnosis methods for stator winding faults in three-phase squirrel-cage induction motors. *24(6)*, 891-912.
- Omari, A., Khalil, B. I., Hazzab, A., Bouchiba, B., Benmohamed, F. E. J. C.-T. i. j. f. c., electrical, m. i., & engineering, e. (2019). Real-time implementation of MRAS rotor time constant estimation for induction motor vector control based on a new adaptation signal.
- Ouchen, S., Benbouzid, M., Blaabjerg, F., Betka, A., Steinhart, H. J. I. J. o. E., & Electronics, S. T. i. P. (2020). Direct Power Control of Shunt Active Power Filter using Space Vector Modulation based on Super Twisting Sliding Mode Control.
- Potamianakis, E. G., & Vournas, C. D. (2006). Short-term voltage instability: effects on synchronous and induction machines. *IEEE Transactions on Power Systems*, 21(2), 791-798.
- Qiao, W., Zhou, W., Aller, J. M., & Harley, R. G. (2008). Wind speed estimation based sensorless output maximization control for a wind turbine driving a DFIG. *IEEE Transactions on Power electronics*, 23(3), 1156-1169.
- Rahimi, M., & Parniani, M. (2009). Dynamic behavior and transient stability analysis of fixed speed wind turbines. *Renewable energy*, 34(12), 2613-2624.
- Rangel-Magdaleno, J., Peregrina-Barreto, H., Ramirez-Cortes, J., Morales-Caporal, R., Cruz-Vega, I. J. S., & Vibration. (2016). Vibration analysis of partially damaged rotor bar in induction motor under different load condition using DWT. 2016.
- Rebello, E., Vanfretti, L., & Almas, M. S. (2015). PMU-based real-time damping control system software and hardware architecture synthesis and evaluation. Paper presented at the Power & Energy Society General Meeting, 2015 IEEE.
- Reddy, B. P., & Keerthipati, S. (2017). A three-level inverter configuration for pole-phase modulated nine-phase induction motor drives with single DC link. Paper presented at the 2017 National Power Electronics Conference (NPEC).
- Reddy, B. P., Keerthipati, S., & Iqbal, A. J. I. T. o. I. E. (2020). Phase Reconfiguring Technique for Enhancing the Modulation Index of Multilevel Inverter fed 9-Phase IM Drive.
- Riera-Guasp, M., Antonino-Daviu, J. A., & Capolino, G.-A. J. I. T. o. I. E. (2014). Advances in electrical machine, power electronic, and drive condition monitoring and fault detection: state of the art. *62(3)*, 1746-1759.
- Rivera-Guillen, J. R., De Santiago-Perez, J., Amezcua-Sanchez, J. P., Valtierra-Rodriguez, M., & Romero-Troncoso, R. J. J. M. (2018). Enhanced FFT-based

method for incipient broken rotor bar detection in induction motors during the startup transient. 124, 277-285.

- Roy, S. K., Mohanty, A., & Kumar, C. (2015). Amplitude demodulation of instantaneous angular speed for fault detection in multistage gearbox. In *Vibration Engineering and Technology of Machinery* (pp. 951-961): Springer.
- Sahni, M., Badrzadeh, B., Muthumuni, D., Cheng, Y., Yin, H., Huang, S.-H., & Zhou, Y. (2012). Sub-synchronous interaction in wind power plants-part II: an ERCOT case study. Paper presented at the Power and Energy Society General Meeting, 2012 IEEE.
- Saleh, S., Ahshan, R., & Rahman, M. (2013). Performance Evaluation of an Embedded d - q WPT-Based Digital Protection for IPMSM Drives. *IEEE Transactions on Industry Applications*, 50(3), 2277-2291.
- Saleh, S., Aktaibi, A., Ahshan, R., & Rahman, M. (2012). The development of a d - q axis WPT-based digital protection for power transformers. *IEEE Transactions on Power Delivery*, 27(4), 2255-2269.
- Saleh, S., Aljankawey, A., Meng, R., Meng, J., Chang, L., & Diduch, C. (2015). Impacts of grounding configurations on responses of ground protective relays for DFIG-based WECSs—Part I: solid ground faults. *IEEE Transactions on Industry Applications*, 51(4), 2804-2818.
- Saleh, S., Aljankawey, A., Ozkop, E., & Meng, R. J. I. T. o. P. E. (2016). On the experimental performance of a coordinated antiislanding protection for systems with multiple DGUs. 32(2), 1106-1123.
- Saleh, S., Meng, R., McSheffery, R., Buck, S., & Ozkop, E. (2017a). Performance of multiframe digital interconnection protection for distributed cogeneration systems. *IEEE Transactions on Industry Applications*, 54(2), 1166-1181.
- Saleh, S., Meng, R., McSheffery, R., Buck, S., & Ozkop, E. J. I. T. o. I. A. (2017b). Performance of multiframe digital interconnection protection for distributed cogeneration systems. 54(2), 1166-1181.
- Saleh, S., Meng, R., & Meng, J. (2016). The performance of a digital interconnection protection for grid-connected WECSs. *IEEE Transactions on Industry Applications*, 52(5), 3714-3728.
- Saleh, S., & Ozkop, E. J. I. T. o. I. A. (2016a). Phaselet-Based Method for Detecting Electric Faults in ϕ Induction Motor Drives—Part I: Analysis and Development. 53(3), 2976-2987.
- Saleh, S., & Ozkop, E. J. I. T. o. I. A. (2016b). Phaselet-Based Method for Detecting Electric Faults in ϕ Induction Motor Drives—Part II: Performance Evaluation. *IEEE Trans. on Industry Applications*, 53(3), 2988-2996.
- Saleh, S., & Ozkop, E. J. I. T. o. I. A. (2016c). Phaselet-Based Method for Detecting Electric Faults in ϕ Induction Motor Drives—Part II: Performance Evaluation. 53(3), 2988-2996.

- Saleh, S., Radwan, T., & Rahman, M. (2007). Real-time testing of WPT-based protection of three-phase VS PWM inverter-fed motors. *IEEE Transactions on Power Delivery*, 22(4), 2108-2115.
- Saleh, S. A., Ahshan, R., Abu-Khaizaran, M. S., Alsayid, B., & Rahman, M. (2013). Implementing and Testing \$ d \$-\$ q \$ WPT-Based Digital Protection for Microgrid Systems. *IEEE Transactions on Industry Applications*, 50(3), 2173-2185.
- Saleh, S. A., Ahshan, R., Abu-Khaizaran, M. S., Alsayid, B., & Rahman, M. (2014). Implementing and Testing \$ d \$-\$ q \$ WPT-Based Digital Protection for Microgrid Systems. *IEEE Transactions on Industry Applications*, 50(3), 2173-2185.
- Saleh, S. A., Ozkop, E., & Aljankawey, A. S. (2016). Performance of the Phaselet Frames-Based Digital Protection for Distributed Generation Units. *IEEE Transactions on Industry Applications*, 52(3), 2095-2109.
- Saleh, S. A., Ozkop, E., & Aljankawey, A. S. *J. I. T. o. I. A.* (2015). Performance of the phaselet frames-based digital protection for distributed generation units. 52(3), 2095-2109.
- Saleh, S. A., Richard, C., Onge, X. F. S., Meng, J., & Castillo-Guerra, E. *J. I. T. o. I. A.* (2018). Comparing the Performance of Protection Coordination and Digital Modular Protection for Grid-Connected Battery Storage Systems. 55(3), 2440-2454.
- Saleh, S. A., Scaplen, B., & Rahman, M. A. (2011). A new implementation method of wavelet-packet-transform differential protection for power transformers. *IEEE Transactions on Industry Applications*, 47(2), 1003-1012.
- Saleh, S. A. *J. I. T. o. I. A.* (2017). Testing the performance of a resolution-level MPPT controller for PMG-based wind energy conversion systems. 53(3), 2526-2540.
- Salomon, C. P., Ferreira, C., Sant'Ana, W. C., Lambert-Torres, G., Borges da Silva, L. E., Bonaldi, E. L., . . . Torres, B. S. *J. E.* (2019). A Study of Fault Diagnosis Based on Electrical Signature Analysis for Synchronous Generators Predictive Maintenance in Bulk Electric Systems. 12(8), 1506.
- Samaga, B. R., Vittal, K. *J. I. J. o. E. P.*, & Systems, E. (2012). Comprehensive study of mixed eccentricity fault diagnosis in induction motors using signature analysis. 35(1), 180-185.
- Samanta, A. K., Naha, A., Routray, A., Deb, A. K. *J. M. S.*, & Processing, S. (2018). Fast and accurate spectral estimation for online detection of partial broken bar in induction motors. 98, 63-77.
- Samantaray, S., & Dash, P. (2007). Wavelet packet-based digital relaying for advanced series compensated line. *IET Generation, Transmission & Distribution*, 1(5), 784-792.
- Sapena-Bañó, A., Chinesta, F., Pineda-Sanchez, M., Aguado, J., Borzacchiello, D., Puche-Panadero, R. *J. I. J. o. E. P.*, & Systems, E. (2019). Induction machine

model with finite element accuracy for condition monitoring running in real time using hardware in the loop system. 111, 315-324.

- Semwal, R., Selvaraj, R., Desingu, K., Chelliah, T. R., & Joseph, A. J. I. T. o. I. A. (2019). Two-Stage Protection Circuit for Multi-Channeled Power Electronic Converter Fed Large Asynchronous Hydro-Generating Unit.
- Seshadrinath, J., Singh, B., & Panigrahi, B. K. (2012). Single-turn fault detection in induction machine using complex-wavelet-based method. *IEEE Transactions on Industry Applications*, 48(6), 1846-1854.
- Seshadrinath, J., Singh, B., & Panigrahi, B. K. J. I. T. o. I. I. (2013). Vibration analysis based interturn fault diagnosis in induction machines. 10(1), 340-350.
- Shao, S., Yan, R., Lu, Y., Wang, P., Gao, R. X. J. I. T. o. I., & Measurement. (2019). DCNN-based multi-signal induction motor fault diagnosis. 69(6), 2658-2669.
- Shuai, Z., He, D., Xiong, Z., Lei, Z., & Shen, Z. J. (2018). Comparative Study of Short-Circuit Fault Characteristics for VSC-based DC Distribution Networks with Different Distributed Generators. *IEEE Journal of Emerging and Selected Topics in Power Electronics*.
- Silva, K., Souza, B. A., & Brito, N. S. (2006). Fault detection and classification in transmission lines based on wavelet transform and ANN. *IEEE Transactions on Power Delivery*, 21(4), 2058-2063.
- Simoes, M. G., & Farret, F. A. (2007). *Alternative energy systems: design and analysis with induction generators*: CRC press.
- Simoes, M. G., & Farret, F. A. (2011). *Alternative energy systems: design and analysis with induction generators (Vol. 13)*: CRC press.
- Simon, L., & Swarup, K. S. (2017). Wide area oscillation damping control with DFIG based wind turbines using WAMS. Paper presented at the Power & Energy Society General Meeting, 2017 IEEE.
- Singh, G., Naikan, V. J. M. S., & Processing, S. (2018). Detection of half broken rotor bar fault in VFD driven induction motor drive using motor square current MUSIC analysis. 110, 333-348.
- Singh, M., & Shaik, A. G. J. M. (2019). Faulty bearing detection, classification and location in a three-phase induction motor based on Stockwell transform and support vector machine. 131, 524-533.
- Sitharthan, R., Sundarabalan, C., Devabalaji, K., Nataraj, S. K., & Karthikeyan, M. (2018). Improved fault ride through capability of DFIG-wind turbines using customized dynamic voltage restorer. *Sustainable cities and society*, 39, 114-125.
- Skogestad, S., & Postlethwaite, I. (2007). *Multivariable feedback control: analysis and design (Vol. 2)*: Wiley New York.
- Skowron, M., Wolkiewicz, M., Kowalski, C. T., & Orłowska-Kowalska, T. (2019). Application of Hybrid Neural Network to Detection of Induction Motor Electrical

Faults. Paper presented at the 2019 International Conference on Electrical Drives & Power Electronics (EDPE).

- Sobanski, P., Orłowska-Kowalska, T. J. M., & Simulation, C. i. (2017). Faults diagnosis and control in a low-cost fault-tolerant induction motor drive system. 131, 217-233.
- Soeth, A. B., de Souza, P. R. F., Custódio, D. T., & Voloh, I. (2018). Traveling wave fault location on HVDC lines. Paper presented at the Protective Relay Engineers (CPRE), 2018 71st Annual Conference for.
- Stojčić, G., Pašanbegović, K., & Wolbank, T. M. (2014). Detecting faults in doubly fed induction generator by rotor side transient current measurement. *IEEE Transactions on Industry Applications*, 50(5), 3494-3502.
- Strang, G., & Nguyen, T. (1996). *Wavelets and filter banks*: SIAM.
- Strang, G., & Nguyen, T. (1996). *Wavelets and Filter Banks*, Wellesley-Cambridge Press, Wellesley, MA.
- Sukumar, D., Jithendranath, J., Saranu, S. J. E. P. C., & Systems. (2014). Three-level inverter-fed induction motor drive performance improvement with neuro-fuzzy space vector modulation. 42(15), 1633-1646.
- Sun, J., Liu, Z., Zheng, Z., & Li, Y. J. I. T. o. P. E. (2019). An Online Global Fault-Tolerant Control Strategy for Symmetrical Multiphase Machines With Minimum Losses in Full Torque Production Range. 35(3), 2819-2830.
- Taj, T. A., Hasanien, H. M., Alolah, A. I., & Muyeen, S. M. (2015). Transient stability enhancement of a grid-connected wind farm using an adaptive neuro-fuzzy controlled-flywheel energy storage system. *IET Renewable Power Generation*, 9(7), 792-800.
- Tajdinian, M., Seifi, A. R., & Allahbakhshi, M. (2018). Transient Stability of Power Grids Comprising Wind Turbines: New Formulation, Implementation, and Application in Real-Time Assessment. *IEEE Systems Journal*.
- Tang, J., Chen, J., Dong, K., Yang, Y., Lv, H., & Liu, Z. J. E. (2020). Modeling and evaluation of stator and rotor faults for induction motors. 13(1), 133.
- Tang, J., Yang, Y., Chen, J., Qiu, R., & Liu, Z. J. E. (2020). Characteristics analysis and measurement of inverter-fed induction motors for stator and rotor fault detection. 13(1), 101.
- Tang, W., Hu, J., Chang, Y., Yuan, X., & Liu, F. (2018). Modeling of DFIG-based WT for System Transient Response Analysis in Rotor Speed Control Timescale. *IEEE Transactions on Power Systems*.
- Tang, Y., Dai, J., Ning, J., Dang, J., Li, Y., & Tian, X. (2017). An Extended System Frequency Response Model Considering Wind Power Participation in Frequency Regulation. *Energies*, 10(11), 1797.

- Tao, T., Zhao, W., Du, Y., Cheng, Y., & Zhu, J. J. I. T. o. P. E. (2019). Simplified fault-tolerant model predictive control for a five-phase permanent-magnet motor with reduced computation burden. 35(4), 3850-3858.
- Tarvirdilu-Asl, R., Nalakath, S., Xia, Z., Sun, Y., Wiseman, J., & Emadi, A. J. I. T. o. P. E. (2020). Improved Online Optimization-Based Optimal Tracking Control Method for Induction Motor Drives.
- Teja, A. R., Verma, V., & Chakraborty, C. J. I. T. o. I. E. (2015). A new formulation of reactive-power-based model reference adaptive system for sensorless induction motor drive. 62(11), 6797-6808.
- Todeschini, G., & Emanuel, A. E. (2011). Transient response of a wind energy conversion system used as active filter. *IEEE Transactions on Energy Conversion*, 26(2), 522-531.
- Toma, S., Capocchi, L., & Capolino, G.-A. (2012). Wound-rotor induction generator inter-turn short-circuits diagnosis using a new digital neural network. *IEEE Transactions on Industrial Electronics*, 60(9), 4043-4052.
- Torkaman, H., & Keyhani, A. (2018). A review of design consideration for Doubly Fed Induction Generator based wind energy system. *Electric Power Systems Research*, 160, 128-141.
- Trabelsi, M., Boussak, M., & Benbouzid, M. J. E. P. S. R. (2017). Multiple criteria for high performance real-time diagnostic of single and multiple open-switch faults in ac-motor drives: Application to IGBT-based voltage source inverter. 144, 136-149.
- Vázquez Pérez, S., Rodríguez, J., Rivera, M., García Franquelo, L., & Norambuena, M. J. I. T. o. I. E., 64 , 935-947. (2017). Model Predictive Control for Power Converters and Drives: Advances and Trends.
- Villanueva, I., Rosales, A., Ponce, P., & Molina, A. J. I. T. o. S. E. (2018). Grid-voltage-oriented sliding mode control for DFIG under balanced and unbalanced grid Faults. 9(3), 1090-1098.
- Wang, L., Xie, X., Jiang, Q., Liu, H., Li, Y., & Liu, H. (2015). Investigation of SSR in practical DFIG-based wind farms connected to a series-compensated power system. *IEEE Transactions on Power Systems*, 30(5), 2772-2779.
- Wang, S., Xiang, J., Zhong, Y., & Zhou, Y. J. K.-B. S. (2018). Convolutional neural network-based hidden Markov models for rolling element bearing fault identification. 144, 65-76.
- Wang, X., & Shen, Y. (2018). Fault-Tolerant Control Strategy of a Wind Energy Conversion System Considering Multiple Fault Reconstruction. *Applied Sciences*, 8(5), 794.
- Wang, Y., Wu, Q., Gong, W., & Gryning, M. P. S. (2016). \mathcal{H}_∞ Robust Current Control for DFIG-Based Wind Turbine Subject to Grid Voltage Distortions. *IEEE Transactions on Sustainable Energy*, 8(2), 816-825.

- Wickerhauser, M. V. (1996). *Adapted wavelet analysis: from theory to software*: AK Peters/CRC Press.
- Wu, F., Sun, J., Zhou, D., Liu, Y., Geng, T., & Zhao, J. J. I. A. (2020). Simplified Fourier Series Based Transistor Open-Circuit Fault Location Method in Voltage-Source Inverter Fed Induction Motor. 8, 83953-83964.
- Wu, L., Zheng, Y., Fang, Y., & Huang, X. J. I. T. o. I. E. (2020). A novel fault-tolerant doubly-fed flux reversal machine with armature windings wound on both stator and rotor teeth.
- Xie, Y., Pi, C., & Li, Z. J. E. (2019). Study on Design and Vibration Reduction Optimization of High Starting Torque Induction Motor. 12(7), 1263.
- Yang-Wu, S., De-Ping, K., Yuan-Zhang, S., Kirschen, D., Yi-Shen, W., & Yuan-Chao, H. (2015). A novel transient rotor current control scheme of a doubly-fed induction generator equipped with superconducting magnetic energy storage for voltage and frequency support. *Chinese Physics B*, 24(7), 070201.
- Yang, B., Yu, T., Shu, H., Qiu, D., Zhang, Y., Cao, P., & Jiang, L. (2018). Passivity-based Linear Feedback Control of Permanent Magnetic Synchronous Generator based Wind Energy Conversion System: Design and Analysis. *IET Renewable Power Generation*.
- Yang, S., Sun, X., Ma, M., Zhang, X., & Chang, L. J. I. T. o. I. E. (2019). Fault Detection and Identification Scheme for Dual-Inverter Fed OEWM Drive. 67(7), 6112-6123.
- Yetgin, A. G. J. E. F. A. (2019). Effects of induction motor end ring faults on motor performance. *Experimental results*. 96, 374-383.
- Yin, Z., & Hou, J. J. N. (2016). Recent advances on SVM based fault diagnosis and process monitoring in complicated industrial processes. 174, 643-650.
- Yu, Y., Zhao, Y., Wang, B., Huang, X., & Xu, D. J. I. T. o. P. E. (2017). Current sensor fault diagnosis and tolerant control for VSI-based induction motor drives. 33(5), 4238-4248.
- Yuan, H., Yuan, X., & Hu, J. (2016). Modeling and large-signal stability of DFIG wind turbine in dc-voltage control time scale. Paper presented at the Power and Energy Society General Meeting (PESGM), 2016.
- Zafari, Y., & Shoja-Majidabad, S. J. A. (2020). Sensorless fault-tolerant control of five-phase IPMSMs via model reference adaptive systems. 61(4), 564-573.
- Zhang, J., Zhan, W., & Ehsani, M. J. I. T. o. E. C. (2019). Fault Tolerant Control of PMSM with Inter-turn Short Circuit Fault.
- Zhang, L., Zhu, X., Gao, J., & Mao, Y. J. I. T. o. I. E. (2019). Design and Analysis of New Five-Phase Flux-Intensifying Fault-Tolerant Interior-Permanent-Magnet Motor for Sensorless Operation. 67(7), 6055-6065.
- Zhang, T., Wang, F., & Fu, W. (2018). Fault Detection and Isolation for Redundant Inertial Measurement Unit under Quantization. *Applied Sciences*, 8(6), 865.

- Zhang, X., Wu, J., Yang, J., & Shu, J. (2008). H-infinity robust control of constant power output for the wind energy conversion system above rated wind. *Control Theory & Applications*, 25(2), 2008.
- Zhang, Y., Roes, M., Hendrix, M., Duarte, J. J. I. J. o. E. P., & Systems, E. (2020). Symmetric-component decoupled control of grid-connected inverters for voltage unbalance correction and harmonic compensation. 115, 105490.
- Zhao, J., Guan, X., Li, C., Mou, Q., & Chen, Z. J. I. T. o. I. T. S. (2020). Comprehensive Evaluation of Inter-Turn Short Circuit Faults in PMSM Used for Electric Vehicles.
- Zhao, W., Chen, Z., Xu, D., Ji, J., & Zhao, P. J. I. T. o. I. E. (2018). Unity power factor fault-tolerant control of linear permanent-magnet vernier motor fed by a floating bridge multilevel inverter with switch fault. 65(11), 9113-9123.
- Zhao, Y., Huang, W., Jiang, W., Lin, X., & Dong, D. J. I. T. o. I. E. (2020). A Fault-Tolerant Machine Based on Radial-Flux Dual Stator and Parallel Permanent-Magnet/Reluctance Structure.
- Zhao, Z., Yu, J., Zhao, L., Yu, H., & Lin, C. J. I. S. (2018). Adaptive fuzzy control for induction motors stochastic nonlinear systems with input saturation based on command filtering. 463, 186-195.
- Zhen, D., Wang, Z., Li, H., Zhang, H., Yang, J., & Gu, F. J. A. S. (2019). An improved cyclic modulation spectral analysis based on the CWT and its application on broken rotor bar fault diagnosis for induction motors. 9(18), 3902.
- Zheng, D., Ouyang, J., Xiong, X., Xiao, C., & Li, M. (2018). A System Transient Stability Enhancement Control Method Using Doubly Fed Induction Generator Wind Turbine with Considering Its Power Constraints. *Energies*, 11(4), 945.
- Zhou, X., Sun, J., Li, H., Lu, M., & Zeng, F. J. I. T. o. P. E. (2019). PMSM open-phase fault-tolerant control strategy based on four-leg inverter. 35(3), 2799-2808.
- Zhu, D., Zou, X., Deng, L., Huang, Q., Zhou, S., & Kang, Y. (2016). Inductance-emulating Control for DFIG-Based Wind Turbine to Ride-through Grid Faults. *IEEE Transactions on Power electronics*.
- Zhu, J., Hu, J., Hung, W., Wang, C., Zhang, X., Bu, S., . . . Booth, C. D. (2018). Synthetic Inertia Control Strategy for Doubly Fed Induction Generator Wind Turbine Generators Using Lithium-Ion Supercapacitors. *IEEE Transactions on Energy Conversion*, 33(2), 773-783.
- Zolfaghari, S., Noor, S. B. M., Rezazadeh Mehrjou, M., Marhaban, M. H., & Mariun, N. J. A. S. (2018a). Broken rotor bar fault detection and classification using wavelet packet signature analysis based on fourier transform and multi-layer perceptron neural network. 8(1), 25.
- Zolfaghari, S., Noor, S. B. M., Rezazadeh Mehrjou, M., Marhaban, M. H., & Mariun, N. J. A. S. (2018b). Broken rotor bar fault detection and classification using wavelet packet signature analysis based on fourier transform and multi-layer perceptron neural network. *Applied Sciences*, 8(1), 25.

Universiti Malaya

LIST OF PUBLICATIONS

1. Abubakar, U., Mekhilef, S., Mokhlis, H., Seyedmahmoudian, M., Horan, B., Stojcevski, A., Bassi H., Hosin Rawa, M. (2018). Transient Faults in Wind Energy Conversion Systems: Analysis, Modelling Methodologies and Remedies. *Energies* 2018, 11(9), 2249.

2. Ukashatu Abubakar, Saad Mekhilef, Khalaf S Gaeid, Hazlie Mokhlis, Yousif I Al Mashhadany. Induction Motor Fault Detection Based on Multi-sensory Control and Wavelet Analysis. *IET Electric Power Applications*, 2020, ISSN 1751-8679.

Universiti Malaysia